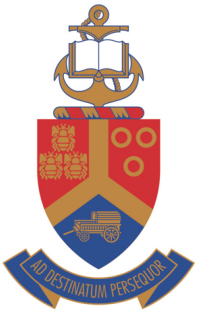

UNIVERSITEIT VAN PRETORIA
UNIVERSITY OF PRETORIA
YUNIBESITHI YA PRETORIA

Fertiliser-catalysed biochar production: an analytical and techno-economic feasibility study

by

Brendon Trollip
17012067

Supervised By

Dr. RD Merckel

Submitted in fulfilment of the requirements for the degree
Master of Engineering (Chemical Engineering)
in the Faculty of Engineering, Built Environment & IT, University of Pretoria

Pretoria, 2024

Statement

The author, whose name appears on the title page of this dissertation, has obtained the required research ethics approval/exemption for the research described in this work.

The author declares that they have observed the ethical standards required in terms of the University of Pretoria's Code of ethics for scholarly activities.

Brendon Trollip
Signature

Date: 27 June, 2024

Abstract

The current agricultural method of burning left over plant material in farm lands before planting a new crop is outdated. While this technique may be fast and cost-effective it is very unsustainable. This practice produces large amounts of carbon black, resulting in health issues, and reduces soil fertility [Pang, 2019]. It is also well known that the process used to produce nitrogen-containing fertilisers, the Haber-Bosch process, is thermodynamically unfavourable at high temperatures. To overcome this limitation, the process is operated at extremely high pressures, making the process very energy intensive [Razon, 2014]. Like fossil fuels, the world's phosphorus reserves are limited and can't sustain current agricultural practices indefinitely, driving the search for sustainable alternatives [Desmidt et al., 2015]. With 71 billion metric tons of phosphate ore available and a production rate of 0.22 billion metric tons in 2021 [Jasinski, 2022], the use of specialty fertilisers is expected to rise due to the irreplaceable role of phosphorus in farming.

The objective of this research was to identify fertilising agents that reduced the pyrolytic onset temperature of biomass, producing a fertilising-biochar. By lowering the pyrolytic ignition temperature, energy reduction were observed, resulting in a more economically viable product. The enriched biochar, containing nitrogen (N), phosphorous (P) and potassium (K), aims to provide essential nutrients to the soil for crop cultivation. 79 prospective fertilising agents, each representing one of the three macro nutrients (NPK) required by biomass, were analysed. K_2CO_3, K_3PO_4 and $Ca(NO_3)_2{\cdot}4H_2O$ were chosen to represent potassium, phosphorous and nitrogen, respectively. As for the biomass of choice, *Eucalyptus grandis* was selected, due to it's widespread abundance, not only in South Africa, but in the world.

The fertilising agents were each added in concentrations of 1 wt.%, 2 wt.% , 5 wt.%, 10 wt.%, 20 wt.% and 50 wt.% to the biomass with deionised water and then dried at 105 °C. Thermogravimetric analysis was conducted on the dried samples with a Hitachi STA7300 horizontal-beam TGA-DTA system and compared to a neat sample of *E. grandis*. It was established that both K_2CO_3 and K_3PO_4 suppressed the pyrolytic onset temperature of the biomass. K_2CO_3 exhibited an ignition temperature suppression of -11 °C, -25 °C, -48 °C, -71 °C, -83 °C, and -97 °C for 1 wt.%, 2 wt.%, 5 wt.%, 10 wt.%, 20 wt.%, and 50 wt.%, respectively, with a maximum possible suppression of -98 °C. This resulted in an energy saving of 18.7 % for the 50 wt.% loading. K_3PO_4 also showed significant suppression of the pyrolytic onset temperature, with 1 wt.%, 2 wt.%, 5 wt.%, 10 wt.%, 20 wt.%, and 50 wt.% loadings resulting in suppressions of -2 °C, -20 °C, -33 °C, -49 °C, -55 °C, and -75 °C, respectively. The highest fertiliser loading (50 wt.%)

indicated an energy saving of 16.7 %. Conversely, $Ca(NO_3)_2{\cdot}4H_2O$ demonstrated no catalytic effect on *E. grandis*.

After establishing that the fertilising agents had a catalytic effect on *E. grandis* and resulted in an energy reduction, a techno-economic feasibility analysis was conducted to investigate the economic viability of an enriched biochar. To quantify the feasibility, four financial indicators were utilised; the net present value (NPV), internal rate of return (IRR), return on investment (ROI), and payback period (PP). In addition to the sale of the nutrient enriched biochar, the by-products (synthesis gas and pyrolysis oil), were also offseted, to increase economic feasibility. Four scenarios for the sale of by-products were considered, with Scenario 2 and Scenario 4 proving to be the most viable. In Scenario 2, electricity was sold to the grid by combusting the synthesis gas and wood vinegar fraction, while the phenolic fraction was distilled and sold separately. In Scenario 4, the phenolic fraction was extracted through distillation, and both the wood vinegar and phenolic fractions were sold. Process parameters including the daily tonnage, fertiliser loading, biochar yield, fertiliser agents ratio and the final selling price were varied to optimise the final selling price.

The first price comparison was between neat biochar to that of coking coal, used in the steel manufacturing industry. It was discovered that at a selling price of 20 R kg^{-1}, neat biochar attained an IRR of 3.4 % and payback period of 10.4 years (with the plant lifespan set at 20 years). The selling price of neat biochar was calculated as almost four times the current price of coking coal (5.04 R kg^{-1}). The other price comparison that was investigated was between NPK fertilising products, currently used in agriculture, to the enriched biochar. Due to the difficulty of obtaining bulk prices for K_2CO_3, K_3PO_4 and $Ca(NO_3)_2{\cdot}4H_2O$, wholesale prices for muriate of potash, diammonium phosphate and urea were used, respectively. Although the selling price was kept as low as possible, an IRR level of 16 % was set to attract investors, given that the plant would require a major fixed capital investment. The analysis indicated that employing a biochar with 51.7 % loaded fertiliser resulted in a 32-fold price increase per hectare, if the required amount of fertiliser is applied. Using a 5.3 % loading, the cost increase would soar to 127 times higher per hectare. The price increase is primarily attributed to the large amount of biochar needed, if an enriched biochar of 5.3 % loading is used, 19 times more product is required per hectare compared to using neat fertilisers.

Acknowledgments

This dissertation would not have been possible without the support and guidance of my supervisor and mentor, Dr. Ryan Merckel. I'm truly grateful for his time and effort through all facets of my academic and professional career. His knowledge and expertise in the field of pyrolysis not only enhanced the quality of my research but also provided me with a deeper understanding of the research field, enabling me to overcome various challenges throughout my Masters.

I am also very grateful for the opportunity I had to present my work at the 14th International Conference on Applied Energy (ICAE 2022), held at Ruhr University in Bochum, Germany. This experience was invaluable for my professional growth and academic exposure.

Thank you to the National Research Foundation (NRF) of South Africa for funding this research through the Thuthuka Funding Instrument and for awarding me the NRF Postgraduate Scholarship for my honours year in 2021.

I'd also like to thank Gessica Petrarolo for the help she lended me in the analytical labs. Furthermore, I'd like to thank Thys Rossouw, for allowing me to go to campus when required and for his support during the writing of my dissertation. You are a remarkable mentor whom I deeply respect and will continue to look up to.

I would also like to express my deepest appreciation to my newly wedded wife for her unwavering support and love throughout this time and my entire academic career. Thank you for making dinner when I was working on Masters late at night. It took a bit longer than it should've, but thank you for standing by me and supporting me.

Lastly, I extend my profound gratitude to my parents, because without them, this would have not been possible. Even though they may not fully understand the specifics of my studies and career, their unwavering belief in me and the drive they instilled from my first year have been the foundation of my success. I would not be where I am today without their encouragement and support.

Brendon Trollip
Department of Chemical engineering
Faculty of Engineering, Built Environment & IT
University of Pretoria
Pretoria, South Africa
27 June, 2024

Table of Contents

List of Figures

List of Tables

List of Symbols

Symbols

R	South African Rand (ZAR)	-
US$	United States Dollar	-
M_i	Molecular mass of element i	g mol^{-1}
M_{compound}	Molecular mass of compound i	g mol^{-1}
C_i	Cost per kilogram of compound	R kg^{-1}
T	Temperature	°C
T_{decomp}	Decomposition temperature	°C
T_{onset}	Pyrolytic onset temperature	°C
$\Delta T_{\text{suppression}}$	Catalytic temperature suppression	°C
$\Delta_{\text{c}}\text{h}^{\circ}_{\text{HHV}}$	Standard molar combustion enthalpy	MJ kg^{-1}
$\Delta H_{\text{r}}^{\circ}$	Enthalpy of reaction	MJ kg^{-1}
ΔH_{Cp}	Enthalpy of pyrolytic onset temperature	MJ kg^{-1}
C_p	Heat capacity	kJ kg^{-1} K^{-1}
f_1	Mass fraction factor	-
f_2	Chemical cost factor	-
f_3	Thermal stability factor	-
f_4	Toxicity factor	-
F	Suitability factor	-

Greek letters

ω_i	Mass fraction of component i	-
ν	Stoichiometric entity	-

Abbreviations

HHV	Higher heating value	MJ kg^{-1}
NPV	Net present value	-
IRR	Internal rate of return	-

ROI	Return on investment	-
PP	Payback period	-
TGA	Thermogravimetric analysis	-
DTG	Differential Thermogravimetric	-
TPD	Temperature programmed desorption	-
TCD	Thermal conductivity detector	-
DAF	Dry ash-free	-
SRF	Short rotation forestry	-
NPK	Nitrogen, phosphorous and potassium	-
DAP	Diammonium phosphate	-
MOP	Mutriate of potash	-

Chapter 1

Introduction

The thermochemical conversion of biomass has been practised by human kind for thousands of years. Some archaeological studies indicate that pyrolysis liquids date back to the time of the Neanderthals [Tiilikkala et al., 2010]. The ancient Egyptians used the tar produced by pyrolysis to seal wooden boats against leaks. Furthermore, it has also been shown that the ancient Egyptians used methanol and acetic acid, obtained from the process of pyrolysis, to embalm pharaohs [Garcia-Nunez et al., 2017]. In preceding years, pyrolysis was utilised to produce biochar, as it has a higher calorific value than wood of the same mass [Fahmy et al., 2020].

Biochar has been used for millenia as a source of heat and as an agricultural amendment. Biochar was used by the indigenous tribes of the Amazon to enrich the soil. The soil, known as terra preta, has a dark colouration and has recognised draining characteristics. As *terra preta* soils are less acid and contain more nutrients, it is generally more fertile than other soils [Eden et al., 1984]. Biochar is currently used to improve soil quality, utilising technological advances to optimise the soil's nutrient requirements [Amin et al., 2016]. The presence of biochar in soils result in (i) higher growth rates of crops, (ii) a net increase in soil-specific area, resulting in improved draining and aeration and (iii) a more porous soil which promotes the growth of mycorrhizal fungi and other soil microbiota [Qambrani et al., 2017].

With an evergrowing global population and concerns over fossil fuel depletion, sustainable energy sources have become a hot topic. The sustainable availability of biomass is predicted to be as high as 1.08×10^{11} tons of oil-equivalent, which equates to almost 10 times the world's current energy demand [De Wit and Faaij, 2010].

1.1 Background

1.1.1 Pyrolysis overview

Thermochemical conversion processes encompass the controlled heating and/or oxidation of biomass for the upgradation of the feedstock or for the production of steam/heat [Tanger et al., 2013]. Figure 1.1 depicts different thermochemical conversion routes and their associated products.

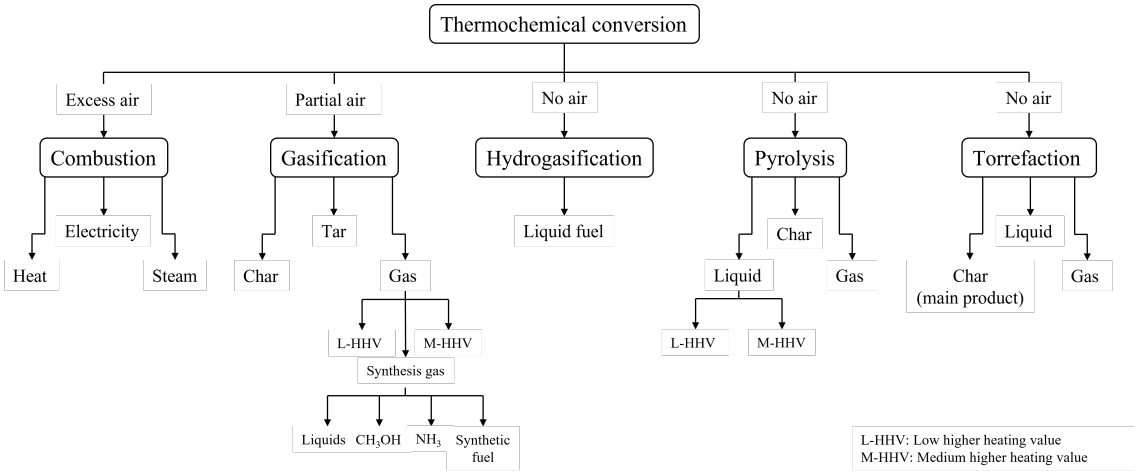

FIGURE 1.1: Thermochemical biomass conversion routes adapted from Küçük and Demirbaş [1997], Verma et al. [2012].

The thermochemical process that has received the most attention in recent years is the pyrolysis of biomass. Pyrolysis converts low-value lignocellulosic biomass to high-value liquid bio-fuels [Meier and Faix, 1999]. Together with the production of char and synthesis gas, pyrolysis facilitates the large-scale production of a cost-effective, renewable fuel [Swart, 2012]. Pyrolysis oil can be utilised as a low-grade fuel for boilers, a high-grade fuel for engines and in the pharmaceutical industry as low-volume, high-value products [Hu and Gholizadeh, 2020]. Biochar, on the other hand, has some very promising and interesting applications, including:

1. the use as a fertiliser to grow crops sustainably, ensure food security by sequestrating carbon back into soil, improving soil and crop health [Bolan et al., 2021],
2. used as a wastewater treatment, filtering out potentially harmful contaminants found in wastewater [Gwenzi et al., 2017], and
3. the ferrous metallurgy industry, potentially replacing coal that is currently in use [Ye et al., 2019].

The pyrolysis of biomass is a very complex process due to the differences in biomass structures and decomposition mechanisms [Kan et al., 2016, Wang et al., 2017]. The process of pyrolysis consist of three main steps: initial evaporation of free moisture, followed by primary thermal decomposition, and subsequent cracking and repolymerisation [Kan et al., 2016]. Various reaction pathways including dehydration, decarboxylation, decarbonlyation, cracking, aromatisation, ketonisation, deoxygenation, and aldol condensation take place during pyrolysis [Albright et al., 1983, Küçük and Demirbaş, 1997]. These reactions result in the pyrolysis oil containing more than 400 different compounds [Lyu et al., 2015]. Figure 1.2 depicts the major reaction pathways and products of pyrolysis. Exemplary reactants and products are shown to depict the various pyrolysis pathways.

Pyrolysis usually takes place between 400 °C and 600 °C, with anything below 400 °C defined as torrefaction and reaction temperature above 600 °C defined as gasification. Pyrolysis can be split into two distinctive categories, slow and fast pyrolysis. The main differentiation between slow and fast pyrolysis is the heating rate, with slow pyrolysis having a heating of about 100 K min^{-1}. On the other hand, fast pyrolysis can reach heating rates in excess of 1000 K min^{-1} [Brown et al., 2011].

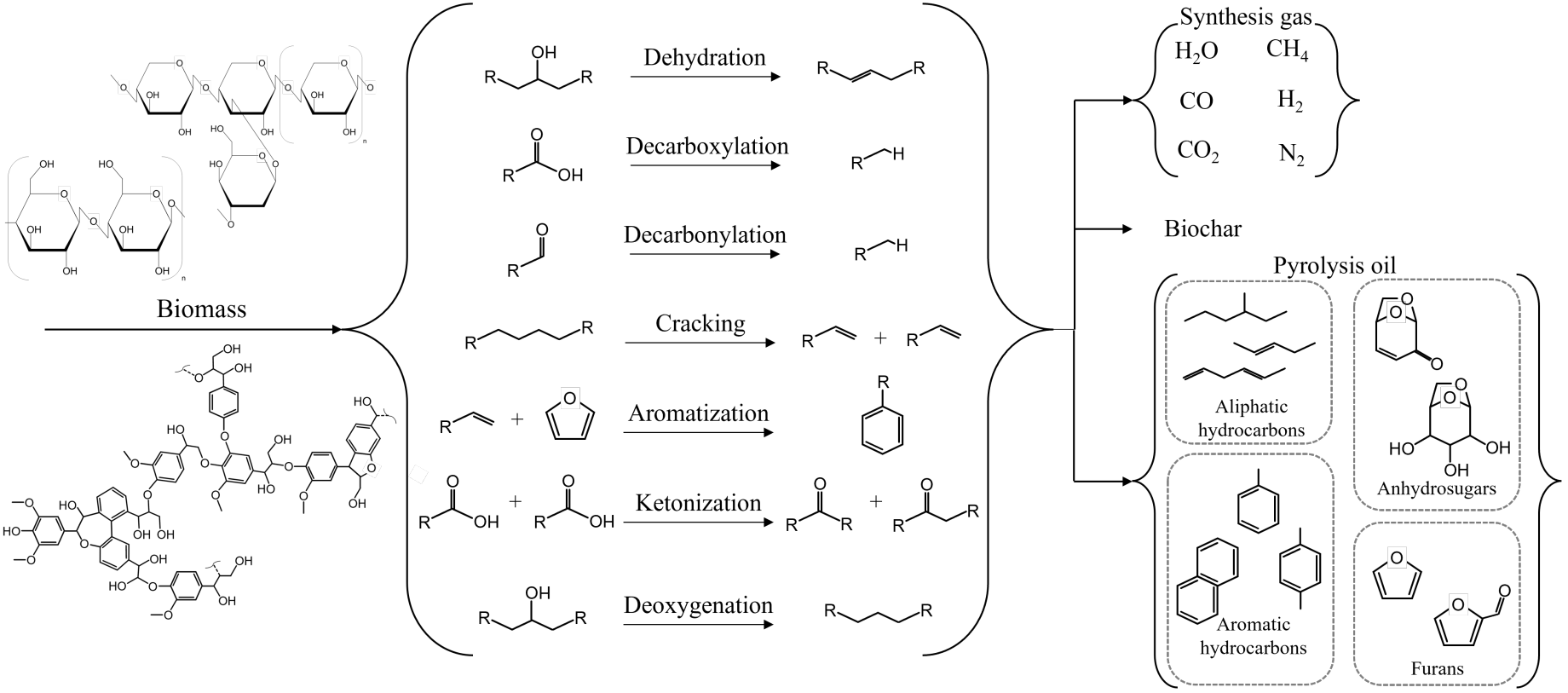

FIGURE 1.2: Pyrolysis reactions and products adapted from Wang et al. [2017].

1.1.2 Current fertilising practise concerns

The concentration of fertilising agents, such as nitrogen, in surface and ground water bodies has steadily increased to levels exceeding acceptable limits [Craswell, 2021]. This study emphasises that fertilisers serve as a significant contributor to nitrogen pollution in water bodies. Rainfall and snowmelt act as transport mechanisms, carrying excess fertilisers into these water bodies. Consequently, nitrogen leaching occurs, resulting in the loss of biodiversity and rendering the water unsuitable for human consumption.

Moreover, another study by Zhang and He [2009] further supports the detrimental effects of excess nitrogen from fertilisers. The study reveals that this excess nitrogen can lead to soil acidification and nutrient depletion. Specifically, the research highlights that soil acidification, caused by the abundance of nitrogen, can adversely impact crop yields. Additionally, the study highlights the negative consequences of excess nitrogen on soil fertility, leading to nutrient depletion and further compromising the overall health of the soil.

Nutrient-enriched biochar can act as a slow-release fertiliser, due to the diffusivity properties of biochar. Biochar has a high surface area and porosity, which allows it to absorb and retain nutrients and water. The nutrient-enhanced biochar can improve soil health by enhancing soil fertility, reducing consumption of fertilisers, promoting sustainable agriculture and recycling nutrients from waste [Karim et al., 2022].

1.2 Research Problem

The aim of the research is to evaluate the economical feasibility of biochar as a soil additive. The investigation includes how biochar functions and participates in the market place. The addition of fertilising agents is also explored to determine what effect they have on the pyrolytic onset temperature. A reduction in the onset temperature of pyrolysis can result in major energy reductions and therefore increase the economic viability. The following hypotheses will be tested:

1. *The addition of fertilising agents will catalyse the pyrolysis reaction and decrease the pyrolytic onset temperature.*
2. *Fertilisers can bring about a significant energy reduction of biochar synthesis such that the technology becomes feasible.*

Numerous discrepancies arose when comparing literature, as some authors [Homagain et al., 2016, Keske et al., 2020] portray biochar as an economically feasible soil additive,

while others remain neutral, concluding that biochar production costs is filled with uncertainties and that the market prices of products have the largest influence on the financial indicators [Campbell et al., 2018, Shackley et al., 2011, Thengane et al., 2020]. This can be due to a lack of understanding of the process particulars of biochar synthesis. It should be noted that biochar is not a fertiliser in itself, but enhances soil fertility and health. Therefore, the research contained in this study aims to incorporate fertilising agents into biochar to deliver essential nutrients to crops.

1.3 Research Objectives

The primary objective of this study is to investigate how fertilising agents impact the pyrolytic onset temperature of *Eucalyptus grandis* by utilising thermogravimetric analysis. Three fertilising agents are identified, each representing nitrogen, phosphorous and potassium, respectively, and their individual effects are studied. The research aims to unravel the intricate relationship between these fertilising agents and the thermal degradation behavior of *Eucalyptus grandis*, shedding light on how each agent influences the pyrolytic ignition temperature. By accomplishing the research objective, we anticipate a reduction in the pyrolysis ignition temperature, leading to significant energy savings.

A second objective of this study is to conduct a comprehensive techno-economic feasibility analysis to investigate the feasibility of producing a catalysed-enriched biochar for the agricultural sector. To evaluate feasibility, four financial indicators are employed, and parameters are optimised to make the end product more attractive to farmers.

1.4 Research Questions

The research objectives are integrated with the need for an investigation of the synergistic effect of fertilising agents on biomass and a comprehensive techno-economic analysis. The following research questions are stated to accomplish the objectives of this research:

1. Are there opportunities to optimise biochar production at the synthesis stage?
2. Will the addition of fertilising agents result in lower energy consumption?
3. Can biochar as a product ever be economically feasible as a substitute for fossil fuel based commodities?
4. Does the addition of fertilising agents make biochar more financially attractive?

Chapter 2

Catalytic suppression of the pyrolytic onset temperature for the production of enriched biochar

The current agricultural operation of incineration of biomass waste has a major impact on human health and is a major source of greenhouse gases. According to Pang [2019], burning woody biomass is a health concern in communities. The study found that burning woody biomass releases particulate matter (PM) which can cause respiratory problems. The study also found that burning woody biomass releases greenhouse gases such as carbon dioxide (CO_2), methane (CH_4), and nitrous oxide (N_2O). According to Huang et al. [2021], pyrolysis is a superior method for upgrading woody biomass due to its reduced greenhouse gas emissions compared to incineration. The study indicates that pyrolysis results in lower levels of carbon dioxide (CO_2), methane (CH_4), and nitrous oxide (N_2O) emissions compared to incineration. Moreover, pyrolysis generates biochar, which serves as both a beneficial soil amendment and a viable fuel source.

This chapter introduces a novel method of incorporating fertilising agents to biochar *via* pyrolysis. Thermogravimetric analysis was employed to examine the impact of the fertilising agents, each representing nitrogen, phosphorus and potassium, respectively, on the pyrolytic onset temperature of woody biomass.

2.1 Materials and methods

2.1.1 Selection of lignocellulosic biomass

Woody biomass is a renewable and abundant source of organic matter that can be used for pyrolysis to produce biochar. Woody biomass can be obtained from different sources such as forest residues, agricultural by-products, energy crops, and urban waste. The amount and quality of woody biomass available for pyrolysis depend on factors such as species, growth conditions, harvesting methods, and storage practices [Simmons et al., 2021].

2.1.1.1 Lignocellulosic biomass

Lignocellulosic biomass is generated by photosynthesis, a process whereby carbohydrates are formed from CO_2, sunlight, and water. Photosynthesis is an incredibly inefficient process to turn sunlight into usable energy. The energy efficiency of photosynthesis is typically less than 1 % for plants [McKendry, 2002]. Lignocellulosic biomass produced as a by-product in the agricultural and forestry sectors are widely available and mostly underutilised [Grobler, 2015]. These industries create an opportunity for the utilisation of biomass that would otherwise be unused. It is estimated that biomass is the fourth largest energy source on the planet, providing 10 % – 14 % of the world's energy supply [Küçük and Demirbaş, 1997, Titiladunayo et al., 2012].

2.1.1.2 Chemical composition

Biomass consists of mainly cellulose, hemicellulose, and lignin — which generally accounts for between 85 % – 90 % of lignocellulosic biomass [Pasangulapati et al., 2012]. The balance comprises of organic extractives (waxes, gums, and resins) and inorganic minerals [Pattiya, 2018]. Cellulose is the most abundant naturally occurring polymer on the planet as it the major structural polymer of the primary cell wall of green plants, several algae and water molds [Gupta et al., 2019]. Cellulose is a complex polysaccharide comprised of thousands of thread-like linear chains of β-(1→4) bonded D-glucose molecules $(C_6H_{10}O_5)_n$ [Pasangulapati et al., 2012]. Hemicellulose is a heterogenous polymer consisting of linked C_5-sugars (xylose and arabinose) and C_6-sugars (mannose and galactose) [Caballero et al., 2003]. β-D-xylopranose ($C_5H_{10}O_5$) forms the backbone of the homoxylans in hemicellulose and other than β-(1→3, 1→4)-glucans — all of the aforementioned compounds are present in the plants cell wall [Scheller and Ulvskov,

2010]. The foremost biological task of hemicellulose is strengthening the cell wall by interacting with cellulose and in some cases, with lignin [Scheller and Ulvskov, 2010]. The most common structures of cellulose and hemicellulose are illustrated in Figure 2.1a) and Figure 2.1b) respectively.

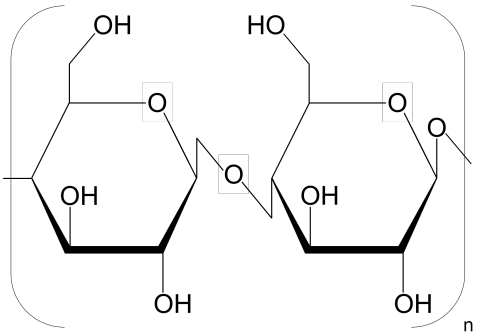

(A) Cellulose representation adapted from Eremenko et al. [2016]

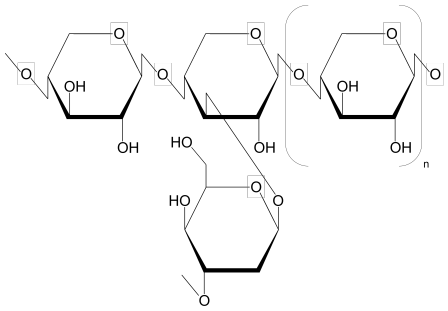

(B) Hemicellulose representation adapted from Alam et al. [2014]

FIGURE 2.1: Lignocellulosic molecule representations.

Second only to cellulose, lignin is the most abundant organic polymer on earth. Lignin is a natural polymer containing three main phenylpropane monolignols: coniferyl; sinapyl; and p-coumaryl alcohols [Liu et al., 2018]. Coniferyl alcohols are the most prevalent of the three components in lignin and is mostly comprised of guaiacyl units. The three phenylpropane monolignols have a high degree of cross-linking, which provides mechanical strength and elasticity to the biomass [Pasangulapati et al., 2012]. Figure 2.2 depicts a snippet of the macromolecular structure of lignin, adapted from Karunarathna and Smith [2020].

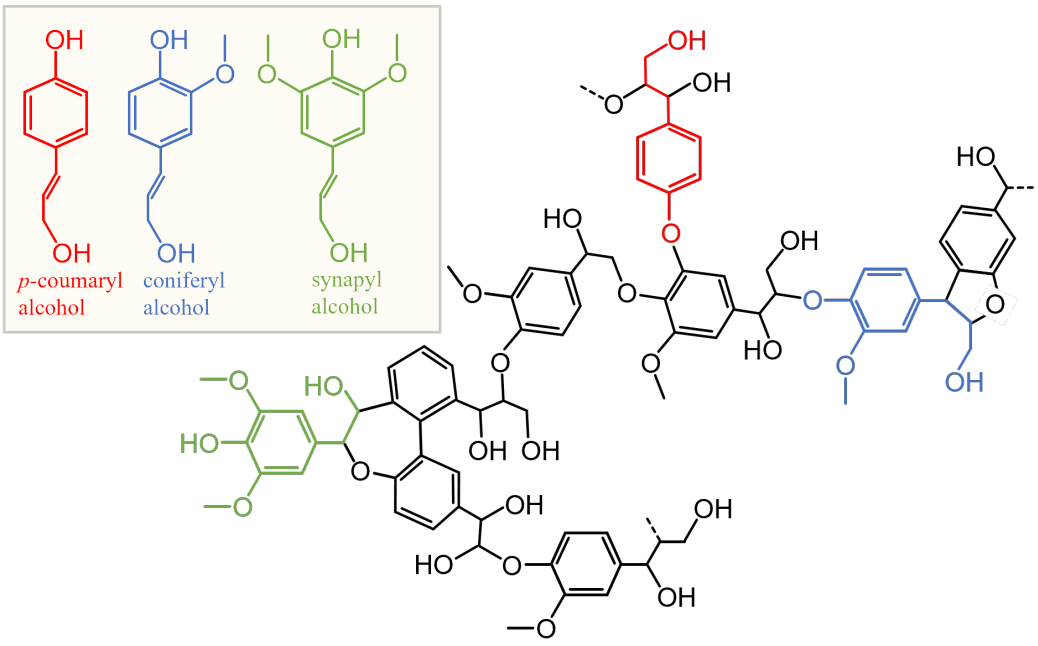

FIGURE 2.2: Chemical structure of lignin.

2.1.1.3 Types of lignocellulosic biomass

The biological and chemical composition of lignocellulosic biomass differs considerably with biomass species. In general, three biomass types are utilised for thermochemical conversion processes: hardwoods, softwoods, and agricultural residues [Pasangulapati et al., 2012]. Hardwoods are produced by angiosperm trees which reproduce by a flowering body. Hardwoods have a more complex structure compared to that of softwoods, and therefore grow much slower [Déjardin et al., 2010]. On average, hardwoods contain about 50 % cellulose, 27 % hemicellulose and 19 % lignin by mass percentage [Di Blasi et al., 2010, Taherzadeh et al., 1997]. On a dry basis, hardwoods contain less lignin but more cellulose than softwoods. Softwoods come from gymnosperms, a type of tree species that produce cones and have needles. Typically, softwoods contain about 43 % cellulose, 23 % hemicellulose, and 30 % lignin [Demirbaş, 2004, Rabemanolontsoa and Saka, 2013]. The technique used to harvest biomass, as well as the storage method, can affect the biological and chemical composition of biomass [Mulkey et al., 2006]. The effects of biomass feedstocks' biological composition (variability in primary constituents) must be better understood to produce products of the desired characteristics [Pasangulapati et al., 2012]. Table 2.1 lists the composition of different lignocellulosic biomass, with the balance being comprised of organic extractives and inorganic minerals. Algae was omitted from the table, as the solid residue of this feedstock is generally high (35 % – 50 %), when undergoing themochemical conversions. This is an indication of low conversion, even at high temperatures [Zhou and Hu, 2020].

TABLE 2.1: Biological composition of different biomass.

Lignocellulosic biomass	Cellulose (%)	Hemicellulose (%)	Lignin (%)	Reference
		Agricultural residues		
Wheat straw	33–38	26–32	17–19	Saini et al. [2015]
Rice straw	28–36	23–28	12–14	Saini et al. [2015]
Rice husks	25–35	12–21	26–31	Rabemanolontsoa and Saka [2013]
Sugarcane bagasse	42–48	19–25	20–42	Saini et al. [2015]
Sorghum bagasse	34–45	18–27	14-21	Saini et al. [2015]
Maize stover	38–40	24–26	7–19	Saini et al. [2015]
Maize leaves	26.9	13.3	15.2	Rabemanolontsoa and Saka [2013]
Switchgrass	5–20	30–50	10–40	McKendry [2002]
Hazelnut shells	25.2	28.2	42.1	Demirbaş [2004]
		Softwoods		
Pine	46.9	20.3	27.3	Taherzadeh et al. [1997]
Spruce	43	29.4	27.6	Demirbaş [2004]
Japanese cedar	38.6	23.1	33.8	Rabemanolontsoa and Saka [2013]
Fir	45	22	30	Di Blasi et al. [2010]
		Hardwoods		
Cherry wood	46	29	18	Di Blasi et al. [2010]
Beech wood	45	33	20	Di Blasi et al. [2010]
Aspen	52.7	21.7	19.5	Taherzadeh et al. [1997]
Poplar	49	24	20	Di Blasi et al. [2010]
Eucalyptus grandis	48.2	22.0	29.8	Pereira et al. [2013]

2.1.1.4 *Eucalyptus grandis*

Eucalyptus grandis emerges as an excellent option for biochar production due to its rapid growth and widespread cultivation, ensuring a steady supply of abundant and renewable woody biomass [Rockwood et al., 2022]. Moreover, *E. grandis* biochar has high carbon content, porosity, and surface area, which are desirable properties for soil amendment and carbon sequestration [Koçak and Ortaş, 2021].

Eucalyptus is a genus of over 700 species of flowering trees and shrubs native to Australia, New Guinea, Indonesia and nearby islands [Myburg et al., 2014]. *E grandis*, also known as flooded gum or rose gum, is one of the most widely planted eucalypts in the world [Chaín et al., 2020]. It is a fast-growing and adaptable tree that can reach heights of over 80 metres in its natural range of eastern Australia [Nakabonge and Matovu, 2021]. It is also cultivated in many other countries, especially in tropical and subtropical regions, for its valuable timber, pulpwood, charcoal, honey and essential oils. In South Africa, the expansive cultivation of the *Eucalyptus* genus spans approximately 1.3 million hectares, primarily for the purpose of pulp and paper production. These extensive *Eucalyptus* plantations make a substantial contribution to the national economy by generating employment opportunities, income, and foreign exchange earnings [Albaugh et al., 2013].

2.1.2 Selection procedure of prospective fertilising agents

Chemical fertilisers are comprised of inorganic salts containing nitrogen, phosphorus, potassium, and sulfur, as well as trace metals that are essential for promoting healthy plant growth [Appleyard et al., 2006]. Nitrogen, phosphorus, potassium were chosen as the three main fertilising compounds due to their widespread usages in agriculture. Due to the low loading requirements of sulfur and other metals, it is assumed that the biochar's inorganic content will suffice. A selection criteria was setup to determine the most suitable fertilising agents to be loaded with *E. grandis*. Four parameters were employed, namely nitrogen, phosphorous, and potassium weight fractions, price per kilogram, thermal stability, and compound toxicity.

2.1.2.1 Mass fraction of fertilising agents

To determine the mass fractions of nitrogen, phosphorous, and potassium in a compound, the basis of one mole of the compound was considered. For instance, the compound potassium nitrate (KNO_3) has one mole of potassium and one mole of nitrogen per mole of the compound. The molecular mass of each element was then utilised to

establish the mass of each element per mole of the compound. Subsequently, the resulting mass was divided by the molecular mass of the compound to calculate the weight fraction of nitrogen, phosphorous, and potassium, respectively. Equation 2.1 depicts this mathematically.

$$\omega_i = \frac{n_i M_i}{M_{\text{compound}}} \tag{2.1}$$

In the given equation, i represents nitrogen, phosphorous, or potassium. ω_i denotes the mass fraction of element i, M_i represents the molecular mass of element i and M_{compound} represents the evaluated molecular mass of the compound. The mass fractions of nitrogen, phosphorous, and potassium were combined to yield a mass fraction factor denoted as f_1 (Equation 2.2). This approach prioritizes the evaluation of compounds with higher levels of the three primary nutrients.

$$0.0 \leq f_1 = \omega_{\text{N}} + \omega_{\text{P}} + \omega_{\text{K}} \leq 1.0 \tag{2.2}$$

2.1.2.2 Chemical cost

To factor in the cost of the chemical, f_2, the cost per kilogram was standardised by comparing it to the most expensive chemical available. If a compound's cost was significantly larger than the average, it was omitted from the analysis as it led to inconclusive findings. The prices of all compounds were obtained from Merck, based on the lowest product grade offered. Equation 2.3 was utilised to derive the cost factor.

$$f_2 = \frac{C_i}{C_{\text{max}}} \tag{2.3}$$

where C_i represents the cost per kilogram of the compound being assessed, while C_{max} represents the cost per kilogram of the most expensive chemical being evaluated. This resulted in more expensive chemicals being penalised in the final selection.

2.1.2.3 Thermal stability

To prevent hazardous situations during pyrolysis, thermal stability is a critical consideration. Fischer Scientific's safety data sheets from 2008 were used to assess thermal stability. Each compound was given a rating, f_{R}, between 1 and 3, with 1 indicating that the compound is an explosive or a strong oxidiser, 2 indicating that it decomposes at

high temperatures, and 3 indicating that it is the most thermally stable. In the absence of any data for a compound, a thermal stability factor of zero was assigned. To obtain a value between 0 and 1, the assigned value was divided by 3 to calculate the thermal stability factor. To ensure that the selected chemicals were suitable for pyrolysis, a quantitative measure was included in addition to the qualitative thermal stability factor. The decomposition temperature was used for this purpose and was standardised against the highest decomposition temperature. To derive an overall thermal stability factor, f_3, the two thermal stability factors were combined.This mathematical calculation is depicted in 2.4.

$$f_3 = \frac{T_{\text{decomp},i}}{T_{\text{decomp,max}}} + f_{\text{R}} \tag{2.4}$$

2.1.2.4 Toxicity

To assess toxicity, the non-human oral rat toxicity (mg kg^{-1} body weight) data was gathered from PubChem. The toxicity factor, f_4, was calculated by dividing the toxicity value by the maximum toxicity value present in the dataset, thus imposing a penalty on smaller values. When non-human toxicity data was not available, a toxicity factor value of zero was assigned to the compound.

2.1.2.5 Prospective fertilising agents analysed

The selection of the most appropriate compounds was determined by adding the four factors together to obtain a suitability factor, F. In total , 79 potential fertilsing agents were analysed. The selection procedure was setup in such a manner that the final three compounds will represent each one of the major fertilising agents, namely nitrogen, phosphorus, potassium.

$$F = f_1 + f_2 + f_3 + f_4 \tag{2.5}$$

Table 2.2 depicts the the three highest scoring chemicals. Potassium carbonate (K_2CO_3), tripotassium phosphate (K_3PO_4) and calcium nitrate tertahydrate [$Ca(NO_3)_2{\cdot}4H_2O$] was chosen to reprensent potassium (K), phosphorus (P) and nitrogen (N), respectively. The extensive list of chemical compounds examined can be viewed in Appendix A.

TABLE 2.2: Criteria scoring card for chosen fertilising agents.

Compound	f_1	Cost (R kg^{-1})	f_2	$T_{Decomposition}$ (°C)	f_3	f_4	F
K_2CO_3	0.70	1167	0.98	891	1.53	0.11	3.19
K_3PO_4	0.57	1473	0.97	1380	1.83	0.12	3.62
$Ca(NO_3)_2$	0.17	1926	0.98	500	0.88	0.02	2.04

Now that the most suitable prospective fertilising agents have been chosen based on a comprehensive selection procedure, it is crucial to assess their properties through thermogravimetic analysis (TGA). TGA is a technique used to investigate the thermal stability and decomposition characteristics of substances. By subjecting the selected compounds to TGA, we can gain valuable insights into their behavior under different temperature conditions, which will further inform their efficacy as fertilising agents.

2.1.3 Sample preparation

E. grandis, in the form of sawdust with a particle size distribution of less than 90 µm and a moisture content of 7.1 %, underwent a drying process in an oven set at 105 °C for 24 hours. The chemicals used in the experiment, namely potassium carbonate (K_2CO_3), calcium nitrate tetrahydrate ($Ca[NO_3]_2 \cdot 4H_2O$), and tripotassium phosphate (K_3PO_4), were procured from Merck & Co., Inc. Two methods were utilised to introduce the fertilising agents to the biomass.

2.1.3.1 Heterogeneous mixing approach

Initially, each fertilising agent was added to the biomass in 1 wt.%, 2 wt.%, 5 wt.% and 10 wt.% concentrations. The mixture was then amalgamated with a mortar and pestle for 5 minutes. Processed samples were stored in a desiccator prior to TGA runs to avoid atmospheric moisture from interfering with the results.

2.1.3.2 Pseudo-homogenous mixing approach

Solutions of K_2CO_3, $Ca(NO_3)_2{\cdot}4H_2O$ and K_3PO_4 were prepared in 250 mL volumetric flasks with deionised water. The biomass samples were mixed with fertiliser agents in mass percentages of around 1 %, 2 %, 5 %, and 10 %, 20 % and 50 %, using 5 mL volumes of the solutions that were prepared.

2.1.4 Ashing

Ashing is a process of burning organic matter at high temperatures to remove all combustible elements and leave behind only inorganic residue [Harris and Marshall, 2017]. The analysis of biomass samples using a TGA requires consideration of the ash content due to its influence on the thermal behavior and kinetics of biomass pyrolysis [Skreiberg et al., 2011]. Furthermore, the ash content also influences the yield and quality of the products obtained from biomass conversion processes Carrier et al. [2011].

Table 2.3 shows the final ash contents of K_2CO_3, $Ca(NO_3)_2{\cdot}4H_2O$ and K_3PO_4, which were determined by subjecting the processed samples to ashing in a muffle furnace for 24 hours at a temperature of 825 °C. The neat biomass also underwent the same ashing procedure and had an ash content of 0.705 % (± 0.025 %).

TABLE 2.3: Ash contents of processed samples.

Target	K_2CO_3	K_3PO_4	$Ca(NO_3)_2{\cdot}4H_2O$
1 %	1.69 %	1.74 %	2.72 %
2 %	2.55 %	2.65 %	2.81 %
5 %	5.43 %	5.64 %	3.11 %
10 %	10.2 %	10.5 %	3.67 %
20 %	19.4 %	20.5 %	4.68 %
50 %	48.3 %	48.8 %	7.92 %

2.1.5 Thermogravimetric analysis

Thermogravimetric analysis (TGA) is a technique used to study the thermal stability and thermal decomposition mechanism of compounds. It can provide thermodynamic data and kinetic parameters of the decomposition process [Zeller et al., 2023]. TGA involves the measurement of the rate at which mass is lost as a function of temperature. The yield of the pyrolysis products can be calculated from the mass loss rate [Quan et al., 2016]. By utilising the dTG (Differential Thermogravimetric) data obtained from TGA, it becomes feasible to predict the locations of peaks and regions with the highest mass loss in relation to temperature. This allows for a deeper understanding of the thermal behavior and decomposition patterns exhibited by the analysed sample [El-Sayed et al., 2023].

The TGA analysis was conducted utilising a Hitachi STA7300 horizontal-beam TGA-DTA system, employing alumina crucibles measuring 5 mm in height and 6 mm in outer diameter. A consistent flow of nitrogen gas was maintained at a volumetric rate

of 80 mL min^{-1}. Each sample, weighing 5.5 mg ± 0.5 mg, underwent preheating to 30 °C, followed by a controlled heating rate of 5 °C min^{-1} (unless stipulated overwise) until reaching a constant temperature of 750 °C, which was maintained throughout the analysis process. These specific parameters and equipment ensured accurate and standardised measurements during the TGA experiments.

2.1.6 Elemental analysis and bomb calorimetry

Elemental analysis was conducted on a Elementar Unicube® organic elemental analyser with direct temperature programmed desorption (direct TPD) and thermal conductivity detector (TCD), using the CHNS mode. Argon gas (≥ 99.999 %) at 1.20 bar – 2.25 bar was used at a flowrate of 200 mL min^{-1} (± 20 mL) as a purge and sweeping gas. Oxygen (≥ 99.999 %) at 2 bar and a flowrate of 25 – 35 mL min^{-1} was used during combustion dosing. The reduction and combustion tube temperatures were set to 850 °C and 1150 °C, respectively. Samples were weighed into tin foil using a microbalance and tightly sealed. Two initial runs were performed with oxygen as the dosing gas, followed by one run with an empty tin sample in oxygen and another run without oxygen. Calibration substances (acitanilide and sulfanilamide standards) were used to correct for drift. The samples were analysed by flushing them with argon and introducing them into the combustion chamber. Combustion gases were swept through the tubes using argon as the sweep gas, and the resulting products were adsorbed onto the TPD column. Selective desorption occurred at preset temperatures, and the gases were analysed for nitrogen, carbon dioxide, water, and sulfur dioxide using TCD.

The bomb calorimetry was conducted on a Parr 6200 bomb calorimeter and a Parr 6510 water handling system pressurised using a 1104B 240 mL high-strength steel bomb. Tests were carried out in a 3.0 MPa oxygen atmosphere. Approximately 500 mg – 1000 mg of samples were weighted out into a platinum pan and ignited using an electrically heated 30-gauge nichrome wire. The cooling bath was maintained at a temperature close to 25 °C. The biochar was produced in a rotary kiln reactor at the University of Pretoria. The neat *E. grandis* was subjected to a pyrolysis temperature of 450 °C, with a residence time of approximately 900 s.

Five instances of neat *E. grandis* samples were subjected to analysis, alongside three instances of *E. grandis* biochar, in order to achieve consistent elemental analysis outcomes. The mean values were subsequently derived and reported in Table 2.4. Bomb calorimetry was conducted three times for both the pure sample and the biochar sample, and the resulting average values were employed. The higher heating value, $\Delta_c h^\circ_{\mathrm{HHV}}$

was computed by utilising the elemental analysis data obtained from the sample. The model relation used is Merckel et al. [2019]

$$\Delta_c h^\circ_{\mathrm{HHV}} = -13.869(1.00v_{\mathrm{C}} + 0.25v_{\mathrm{H}} - 0.50v_{\mathrm{O}}) \times \frac{M_{\mathrm{O_2}}}{M_{\mathrm{feed}}} \tag{2.6}$$

Table 2.4 depicts the results of the elemental analysis and bomb calorimetry.

TABLE 2.4: Elemental analysis of *E. grandis* on a dry ash-free basis.

Elemental analysis	*E. grandis* neat	*E. grandis* biochar
C	44.94	73.92
H	5.62	2.49
N	0.17	0.48
S	0.19	0.23
O[a]	49.08	22.88
H:C (mol_H mol_C^{-1})	1.49	0.40
O:C (mol_O mol_C^{-1})	0.83	0.23
HHV (MJ kg^{-1}, Equation 2.6)	-15.9	-27.1
HHV (MJ kg^{-1}, bomb calorimetry)	-16.9	-27.0

[a]O(wt.%) = 100-C-H-N-S on a DAF basis

Elemental analysis was conducted on a dry-ash free (DAF) basis. The moisture content (7.100 %) and ash content (0.705 %) were entered into the Elementar Unicube®'s program. It was then subsequently subtracted from the elemental analysis to produce a DAF elemental composition.

The formula proposed by Merckel et al. [2019] provides an accurate estimation of the higher heating value indicated by the bomb calorimetry. The pyrolysis of *E. grandis* resulted in a 59.8 % increase in the overall higher heating value.

2.1.7 Energy balance implications

The primary role of the fertilising agents, other than supplying the required nutrients to the biochar, is to function as an catalyst. A catalyst is a compound that reduces the activation energy of a chemical reaction, thereby accelerating the reaction rate. Catalysts achieve this by offering an alternative reaction pathway with a lower energy barrier, allowing reactant molecules to more easily overcome the activation energy and proceed to the product state [Roduner, 2014]. Dupont et al. [2014] examined the heat

capacity of various biomass types under conditions resembling those found in industrial reactors, with the intention of utilising this data in thermal conversion models. As expected, the heat capacities indicated a linear increase between 40 °C and 80 °C. Since the pyrolytic onset temperature of woody biomass is typically greater than 250 °C, the data gathered for short rotation forestry (SRF) eucalyptus was extrapolated to correspond to the pyrolytic ignition temperature. The following linear correlation for heat capacity, C_p (kJ kg^{-1} K^{-1}), was found using the data provide by Dupont et al. [2014] for SRF eucalyptus:

$$C_{p,\text{ biomass}} = 0.005T_{\text{onset}} - 0.2113 \tag{2.7}$$

To assess energy savings and the influence of the fertilising agents, the enthalpy of reaction, $\Delta H_{\text{r}}^{\circ}$, and the enthalpy required to reach the pyrolytic onset temperature, ΔH_{Cp} was summated. The resulting calculation, Equation 2.9 (MJ kg^{-1}), was compared to the base case of neat biomass and an energy saving was calculated which is depicted in Equation 2.8. The heat capacity of each of the fertilising agents were obtained from Green and Perry [2008] at their representative temperatures. The enthaply of reaction of eucalyptus pyrolysis is a complex topic that requires detailed analysis. The pyrolysis process of eucalyptus involves three stages: dehydration, decomposition of organic matter, and the breakdown of oxalate, lignin, and other constituents [Fu et al., 2020]. As a result, an conservative estimate of $\Delta \text{H}_{\text{r}}^{\circ} = 1.2$ MJ kg^{-1} [Swart, 2012] was used for all the cases in this study.

$$\text{Energy saving} = \frac{\Delta H_i}{\Delta H_{\text{neat biomass}}} \tag{2.8}$$

and

$$\Delta H_i = \Delta H_{\text{r}}^{\circ} + C_p \Delta T \tag{2.9}$$

where,

$$C_p = \omega_{\text{biomass}} C_{p,\text{ biomass}} + \omega_i C_{p,i} \tag{2.10}$$

with ω_{biomass} the mass fraction of biomass, ω_{i} the loading fraction of fertilising agent and $\text{C}_{\text{p, i}}$ the heat capacity of the specific fertilising agent.

2.2 Results and discussion

2.2.1 Neat biomass

The TGA-dTG analysis of the neat biomass (Figure 2.3) is important to establish an unadulterated baseline characterisation of its intrinsic thermal behavior. The neat assessment creates an inherent thermal stability benchmark to which the fertlised-catalised biochar can be compared to. This comparative approach is instrumental in uncovering the impact of fertilising agents on the pyrolytic onset temperature of the biomass. The TGA data indicates a 23.6 wt.% mass loss with three distinctive dTG peaks. An initial peak at approximately 44.0 °C signifies the evaporation of moisture content inherent to the biomass. Followed by a peak at 261 °C, corresponding to the degradation of hemicellulose, one of the major components of plant cell walls. The thermal decomposition of hemicellulose results in the release of volatile organic compounds and the formation of char. At around 325 °C, two convoluted peaks are observed, associated with the degradation of cellulose and lignin, which are the primary structural components of biomass. The cellulose-lignin complex begins to break down, leading to further release of gases and the formation of biochar, resulting in the maximum dTG weight loss.

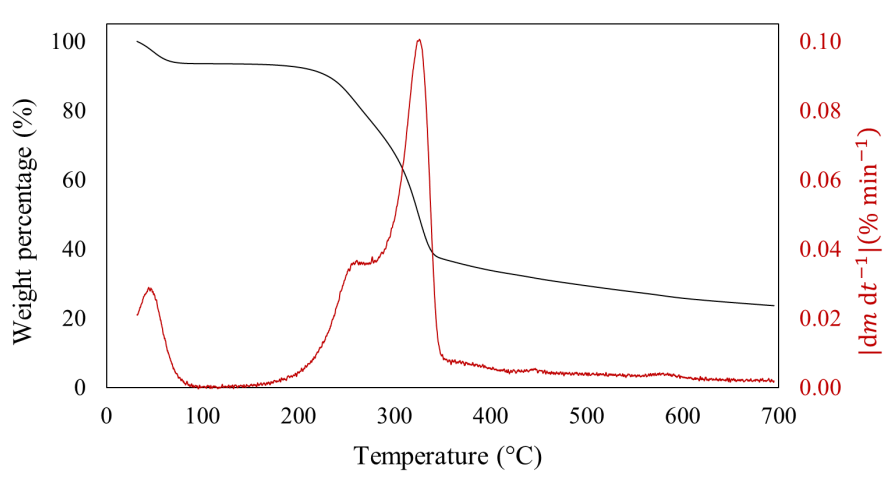

FIGURE 2.3: TG and dTG analysis for neat biomass.

2.2.1.1 Effect of heating rate on the pyrolytic onset temperature

The effect of the heating rate was examined for the neat biomass at 5 °C min^{-1}, 10 °C min^{-1}, 15 °C min^{-1} and 20 °C min^{-1}, respectively. As observed by Parthasarathy et al. [2023] and El-Sayed and Mostafa [2015], the heating rate had negligible impact on the thermal decomposition mechanism of biomass. The results of the TGA and dTGA at different heating rates are illustrated in Figure 2.4 and Figure 2.5, respectively.

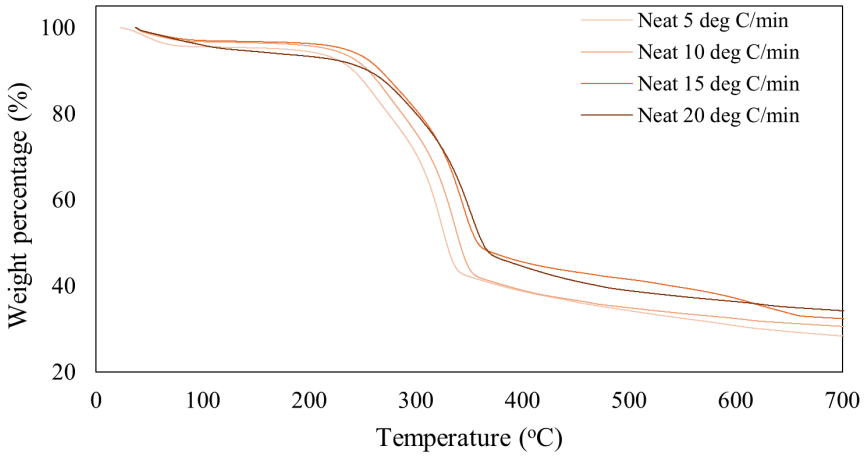

FIGURE 2.4: TGA result of different heating rates on *E. grandis*.

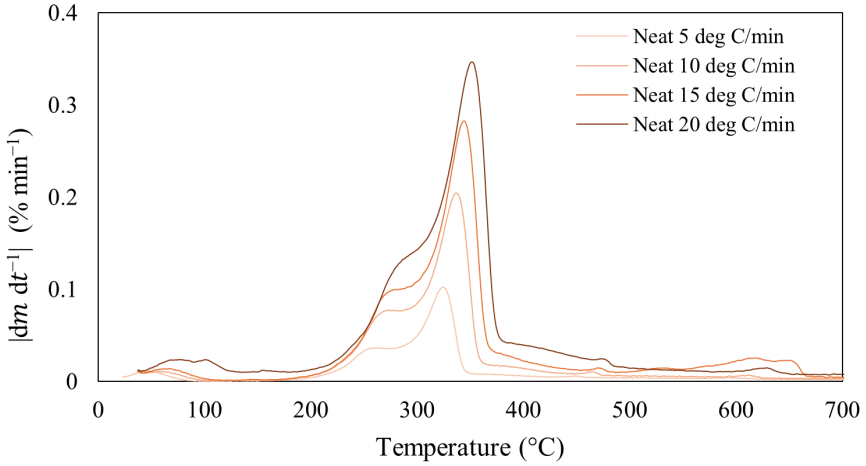

FIGURE 2.5: dTG result of different heating rates on *E. grandis*.

It was observed that an increase in heating rate resulted in a shift of the pyrolytic onset temperature, the inflection point and final mass content to higher temperatures. This shift can be attributed to fluctuations in heat transfer rates, which impact temperature differentials, gradients, and thermal lag between the outer layer and interior of the material as the heating rate is increased from 5 °C min^{-1} to 20 °C min^{-1}.

2.2.2 Neat fertilising agents

It is also important to establish The TGA-dTG analysis of the individual fertilizing agents, namely K_2CO_3, K_3PO_4, and $Ca(NO_3)_2{\cdot}4H_2O$, plays a crucial role in establishing a foundational understanding of their inherent thermal behaviors. Much like the neat biomass analysis discussed previously, this examination of the pure fertilizing agents serves as a important baseline. It is worth noting that despite the significance of this

comparative analysis, a notable gap exists in the existing literature. A thorough search revealed a lack of available TGA data for these specific fertilising agents, with only Victor et al. [2016] and Lehman et al. [1998] having done TG analysis on K_2CO_3 and ,Zhao et al. [2022] on $Ca(NO_3)_2)\cdot 4H_2O$, under an inert environment.

2.2.2.1 TG analysis on K_2CO_3

The TGA-dTG results correlate with that found by Victor et al. [2016] and Lehman et al. [1998]. An initial peak at approximately 76 °C is observed which results in a weight loss of 3 wt.%. This is mainly due to moisture absorbed by the fertilising agent. The initial peak is followed by a state of thermal stability, with the total mass loss for the sample being 3.8 wt.%. Lehman et al. [1998] studied the thermal stability of K_2CO_3 near the melting point and found that the melting point of K_2CO_3 is around 900 °C in N_2.

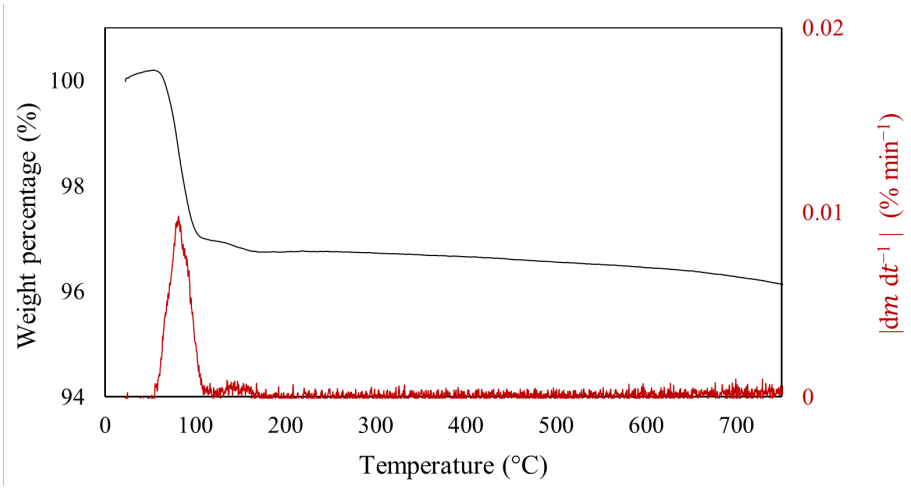

FIGURE 2.6: TG and dTG analysis of K_2CO_3.

2.2.2.2 TG analysis on K_3PO_4

As noted earlier, there is a lack of TGA data for K_3PO_4 in the existing literature. Once again, an initial peak is detectable around ± 85 °C, attributable to the evaporation of moisture, which leads to a reduction in mass by 0.7 wt.%. A subsequent peak becomes apparent at 152 °C, causing the most substantial mass loss at 1.9 wt.%. Lastly, the third peak is observed at approximately 251 °C, contributing to a mass loss of 0.6 wt.%, thereby resulting in a cumulative total mass loss of 3.2 wt.%.

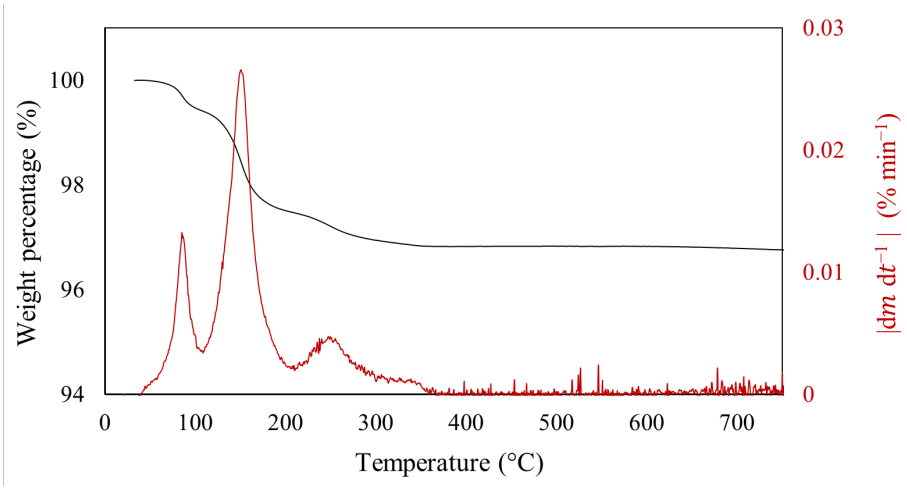

FIGURE 2.7: TG and dTG analysis of K_3PO_4.

The most common hydrated crystalline structure of tripotassium phosphate is $K_3PO_4 \cdot H_2O$. Therefore, the dehydration reaction will proceed as follows:

$$K_3PO_4 \cdot H_2O \rightarrow K_3PO_4 + H_2O \tag{2.11}$$

Doing a mass balance for this reaction, the weight loss is 7.8 wt.%, compared to the 0.7 wt.% observed in Figure 2.7. To explore if the sample necessitates more time to attain the calculated 7.8 wt.% mass loss, the neat K_3PO_4 sample was analysed again at a lower heating rate of 5 °C min^{-1}.

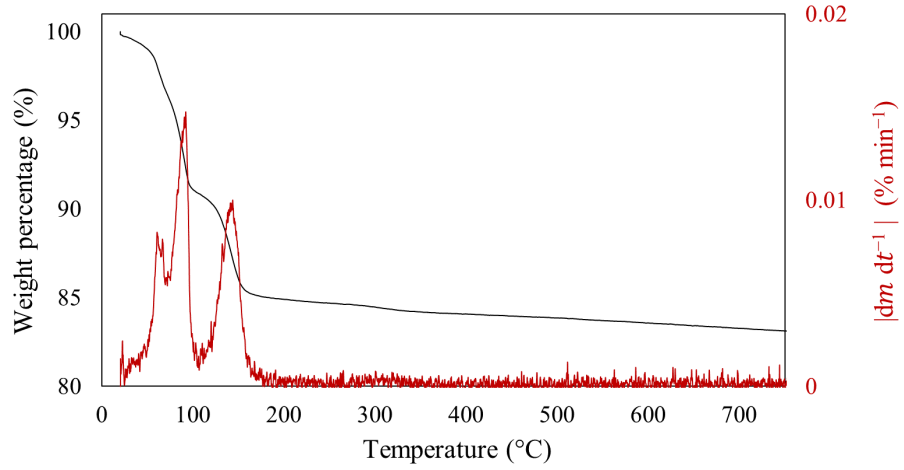

FIGURE 2.8: TG and dTG analysis of K_3PO_4 with 5 °C min^{-1} heating rate.

Figure 2.8 indicated a mass loss of 8.9 wt.% at the end of the initial two peaks (104 °C). Another peak is observed at 153 °C and 147 °C for Figure 2.7 and Figure 2.8, respectively. Figure 2.7 also indicates a smaller peak at 251 °C, which becomes convoluted in Figure

2.8. In the absence of literature data, it is conceivable that the following reaction occurs at 147 °C:

$$K_3PO_4 \rightarrow K_3PO_3 + O_2 \tag{2.12}$$

This reaction will result in a further theoretical mass loss of 6.9 wt.%, bringing the total mass loss to 85.2 wt.%, which aligns with the total mass loss of 84.7 wt.% observed in Figure 2.8.

2.2.2.3 TG analysis on $Ca(NO_3)_2{\cdot}4H_2O$

Zhao et al. [2022] investigated the thermal decomposition of $Ca(NO_3)_2{\cdot}\ 4H_2O$ by subjecting samples to TG/DSC-FTIR. This was accomplished by heating samples from 30 °C to 700 °C at 10 °C min^{-1} under a N_2 flow of 100 ml min^{-1}. The data produced in Figure 2.9 coincides with that observed by Zhao et al. [2022]. The process of water decomposition occurs within the temperature range of 50 °C to 220 °C, leading to a mass reduction of 30.2 wt.%, which is notable considering that the crystalline structure of N_2 flow of 100 ml min^{-1} contains 30.5 wt.% water. Subsequently, a distinct peak emerges between 550 °C and 600 °C. This second peak follows a reaction pathway that results in the liberation of NO, NO_2, and O_2, while simultaneously forming solid CaO. This series of reactions has been documented by Zhao et al. [2022]:

$$Ca(NO_3)_2(l) \rightarrow CaO(s) + 2NO(g) + 1.5O_2(g) \tag{2.13}$$

$$Ca(NO_3)_2(l) \rightarrow CaO(s) + 2NO_2(g) + 0.5O_2(g) \tag{2.14}$$

$$Ca(NO_3)_2(l) \rightarrow CaO(s) + NO(g) + NO_2(g) + O_2(g) \tag{2.15}$$

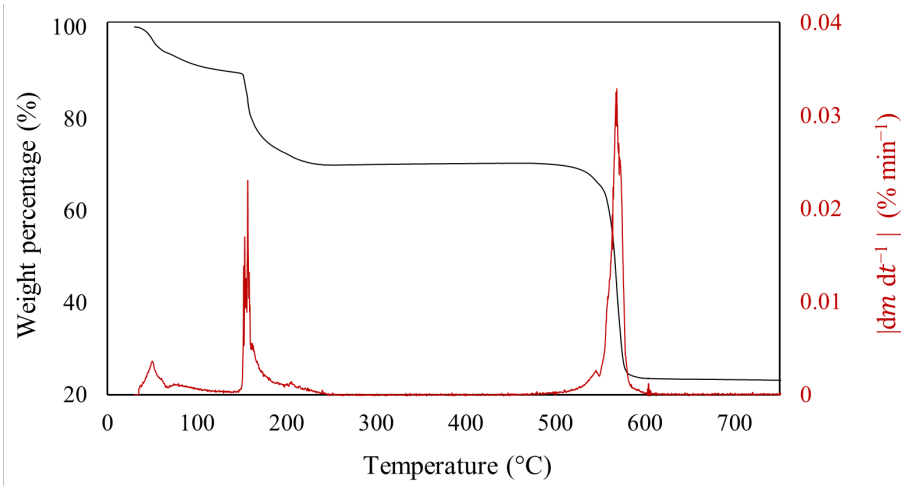

FIGURE 2.9: TG and dTG analysis of $Ca(NO_3)_2 \cdot 4H_2O$.

2.2.3 Heterogeneous mixing approach

The data obtained through the heterogeneous mixing approach exhibited a level of unreliability due to the detection of minor shifts in peak intensities at concentrations of 1 wt.%, 2 wt.%, and 5 wt.%. In contrast, a significantly more pronounced catalytic suppression of the pyrolytic temperature was observed at the 10 wt.% concentration level, as depicted in Figure 2.10. This outcome potentially stems from inadequate mixing between the fertilizing agents and biomass components. Nevertheless, these findings indicate the feasibility of achieving some degree of catalytic temperature suppression through improvements in the mixing procedure.

In response to these observations, an alternative technique for incorporating fertilizer agents was devised, employing the pseudo-homogeneous mixing approach. This method involves introducing fertilizer agents to the biomass in a solute state, aiming to achieve a more uniform distribution.

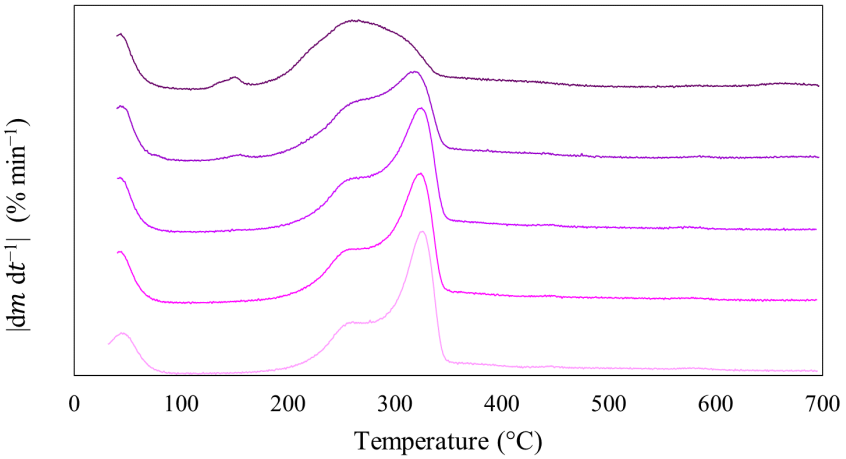

FIGURE 2.10: dTG data for heterogeneous mixing approach.

2.2.4 Pseudo-homogeneous mixing approach

2.2.4.1 Catalytic effect of K_2CO_3

As indicated in Figure 2.6, K_2CO_3 indicated thermal stability after the initial mass loss of free moisture. This indicates that any peak alteration of the neat biomass would indicate a catalytic effect. Figure 2.11 depicts the TG data of *E. grandis* neat, and loaded with 1 wt.%, 2 wt.%, 5 wt.%, 10 wt.%, 20 wt.% and 50 wt.% K_2CO_3, respectively. The mass loss clearly decreased with an increase in K_2CO_3 loading, which is expected, as K_2CO_3 only had a 3.8 wt.% mass loss.

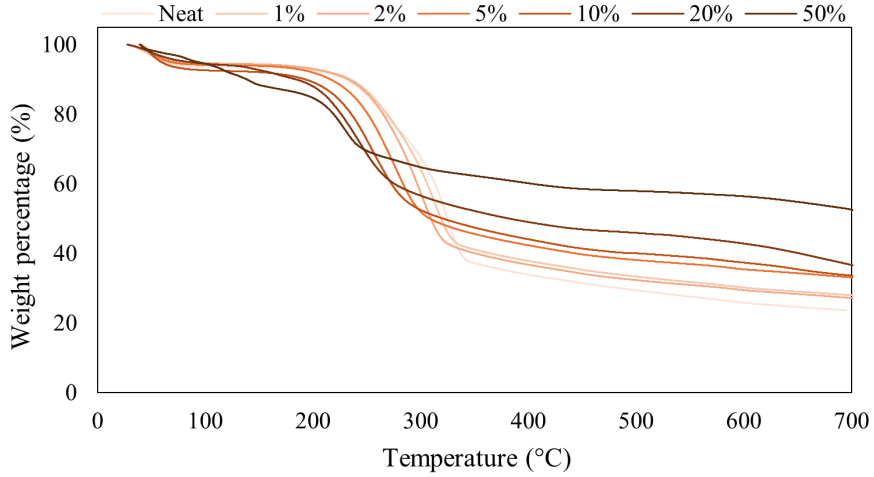

FIGURE 2.11: TG analysis for Eucalyptus grandis pre-loaded with K_2CO_3.

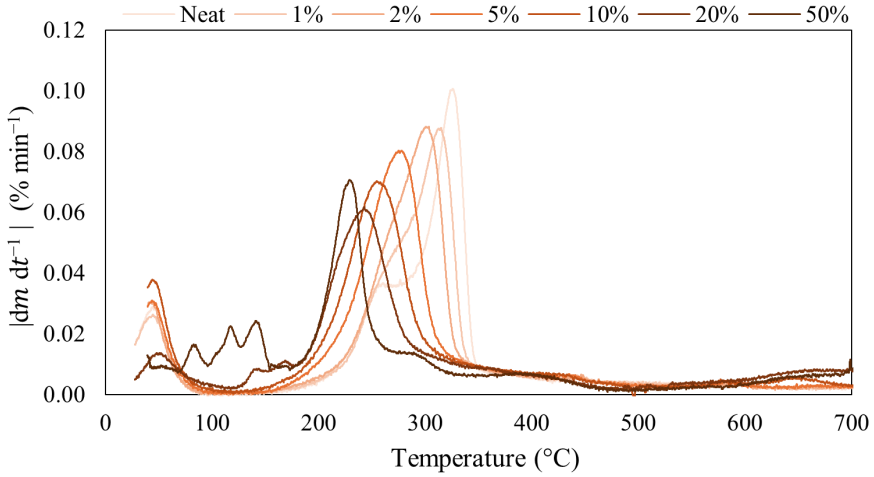

FIGURE 2.12: dTG analysis for Eucalyptus grandis pre-loaded with K_2CO_3.

The dTG data, illustrated in Figure 2.12, indicates a significant suppression of the pyrolytic onset temperature. Peaks around 100 °C is observed at concentrations of 20 wt.% and 50 wt.%, which can be attributed to the moisture contained in K_2CO_3. Table 2.5 displays the final mass, pyrolytic onset temperature and the temperature suppression observed. With a fertiliser loading of 50 wt.%, a temperature suppression of 97 °C is observed.

TABLE 2.5: Catalytic suppression of the pyrolytic onset temperature using K_2CO_3.

Fertiliser loading	Final mass (wt.%)	$T_{Pyrolytic\ onset}$ (°C)	$\Delta T_{suppression}$ (°C)
Neat	24	326	0
1 wt.%	27	315	-11
2 wt.%	26	301	-25
5 wt.%	32	278	-48
10 wt.%	33	254	-71
20 wt.%	37	243	-83
50 wt.%	48	229	-97

2.2.4.2 Catalytic effect of K_3PO_4

As previously mentioned, K_3PO_4 depicted three distinctive peaks between 85 °C and 251 °C, where the first peak is attributed to the evaporation of moisture. Although three peaks are observed, the mass loss of K_3PO_4 is minuscule, with only 3.2 wt.% total mass loss.

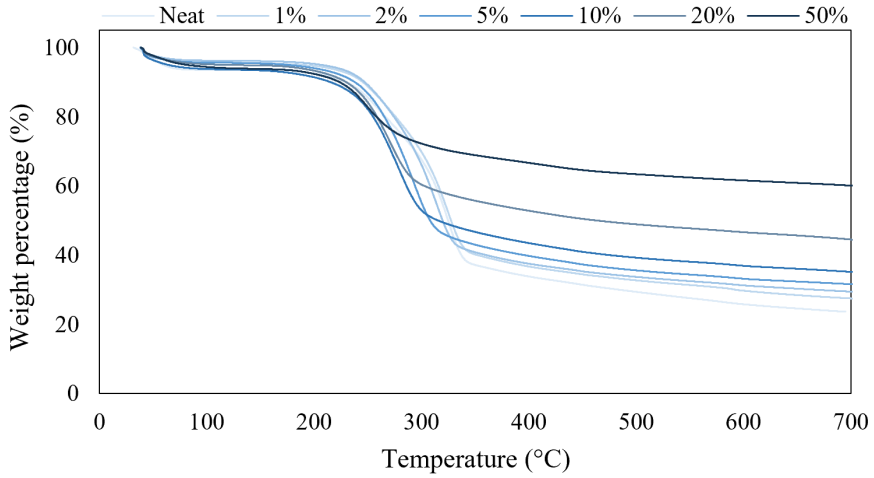

FIGURE 2.13: TG analysis for Eucalyptus grandis pre-loaded with K_3PO_4.

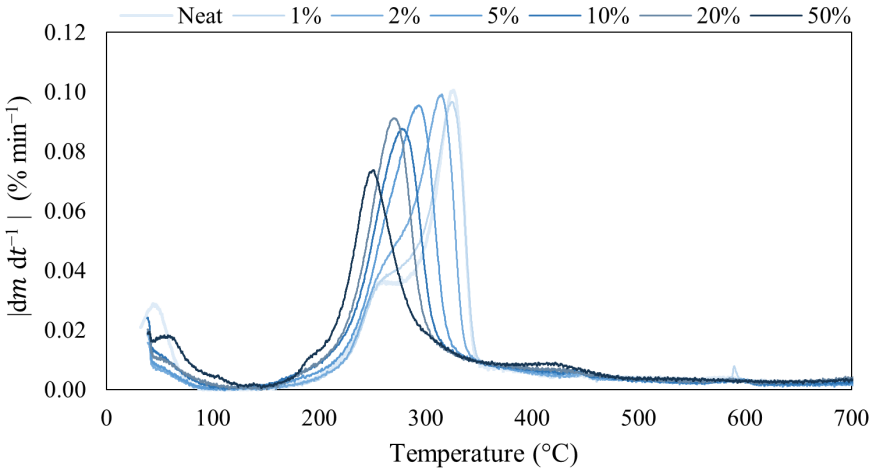

FIGURE 2.14: dTG analysis for Eucalyptus grandis pre-loaded with K_3PO_4.

As with K_2CO_3, a noteworthy suppression of the pyrolytic onset temperature is observed for K_3PO_4. The increase of fertiliser loading convoluted the cellulose, hemicellulose and lignin peaks even further, with 50 wt.% loading seemingly only having one peak. The inflection points of Figure 2.14 shifts dramatically to lower temperatures with an increase in K_3PO_4 loading. Table 2.6 illustrates the char and inoragnic content as well as the pyrolytic ignition temperature and the suppression of the onset temperature.

TABLE 2.6: Catalytic suppression of the pyrolytic onset temperature using K_3PO_4.

Fertliser loading	Final mass (wt.%)	$T_{Pyrolytic\ onset}$ (°C)	$\Delta T_{suppression}$ (°C)
Neat	24	326	0
1 wt.%	27	324	-2
2 wt.%	29	315	-20
5 wt.%	31	293	-33
10 wt.%	34	277	-49
20 wt.%	43	271	-55
50 wt.%	59	251	-75

2.2.5 Catalytic effect of $Ca(NO_3)_2{\cdot}4H_2O$

The addition of $Ca(NO_3)_2{\cdot}4H_2O$ did not result in the desired suppression of the pyrolytic onset temperature for 1 wt.% to 20 wt.% loading. Interestingly, an observable shift to the left in the inflection peak was noted for 50 wt.% loading. However, this shift can be primarily attributed to the relatively high loading of $Ca(NO_3)_2{\cdot}4H_2O$, as evident from Figure2.9, where an inflection peak is observed at approximately 170 °C.

Furthermore, it is noteworthy that both peaks that where observed in Figure 2.9 seems to have shifted about 100 °C to higher temperatures. This intriguing observation could be attributed to various factors, including thermal delays and the complex kinetics of the reaction involved in loading biomass with $Ca(NO_3)_2{\cdot}4H_2O$.

It also appears that the two peaks associated with hemicellulose and cellulose-lignin degradation convoluted with the initial peak of $Ca(NO_3)_2{\cdot}4H_2O$ decomposition. This convolution of peaks further highlights the intricate interplay of reactions occurring during the pyrolysis of biomass loaded $Ca(NO_3)_2{\cdot}4H_2O$ and emphasizes the need for a more comprehensive understanding of the underlying mechanisms at play. The TG and dTG data is depicted in Figure 2.15 and Figure 2.16, respectively.

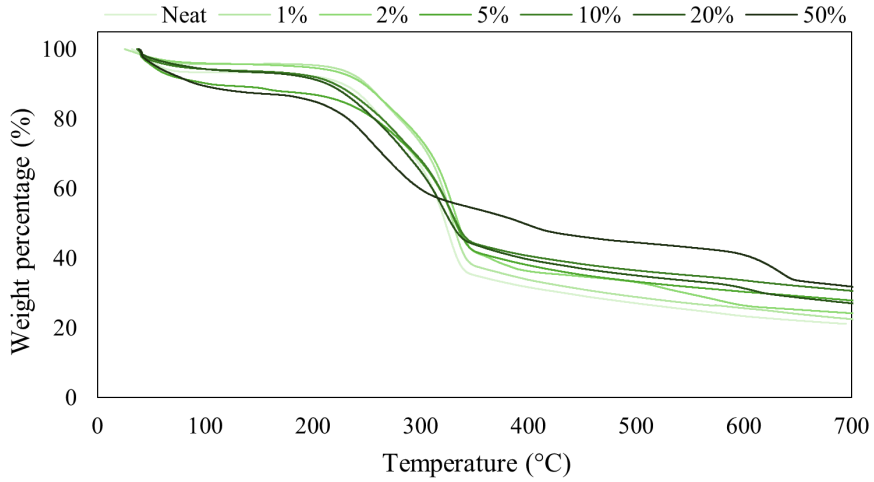

FIGURE 2.15: TG analysis for Eucalyptus grandis pre-loaded with $Ca(NO_3)_2{\cdot}4H_2O$.

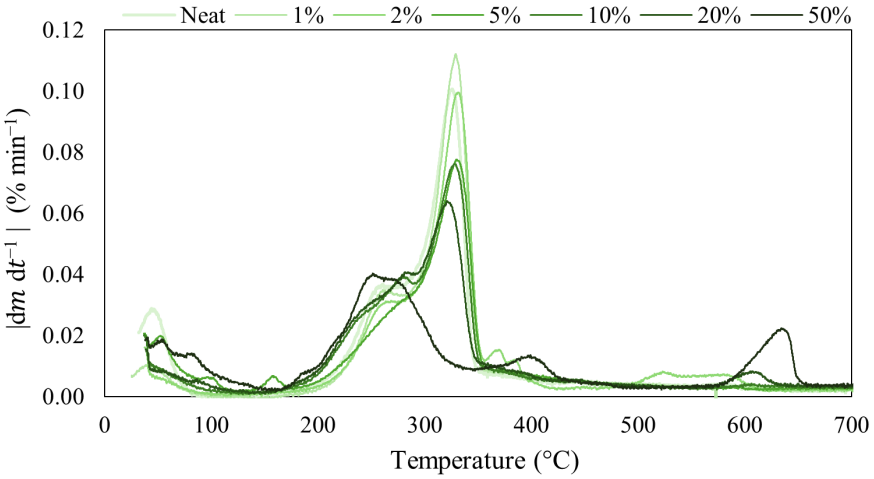

FIGURE 2.16: dTG analysis for Eucalyptus grandis pre-loaded with $Ca(NO_3)_2{\cdot}4H_2O$.

2.2.6 Suppression of pyrolytic onset temperature

It is clear that K_2CO_3 and K_3PO_4 successfully lowered the pyrolytic onset temperature, whereas reduction in temperature caused by $Ca(NO_3)_2{\cdot}4H_2O$ loading is negligible. The TGA data offers insights into the ash content of the samples. As depicted in Figures 2.11 and 2.13, it is evident that an increase in the amount of fertiliser results in a higher ash content, consequently leading to a greater final mass, as anticipated. However, this trend is not as noticable when examining $Ca(NO_3)_2{\cdot}4H_2O$ (Figure 2.15). This discrepancy may suggest a transformation or degradation of the compound in question and a potential deactivation of catalytic properties prior to the pyrolysis process. To estimate the maximum temperature suppression, a non-linear regression model was employed, as

illustrated in Equation 2.16. The model was executed within Anaconda's Jupyter Notebook, utilising the Python programming language and employing the *scipy.optimize* library in conjunction with *curve˙fit*.

$$\Delta T = A + \frac{B + A}{1 + \frac{\omega_{\text{fertiliser loading}}}{C^D}} \tag{2.16}$$

This model utilised the pyrolytic ignition temperature as well as the fertiliser loading to estimate the maximum suppression of the pyrolytic onset temperature. Figure 2.17 depicts the non-linear regression model for K_2CO_3 and K_3PO_4. As $Ca(NO_3)_2{\cdot}4H_2O$ did not act as a catalyst, a simple polynomial trend line was employed.

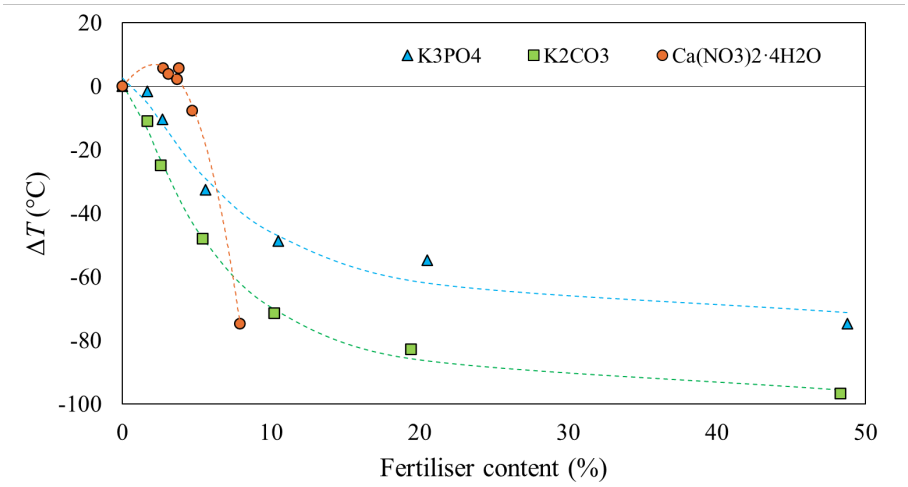

FIGURE 2.17: Modelled temperature suppression of major pyrolysis peak as a function of fertiliser content.

The maximum suppression of the pyrolytic onset temperature for K_2CO_3 and K_3PO_4 was calculated as 98 °C and 76 °C, respectively. Table 2.5 and 2.6 indicated a ignition temperature suppression of -97 °C and -75 °C for K_2CO_3 and K_3PO_4, respectively. Both experimental values were found to be only 1 °C less than the modelled values, indicating further experimental work is not required, as the 50 wt.% provided adequate temperature suppression.

K_2CO_3 and K_3PO_4 are alkaline when dissolved in deionised water, in contrast to $Ca(NO_3)_2{\cdot}4H_2O$, which remains neutral under the same conditions. This difference in behavior can be attributed to the distinct origins of these compounds.

K_2CO_3 and K_3PO_4 are the products of reactions involving a weak acid and a strong base [Kolthoff, 1944]. When these compounds dissolve in water, they release hydroxide ions (OH^-) into the solution, leading to an increase in pH and resulting in an alkaline

solution. This alkalinity results from the ability of the hydroxide ions to accept protons (H^+) from the water, making the solution more basic Kolthoff [1944].

On the other hand, $Ca(NO_3)_2{\cdot}4H_2O$ is the product of a reaction involving both a strong acid and a strong base. Consequently, when dissolved in deionised water, it neither donates nor accepts protons to a significant extent [Kolthoff, 1944]. As a result, the pH of the solution remains relatively stable, and it is classified as neutral.

Saccharides are susceptible to both acid- and alkaline-hydrolysis, therefore the addition of either acidic or alkaline solutions results in the breakdown of the saccharide molecules. Interestingly, the proximity of acetyl groups to the xylan polymer structure ensures that lysis occurs before alkaline hydrolysis takes place, as observed by [Zhang et al., 2011]. This observation provides a potential explanation for why K_2CO_3 and K_3PO_4 had an impact on the pyrolytic onset temperature of *E. grandis*, while $Ca(NO_3)_2{\cdot}4H_2O$ did not.

Furthermore, the existence of pyrolytic vapors, including water as a result of hemicellulose pyrolysis, in conjunction with alkaline compounds, may explain the observed suppression of pyrolytic temperatures compared to cellulose. This suggests that a combination of factors, including the introduction of alkaline substances, influences the thermal decomposition of cellulose.

2.2.6.1 Energy balance implications

Table 2.7 and 2.8 depicts the energy saving of the addition (Equation 2.8) of K_2CO_3 and K_3PO_4, respectively. The heat capacity, C_p, of K_2CO_3 is 0.1147 kJ kg^{-1} K^{-1} for a temperature range of 296 K – 372 K [Green and Perry, 2008] and estimated as 0.3124 kJ kg^{-1} K^{-1} for K_3PO_4 by calculating the the specific heat capacities of its individual elements and compounds.

TABLE 2.7: Energy saving observed for K_2CO_3.

Fertliser loading	ΔH_{Cp} (MJ kg^{-1})	ΔH_i (MJ kg^{-1})	Energy saving
Neat	0.43	1.63	0.0 %
1 wt.%	0.40	1.60	1.5 %
2 wt.%	0.37	1.57	3.6 %
5 wt.%	0.30	1.50	7.7 %
10 wt.%	0.24	1.44	11.2 %
20 wt.%	0.21	1.41	13.6 %
50 wt.%	0.12	1.32	18.7 %

TABLE 2.8: Energy saving observed for K_3PO_4.

Fertliser loading	ΔH_{Cp} (MJ kg^{-1})	ΔH_i (MJ kg^{-1})	Energy saving
Neat	0.43	1.63	0.0 %
1 wt.%	0.42	1.62	0.6 %
2 wt.%	0.39	1.59	2.3 %
5 wt.%	0.32	1.52	6.4 %
10 wt.%	0.27	1.47	9.4 %
20 wt.%	0.24	1.44	11.5 %
50 wt.%	0.16	1.36	16.7 %

The data presented in the tables above clearly indicate that K_2CO_3 and K_3PO_4 led to significant reductions in energy consumption. Table 2.7 illustrated that 50 wt.% K_2CO_3 loading exhibited the most substantial energy saving, amounting to 18.7 %. Furthermore, the highest K_3PO_4 loading also resulted in an impressive energy saving of 16.7 %. To determine the point at which the energy savings from different fertiliser loadings offset the associated fertliser purchasing costs, it is crucial to perform a threshold analysis. Chapter 3 introduces a techno-economical feasibility analysis, which includes factors such as optimal daily tonnage, fertiliser loading, biochar yield, NPK ratio of fertilising agents, amongst others.

2.3 Summary

Both K_2CO_3 and K_3PO_4 successfully suppressed the pyrolytic onset temperature of *E. grandis*. *E. grandis* was chosen as the biomass of choice due to it's abundance, not only in South Africa, but across the world. From 79 prospective compounds, K_2CO_3, K_3PO_4 and $Ca(NO_3)_2{\cdot}4H_2O$ were selected as fertilising agents to represent potassium (K), phosphorus (P) and nitrogen (N), respectively. $Ca(NO_3)_2{\cdot}4H_2O$ did not exhibit any catalytic effect on the biomass, although with 50 wt.% loading, the peak did shift, but this is assumed to be the convolution of the hemicellulose, cellulose-lignin and $Ca(NO_3)_2{\cdot}4H_2O$ peaks.

K_2CO_3 presented an ignition temperature suppression of -11 °C, -25 °C, -48 °C, -71 °C, -83 °C and -97 °C, for 1 wt.%, 2 wt.% , 5 wt.%, 10 wt.%, 20 wt.% and 50 wt.%, respectively, with a maximum possible suppression of -98 °C. This translated in an energy saving of 18.7 % for the 50 wt.% loading.

K_3PO_4, also indicates significant suppression of the pyrolytic onset temperature with 1 wt.%, 2 wt.% , 5 wt.%, 10 wt.%, 20 wt.% and 50 wt.% loading resulting in a suppression of -2 °C, -20 °C, -33 °C, -49 °C, -55 °C and -75 °C, respectively. The highest fertiliser loading (50 wt.%) indicated an energy saving of 16.7 %.

Chapter 3

Techno-economic feasibility analysis

Major discrepancies exist in literature whereby some authors depict biochar as a *miracle* commodity with economic opportunities [Campbell et al., 2018, Homagain et al., 2016, Keske et al., 2020, Shackley et al., 2011, Thengane et al., 2020]. This chapter investigates the economic feasibility of producing a novel, nutrient-enhanced biochar as a replacement of commercial fertiliser. The addition of fertilising agents was introduced in Chapter 2 and the effect it has on the pyrolytic onset temperature. This resulted in energy savings as eluded to in Section 2.2.6.1.

The chapter aims to optimise the selling price of the enriched biochar to make it appealing for farmers, while maintaining an internal rate of return (IRR) of 16 %, ensuring attractiveness to investors. A comprehensive techno-economic feasibility analysis was conducted, incorporating factors such as an equipment bill, fixed capital investment, working capital, production costs and discounted cash flow. Three other financial indicators were also used including the net present value (NPV), return on investment (ROI) and payback period (PP) over a 20 year lifespan.

3.1 Analysis description

The techno-economic feasibility analysis was conducted on Microsoft® Excel® for Microsoft 365 MSO (Version 2301 Build 16.0.16026.20196). This program was chosen as the initial tool for setting up the analysis. To explore and iterate through different scenarios, Anaconda's Jupyter Notebook was utilised, employing the Python coding

language. The open-core spreadsheet automation package, xlwings, was specifically employed within Jupyter Notebook to facilitate the manipulation and automation of the Excel spreadsheets. The following process variables were iterated to optimise financial indicators (Table 3.1):

- Price comparison of biochar to coal
- Daily tonnage
- Fertiliser loading
- Biochar yield
- Fertiliser agents ratio
- Selling price

As eluded to in Chapter 1, pyrolysis oil can be utilised as a energy carrier or be separated into different fractions. For this analysis, two fractions were identified; wood vinegar, an inexpensive fraction that can be used as herbicide and pesticide [Chu et al., 2022, Dewi et al., 2020] and a phenolic fraction, a high value fraction that is used as an antiseptic and plastic precursor [Chen et al., 2020]. In an attempt to make the plant as economically viable as possible, four scenarios were investigated, in addition to the sale of enriched biochar:

1. Selling electricity to the grid through the combustion of the synthesis gas and all the pyrolysis oil (both wood vinegar and phenolic fraction).
2. Selling electricity to the grid through the combustion of the synthesis gas and the wood vinegar fraction, while extracting the phenolic fraction through distillation and selling it.
3. Selling of all the pyrolysis oil as wood vinegar.
4. Extraction of phenolic fraction through distillation and selling a wood vinegar fraction and a phenolic fraction.

Even though the extraction of the phenolic fraction is a difficult process, which has not yet been industrially established, it is added as a theoretical calculation for when the technology is available.

Financial indicators such as the net present value (NPV), internal rate of return (IRR), return on investment (ROI), and payback period (PP) play a crucial role in evaluating

the economic feasibility of a chemical plant. The utilisation of these financial indicators offers investors, directors and financial managers valuable insight into the projects profitability and future financial position [Towler and Sinnott, 2021]. Both the NPV and IRR accounts for the time value of money and provide a comprehensive analysis of the potential returns of a project in the lifespan. The ROI provides insight into the possible profitability of the initial investment, helping decision-makers compare different business opportunities. Furthermore, the PP indicates how quickly the initial investment can be repayed [Towler and Sinnott, 2021]. Together, the financial indicators, described in Table 3.1, enable investors to make informed decisions on the feasibility, investment opportunity of a project. A judgement can then be formulated of the profitability of a project and if it aligns with a company's financial objectives and risk tolerance.

TABLE 3.1: Financial indicators used in the analysis.

Financial indicator	Abbreviation	Description
Net present value	NPV	Financial metric used to calculate the present value of future cash inflows and outflows, taking into account the time value of money.
Internal rate of return	IRR	Financial indicator used to calculate the discount rate that makes the net present value of future cash inflows and outflows equal to zero.
Return on investment	ROI	Financial ratio used to evaluate the profitability of an investment by dividing the net profit by the cost of the investment.
Payback period	PP	The amount of time it takes to recover the initial cost of an investment based on the expected cash inflows.

A mass and energy balance was conducted to estimate the liquid, solid and gas yield. The yields are iterated in subsequent sections, within the attainable ranges, to financially optimise the yields. Table 2.4 in Chapter 2 depicts the element analysis results of *E. grandis*. The parameters depicted in Table 3.2 were set to constant values for the entire analysis, as they cannot be changed during the process:

TABLE 3.2: Constant parameters of analysis.

Operation period per annum		
Parameter	Value	Unit
Daily operating hours	24	h day^{-1}
Operating period	92	% a^{-1}
Planned maintenance	4	% a^{-1}
Unplanned maintenance	4	% a^{-1}
Yearly inflation	6	% a^{-1}
Biomass parameters		
Parameter	Value	Unit
Neat moisture content	35.5	%
Ash content	1	%
Dried moisture content	8	%
Costing of feedstock		
Parameter	Value	Unit
E. grandis	550	R ton^{-1}
Urea	5963	R ton^{-1}
DAP	7896	R ton^{-1}
MOP	5637	R ton^{-1}
Fuel to energy: Internal combustion turbine		
Electricity selling price	2.8	R kWh^{-1}
Energy efficiency	29	%

The plant performance was set to 0 % for year one, as it is assumed that the plant will be constructed within year one. For year two, the plant performance is assumed to be 75 %, as the facility undergoes a ramp-up period, allowing operators to fine-tune and optimise processes. Thereafter, it is assumed that the process and equipment has reached maturity, therefore the plant performance is taken as 100 %. The plants lifespan is taken as 20 years for all iterations. The electricity selling price of R2.80 per kWh was attained from the National Energy Regulator of South Africa (NERSA) for agricultural use. The energy efficiency was calculated as illustrated in Equation 3.1.

$$\eta_{\text{energy}} = \frac{E_{gen}}{\text{HHV}_{\text{diesel}}} \tag{3.1}$$

E_{gen} is the energy density of diesel in kWh kg^{-1} at 65 % – 70 % loading and HHV_{diesel} is the higher heating value of diesel.

As mentioned in Chapter 2, K_2CO_3, K_3PO_4 and $Ca(NO_3)_2{\cdot}4H_2O$ were selected as fertilising agents to represent potassium (K), phosphorus (P) and nitrogen (N), respectively. As these compounds are currently utilised for niche applications, it was very difficult to attain bulk prices for them. Therefore, the bulk prices of agricultural fertilisers urea, diammonium phosphate (DAP) and muriate of potash (MOP) were used for N, P and K, respectively. Urea, the most concentrated solid nitrogen fertiliser, is commonly marketed in prilled form and is widely recognised as the most prevalent nitrogen fertiliser [Lockhart and Wiseman, 2014]. DAP is a highly soluble fertiliser and an exceptional source of phosphorus and nitrogen [Maqsood et al., 2022]. MOP is the most common from of potash and usually contains at least 60 % K_2O, making it an excellent source of potassium [Lockhart and Wiseman, 2014]. The prices illustrated in Table 3.2, were calculated as the average price over a 10-year span, between April 2012 and April 2022, as reported by Baffes and Koh [2022] for World Bank.

3.1.1 Growing *Eucalyptus*

This section delves into the intricacies of assessing the economic viability of cultivating *Eucalyptus* trees from seed, encompassing essential factors such as seedling acquisition, fertiliser and pesticide acquirement, cultivation practices like plowing, thinning, weeding, maintenance, and eventual harvesting. In total six papers [Agrifarming, 2021, Langat et al., 2015, Olivier and Rusk, 1997, Phimmavong et al., 2019, Silva et al., 2020, Sudha et al., 2007] were evaluated and compared. Langat et al. [2015], Silva et al. [2020] and Phimmavong et al. [2019] delve into detail regarding every facet of the growing process from seed. To ensure the economic analysis remains meaningful and comparable, adjustments were made to account for inflation and current-day costs, considering the studies conducted over a period of two decades. To estimate the present net value, a country-specific inflation calculator from World Data was employed to the year 2022.

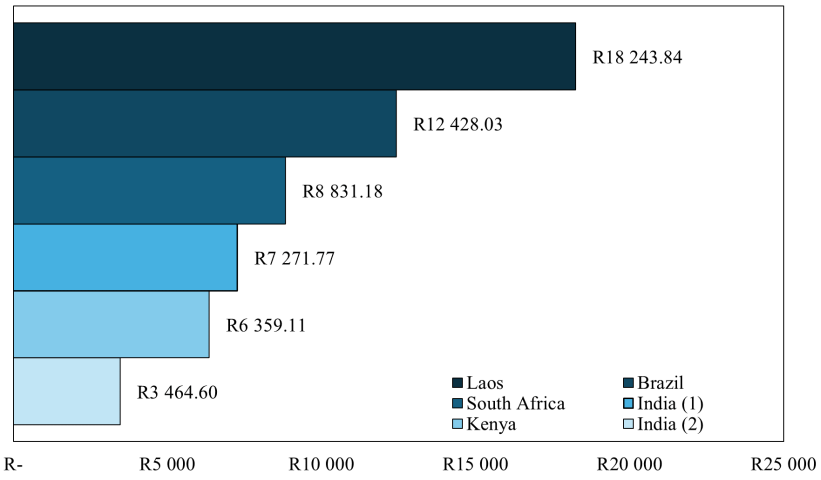

FIGURE 3.1: Total costs per hectare per year in 2022 (R ha^{-1} y^{-1}).

Silva et al. [2020] conducted an in-depth investigation into the economic viability of an *Eucalyptus* plantation for pulp production in the mesoregion of Southern Pará, Brazil. It is worth noting that Figure 3.1 does not incorporate the cost of land acquisition, as this aspect was considered solely by Silva et al. [2020], ensuring comparability across studies. Consequently, the cost of land acquisition was excluded to facilitate meaningful comparisons. Based on the data provided in the paper, the yearly cost over a span of 7 years amounts to 12 428.03 R ha^{-1} y^{-1}, resulting in a cumulative cost of 86 996.21 R ha^{-1}. This cost translates to 579.97 R ton^{-1} – 869.96 R ton^{-1} when assuming a yield of 100 ton ha^{-1} – 150 ton ha^{-1}. The study used a selling price of 50 R$ m^{-3} – 70 R$ m^{-3} and an annual intrest rate of 5 % y^{-1} – 15 % y^{-1} in their analysis with a Mean Annual Increment (MAI) of 35 m^3 ha^{-1} y^{-1} – 45 m^3 ha^{-1} y^{-1}, resulting in a production of 245 m^3 ha^{-1} – 315 m^3 ha^{-1}. Using the previously mentioned values, and assuming a yield of 100 ton ha^{-1} – 150 ton ha^{-1}, the selling price would be between 273.59 R ton^{-1} and 738.68 R ton^{-1}. An exchange rate of R$ 3.35 to the Rand was used.

Langat et al. [2015] presented a financial analysis of growing *Eucalyptus grandis* for production of medium size power transmission poles and firewood in Kenya. The financial analysis was undertaken using Net Present Value (NPV), Equal Annual Equivalent (EAE) and Internal Rate of Return (IRR) for a 10-year rotation period for medium power transmission poles and firewood production at discount rates of 8, 12 and 16 percent. As the production of transmission poles lies outside the scope of this dissertation, it will not be considered in the analysis. Based on the data provided in the paper, the annual cost over a 10-year period totals 6 359.11 R ha^{-1} y^{-1}, with a cumulative cost of 63 591.14 R ha^{-1}. When assuming a yield of 100 ton ha^{-1} – 150 ton ha^{-1}, this cost translates to 423.94 R ton^{-1} to 635.91 R ton^{-1}. The total cost and undisclosed net revenue

was calculated as R65 374.88 and R82 391.42, respectively, resulting in an IRR of 5.2 %. This puts the selling price of the *E. grandis* at 534.29 R ton^{-1} to 801.43 R ton^{-1}. The exchange rate used was KES 0.14 to the Rand.

Phimmavong et al. [2019] presented a financial analysis of three plantation models - monoculture *Eucalyptus*, rice mixed with *Eucalyptus* and cassava mixed with *Eucalyptus* in four provinces in Laos. As polyculture plantations extends further than the scope of this dissertation, only the monoculture *Eucalyptus* was considered. A overall cost of 104 752 R ha^{-1} was calculated using a US Dollar to Rand exchange rate of R16 to the US Dollar. This equates to 18 243.84 R ha^{-1} y^{-1}, when inflation in Laos to 2022 was considered, as mentioned above. The total revenue was calculated as 205 180.50 R ha $^{-1}$, resulting in a yearly income of 29 311.50 R ha^{-1} y^{-1} calculated back over the 7 year span. Again using a yield of 100 ton ha^{-1} – 150 ton ha^{-1}, the cost price of the *Eucalyptus* would be 851.38 R ton^{-1} to 1 277.07 R ton^{-1} and a selling price of 1 367.87 R ton^{-1} to 2 051.81 R ton^{-1}. This is significantly higher than the calculated cost price per ton of similar studies [Langat et al., 2015, Silva et al., 2020].

Similar calculations were done for Agrifarming [2021], Olivier and Rusk [1997], Sudha et al. [2007], with the data available in their study. Figure 3.2 depicts the cost and selling price per ton of harvested *Eucalyptus* for each of the studies.

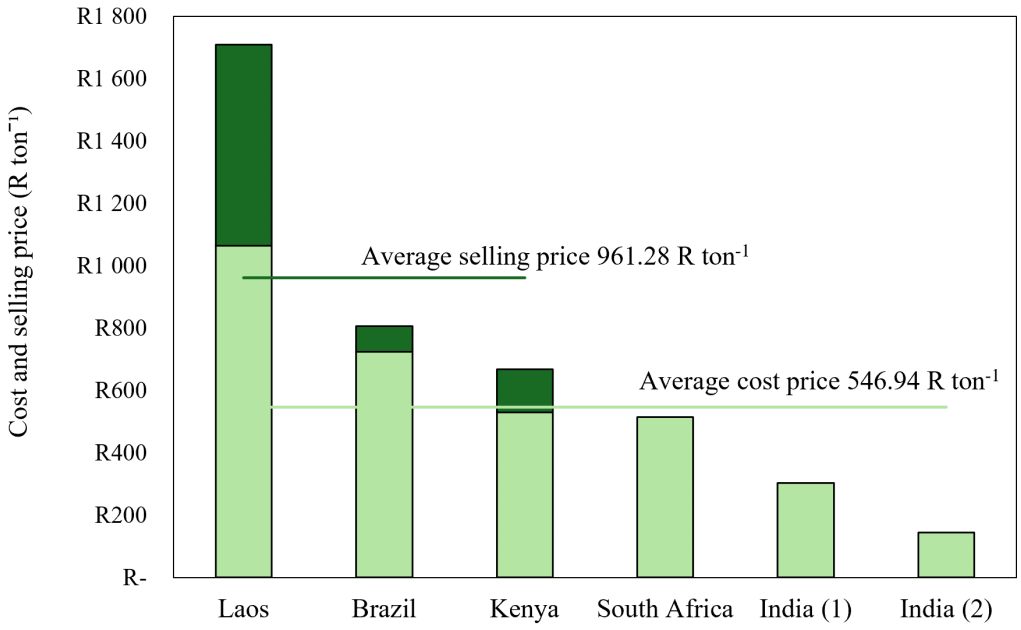

FIGURE 3.2: Cost and selling price of harvested *Eucalyptus*.

Figure 3.2 indicates that the assumed value of 550 R ton^{-1} was inline with studies conducted on the average cost price of growing *E. grandis*.

3.2 First iteration depiction of financial metrics calculations

The parameters depicted in Table 3.3 were used for an initial estimation and illustration of the cost estimation. As mentioned in Section 3.1, these values will then be optimised using the xlwings automation package in Jupyter Notebook. All four scenarios involving the sale of oils and/or electricity will be depicted. The financial metrics (equipment bill, fixed capital cost, sales and costing, production costs and discounted cash flow) will dynamically adjust with variations in the variable parameters, as influenced by the optimisation process.

TABLE 3.3: Constant parameters of analysis.

Feed rate		
Parameter	Value	Unit
Feed rate (incl. fertilising agents)	10 000	kg d^{-1}
Fertiliser loading	10	%
Fertilising compound loading ratio	1:1:1	-
Pyrolysis yields		
Parameter	Value	Unit
Liquid yield	0.45	%
Water contained in liquid	0.15	%
Biochar yield	0.4	%
Non-condensable gas yield	0.15	%
Selling price		
Parameter	Value	Unit
Average biochar price: bulk	20	R kg^{-1}
Average biochar price: niche	110	R kg^{-1}
Sales ratio, biochar niche %	10	%
Sales ratio, biochar bulk %	90	%
Biochar selling price	29	R kg^{-1}
Mark-up on fertiliser	75	%
Fertiliser selling price	26.43	R kg^{-1}
Enriched biochar selling price	28.61	R kg^{-1}

3.2.1 Equipment bill

The equipment bill was derived and adapted from Wright et al. [2010]. It is important to note that although the referenced study is dated, there is no more recent version available. Since the establishment of an equipment bill is beyond the scope of this study, the values from Wright et al. [2010] were utilised and adapted. To ensure the validity of the techno-economic feasibility study, the Chemical Engineering Plan Cost Indices (CEPCI) of 2021 was used, to account for the changes in the cost of constructing process plants in the chemical and manufacturing industries. Additionally, the maximum USD to Rand trading prices of 7.97 (2010) and 17.02 (2021) was used to account for depreciation of the Rand to the USD. Lastly, the *six-tenths rule* [Towler and Sinnott, 2021] and sizing factor was used for the cost estimation. The equation is depicted below,

$$\text{Cost (2021) R} = \text{Exchange rate} \times \frac{CE_{2021}}{CE_{2010}} \times \text{Cost (2010) USD} \times \left(\frac{\text{Feed rate}}{\text{Sizing factor}}\right)^{0.6} \tag{3.2}$$

The following CE (2021) values were used according to Chemical Engineering [2022]. Table 3.4 depicts the CEPCI values used. The equipment bill is depicted in Table 3.5. It should be noted that the total fixed cost only includes applicable equipment, and that all pretreatment equipment and the wet sawdust hopper was excluded.

TABLE 3.4: Chemical Engineering Plan Cost Indices 2010 and 2021.

CEPCI	2010	2021
CE Index	**556.3**	**801.3**
Equipment	667.5	1015.3
Heat Exchanger & tanks	617.8	859
Process machinery	627	1007.8
Pipes, valves & fittings	840.2	1470.03
Process instruments	426	558.1
Pumps & compressors	902	1226.9
Electrical equipment	484.7	726.9
Structural supports & misc.	689.6	1118.8
Construction labour	331	345.5
Buildings	503.3	826
Engineering & supervision	336.6	310.3

TABLE 3.5: Equipment bill.

Description	Unit Operation	# Online	# Spare	Cost (2010) USD unit^{-1}	Cost (2021) R unit^{-1}
Wood chipper	Pretreatment	1	0	$302 200	R308 405
Cutting mill	Pretreatment	1	0	$302 200	R308 405
Biomass chopping screen	Pretreatment	1	0	$22 500	R22 962
Wet sawdust hopper	Storage	1	0	$41 400	R42 250
Rotary dryer	Pretreatment	1	0	$681 400	R695 392
Steam blower	Pretreatment	1	0	$803 300	R819 795
Biomass-to-pyrolyser screw feeder	Pyrolysis	1	0	$163 500	R165 837
Dry sawdust hopper	Storage	1	0	$41 400	R42 250
Pyrolysis fluidised bed reactor	Pyrolysis	1	0	$836 000	R853 167
Pyrolysis vapour cyclone	Separation	1	0	$1 262 000	R1 287 914
NCG-liquid separation	Separation	1	0	$215 400	R219 823
Electrostatic precipitator	Separation	1	0	$292 400	R298 404
Pyrolysis oil condenser	Separation	1	0	$998 700	R1 019 208
Water pump	Separation	1	0	$669 700	R683 452
Fluidised bed sand hopper	Combustion	1	0	$41 400	R42 250
Combustion-pyrolysis screw feeder	Combustion	1	0	$379 600	R387 395
Combustion fluidised bed	Combustion	1	0	$244 300	R249 317
Air preheater	Combustion	1	0	$2 543 600	R2 595 831
Combustion gas blower	Combustion	1	0	$62 200	R63 477
Combustion vapour cyclones	Combustion	1	0	$1 104 700	R1 127 384
Fluegas blower	Combustion	1	0	$214 700	R219 109
Cooling tower	Cooling	1	0	$3 005 100	R3 066 808
Fuel storage	Storage	1	1	$24 300	R49 598
Liquid fuel pump	Storage	1	0	$24 300	R24 799
Total Equipment Cost				**$14 275 300**	**R14 593 233**
Total Fixed Capital				**$12 122 300**	**R12 396 023**

3.2.2 Total capital investment

The total capital investment is the required amount of initial investment (fixed capital investment) and additional investment (working capital) required to build and sustain the plant before it starts generating revenue.

3.2.2.1 Fixed capital investment

A fixed capital investment (FCI) is essential in financial metrics for building a new plant because it depicts the substantial upfront expenditure on long-term assets such as equipment, piping, instrumentation, etc. Assessing and accurately accounting for these investments in financial metrics are crucial for determining the project's return on investment, payback period, and overall feasibility [Piketty, 2014]. The calculations for the fixed capital investment was also attained from Wright et al. [2010] for chemical processing plants. The results are illustrated in Table 3.6.

TABLE 3.6: Fixed capital investment (FCI) based on a chemical processing plant.

Cost type	Description	Factor	Contribution	Total
Equipment cost				R14 593 233
Additional materials		66.2		R9 660 721
	Piping	32	R4 669 835	
	Concrete	8.7	R1 298 798	
	Steel	1.7	R248 085	
	Instruments (1)	7.3	R1 065 306	
	Electricity	8.3	R1 211 238	
	Instruments (2)	3.4	R496 170	
	Paint	0.6	R87 559	
Additional costs				R19 664 861
	Labour costs	0.36	R8 521 281	
	Indirect costs	0.34	R11 143 580	
Contingencies		0.2		R8 783 763
FCI				**R52 702 578**

3.2.2.2 Working capital

Working capital refers to the additional funds required beyond the fixed capital investment of the plant, necessary for initiating and sustaining operations until the plant becomes profitable [Towler and Sinnott, 2021]. Factors that were included, are:

- Cost of purchasing one month's *E. grandis* and fertilising agents
- Cost of 1 month's raw material in-process
- Cost of producing $\frac{1}{2}$ months produced product
- The outstanding accounts for one month
- Petty cash

The working capital is illustrated in Table 3.7.

TABLE 3.7: Working capital derived from Towler and Sinnott [2021].

Item	Cost	Unit
Cost of raw material	R199 411	R month^{-1}
1 month's raw material in-process	R2 658 566	R month^{-1}
Product: $\frac{1}{2}$ month feedstock processed	R1 349 533	R $\frac{1}{2}$month^{-1}
Sales - outstanding accounts	R2 658 566	R month^{-1}
Petty cash	R398 821	R month^{-1}
Total working capital	**R7 264 916**	

The fixed capital investment and working capital is summated to calculate the total capital investment. The total capital investment for this iteration is R59 967 494.

3.2.2.3 Production costs

The costs associated with producing a product can be categorised into two primary groups, production costs and general costs. The production costs are subdivided into three groups, direct production costs, fixed production costs and plant overheads. Direct production costs, as the name indicates, are directly dependant on the production rate. When the production rate is zero, the production costs are expected to be zero as well. The direct production costs are adapted from Towler and Sinnott [2021].

Fixed production costs include local taxation, insurance and depreciation. The straight line method was used for the depreciation, assuming a 20-year plant lifespan. The plant overhead cost, which includes costs such as general engineering services, salary overheads such as bonuses, plant protection (guards), workshops, etc., was calculated as 50 % of the totals of labour, supervision and maintenance. Other appropriate ranges of cost factors [Towler and Sinnott, 2021] are illustrated in Table 3.8. As the moderate case study was investigated, mean values were used for the production sheet depicted in Table 3.9.

TABLE 3.8: Appropriate ranges of costs.

Cost	Range and description
Labour	15 % of production costs
Direct supervision	15 % of labour costs
Utilities	10 % to 20 % of production costs
Maintenance	3 % to 20 % of FCI
Consumables	15 % of maintenance costs
Laboratory fees	10 % to 20 % of labour costs
Patents and royalties	2 % to 6 % of production costs
Local tax	1 % to 2 % of FCI
Insurance	1.25 % of FCI
Plant overhead costs	50 % of labour, supervision and maintenance
Administration costs	40 % to 60 % of labour costs
Distribution and marketing	2 % to 20 % of sales income
Research and development	2 % of sales costs
Contingency	1 % to 5 % of total costs

TABLE 3.9: Production costs per annum: Moderate case.

Direct production costs			**R14 645 851**
Feedstock costs		V	R2 392 928
Labour	0.15	F	R3 357 056
Direct supervision	0.15	F	R503 558
Utilities	0.15	V	R3 357 056
Maintenance	0.06	F	R3 162 155
Consumable	0.15	F	R474 323
Laboratory fees	0.15	F	R503 558
Patents and royalties	0.04	V	R895 215
Fixed production costs			**R4 223 141**
Local tax	0.015	F	R790 539
Insurance	0.0125	F	R658 782
Depreciation	0.053	F	R2 773 820
Plant overheads	**0.5**	**F**	**R3 511 385**
General costs			**R4 549 779**
Administration costs	0.5	F	R1 678 528
Distribution and marketing	0.07	V	R2 233 195
Research and development	0.02	F	R638 056
Contingency	**0.025**	**F**	**R673 254**
Total production costs			**27 603 410**
Fixed cost			**R18 725 015**
Variable cost			**R8 878 395**

3.2.3 Sales and costing

As previously mentioned in Section 3.1, four scenarios were investigated. These scenarios are labelled Scenario 1-4, depicted in Table 3.10, as numbered in Section 3.1. The biochar sales and fertiliser sales are presented individually to emphasize which one significantly

contributes to the enhanced biochar and proves to be more financially viable. This separation aims to highlight the comparative impact of each on the financial indicators.

TABLE 3.10: Sales and costing summary.

Costing factor	Scenario 1	Scenario 2	Scenario 3	Scenario 4	Units
Biochar sales	23 918 040	23 918 040	23 918 040	23 918 040	R y^{-1}
Fertiliser sales	3 883 474	3 883 474	3 883 474	3 883 474	R y^{-1}
Wood vinegar sales	0	0	6 144 724	4 054 085	R y^{-1}
Electricity sales	7 592 120	4 101 273	0	0	R y^{-1}
Phenolics sales	0	8 597 183	0	8 597 183	R y^{-1}
Raw materials costs	173 800	173 800	173 800	173 800	R y^{-1}

As the feed rate, fertiliser loading and mark-up remains constant for this iteration, the selling price and cost price of the enriched biochar will also remain constant. The total purchase cost of the feed stock is 15.31 R kg^{-1}, with the fertilising agents and the *E. grandis* contributing 15.10 R kg^{-1} and 0.21 R kg^{-1}, respectively. The enriched biochar is priced at 28.61 R kg^{-1}, with contributions from fertilising agents and biochar amounting to 26.43 R kg^{-1} and 29.00 R kg^{-1}, respectively. The ratio of biochar to fertiliser selling price is 85 %. Furthermore, the total mark-up, including all other expenses, is 86.87 %.

3.2.4 Financial indicators

As eluded to in Section 3.1, four financial indicators will used to analyse the economical viability of the plant. These financial indicators include the net present value (NPV), interal rate of return (IRR), return of investment (ROI) and the payback period (PP) after the 20-year lifespan of the plant. The discounted cash flow (for the first three years and last three years) used to calculate the financial indicators of the scenarios is attached in Appendix B. The four scenarios are compared in Table 3.11.

TABLE 3.11: Financial indicators of the four scenarios.

Financial indicator	Scenario 1	Scenario 2	Scenario 3	Scenario 4	Units
NPV	-35 745 382	8 731 200	-61 544 826	8 387 109	R
IRR	-5.0	1.1	-9.5	1.1	%
ROI	21.4	28.0	16.2	27.9	%
PP	19.8	11.9	32.9	12.0	years

The financial indicators in Table 3.11 suggests that for this explanatory iteration that only Scenario 2 and Scenario 4 would be economically viable. The IRR remains notably low at 1.1 % for both scenarios, which may require a compelling case to attract potential investors.

In contrast, both Scenario 1 and Scenario 3 exhibit negative NPVs along with negative IRRs. In the case of Scenario 1, the calculation indicates that the plant would only start generating cumulative net cash flow after 19.8 years, a mere 0.2 years prior to the conclusion of the project's lifespan. It's important to highlight that the PP is derived from the cumulative net cash flow and not the cumulative discounted cash flow, as is the case with NPV. Consequently, the occurrence of a negative NPV when the PP is less than the plant's lifespan is plausible. This highlights the importance of considering both the NPV and PP together for a comprehensive assessment of a project's financial viability. Moreover, the prolonged period before positive cumulative net cash flow in Scenario 3 emphasises the challenges associated with this particular scenario, warranting careful consideration in investment decision-making.

In conclusion, none of the Scenario's would sole-heartedly attract potential investors. Therefore, in the next section, optimisation will be introduced in an attempt to make the project more attractive.

3.3 Optimisation through iterations

As eluded to in Section 3.1, Anaconda's Jupyter Notebook was used together with xlwings to automate and manipulate the Excel spreadsheets. For the iterations, Scenario 2 (selling electricity to the grid through the combustion of the synthesis gas and the wood vinegar fraction, while extracting the phenolic fraction through distillation and selling it) will be used as a base line as it was found to be the most economic scenario.

3.3.1 Price comparison of biochar to coking coal

Coal is categorised into four groups, each with distinct properties based on the carbon content and calorific value [Wood et al., 1983]. Anthracite, known for its high carbon content and low impurities, is a premium coal used in residential heating. Bituminous coal, a versatile and widely used type, contains moderate levels of carbon and volatile matter. Subbituminous and lignite coals have lower carbon content but higher moisture levels, making them suitable for electricity generation [US Energy Information Administration, 2022].

Biochar, while not a direct substitute for coking coal in steelmaking due to its impurities and structural limitations, holds promise as a partial replacement. Safarian [2023] found that biochars derived from woody biomass exhibit physico-chemical properties that meet coal and coke substitution requirements. However, further evaluation of different biochar types is necessary, focusing on fixed carbon content (>80 %) and calorific value (>27 MJ kg^{-1}) to assess their suitability as coke alternatives. In the sintering process, biochar can be substituted for coke at levels between 40 % and 60 %, ensuring high-quality sinter products and maintaining a product yield above 80 %. Additionally, in blast furnace technology, biochar shows great potential for complete substitution with pulverised coal resulting in a 25 % reduction in CO_2 emissions [Safarian, 2023].

Biochar, with 0 % fertiliser loading, is compared to the price of metallurgic (coking) coal to evaluate the economic feasibility to replace coke with biochar. The average coke coal price for 2022 [Focus Economics, 2023] was 308 US$ ton^{-1}. This translates to 5.04 R kg^{-1} using the average dollar to rand exchange rate (2022) of R16.47 to the US Dollar. Table 3.12 depicts the 20-year financial indicators of the plant by using different selling prices. The feedrate was kept constant at 1000 kg day^{-1}.

TABLE 3.12: Financial indicators of biochar (0 % loading) with different selling prices.

Indicator	5 R kg^{-1}	10 R kg^{-1}	15 R kg^{-1}	20 R kg^{-1}	Unit
NPV	-124 231 673	-74 113 574	-23 995 475	26 122 264	R
IRR	N/A	-13.2	-3.3	3.4	%
ROI	N/A	8.9	19.0	29.1	%
PP	N/A	51.8	16.8	10.4	Years

Table 3.12 indicates that with a comparable selling price of 5 R kg^{-1}, the project would be economically unviable. Despite a 20-year plant lifespan, the payback period, covering the original capital investment with operational costs, would never be achieved. Only at a price of 20 R kg^{-1}, four times the price of coking coal, is a positive IRR observed, along with a reasonable payback period.

This begs the question, is the price of coal completely undervalued, therefore never allowing renewable energies to substitute or replace fossil-based fuels?

3.3.2 Feedrate optimisation

The pyrolysis yields, average biochar price for bulk and niche applications as well as the mark-up on the fertilising agents was kept the same as that of the initial iteration

(Table 3.3). Figure 3.3 – Figure 3.7 was produced by varying the feedrate of each loading percentages investigated in Chapter 2.

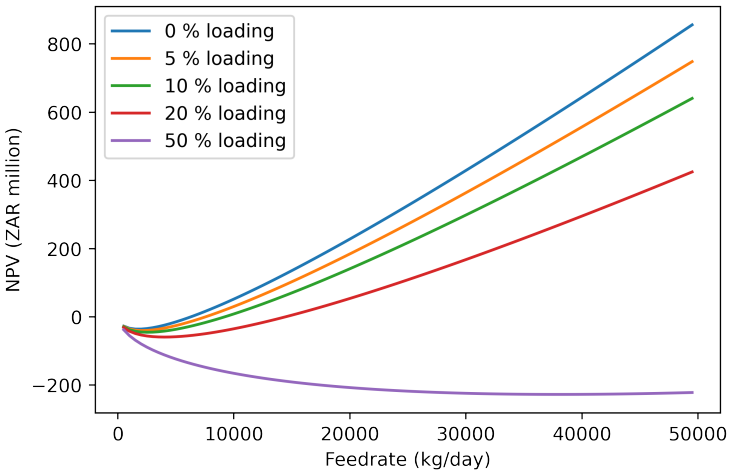

FIGURE 3.3: Net present value of different fertiliser loadings.

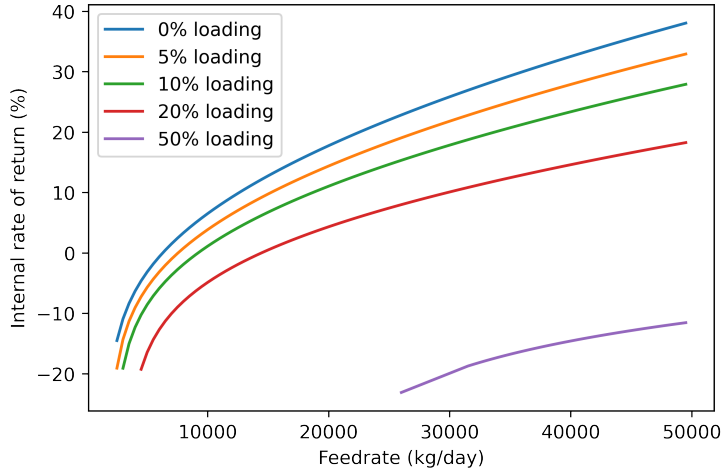

FIGURE 3.4: Internal rate of return of different fertiliser loadings.

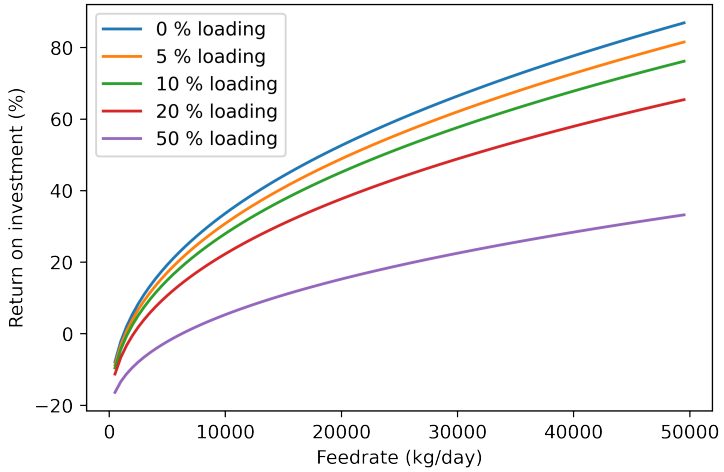

FIGURE 3.5: Return of investment of different fertiliser loadings.

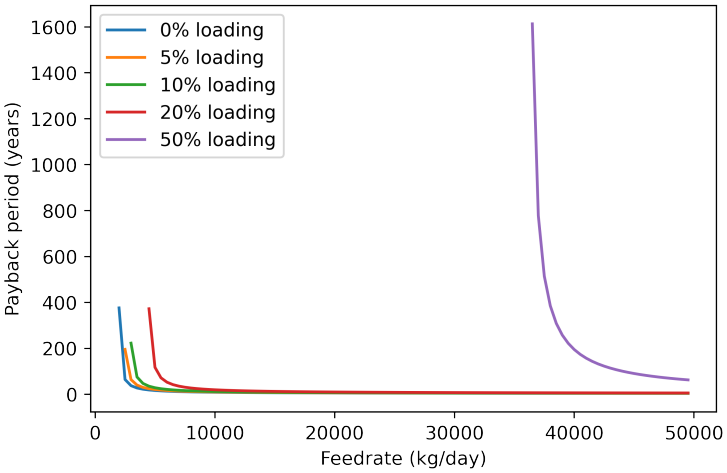

FIGURE 3.6: Payback period of different fertiliser loadings.

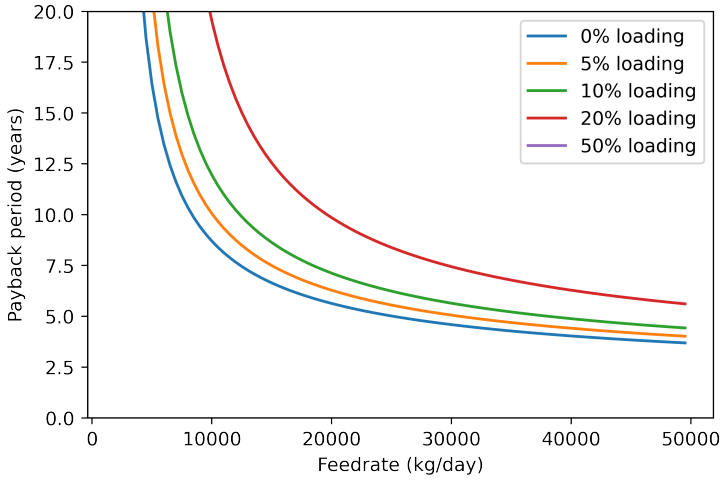

FIGURE 3.7: 20-year payback period of different fertiliser loadings.

Figure 3.3 – Figure 3.7 suggests that an increase in feedrate results in more favourable financial indicators. Furthermore, the modeling suggests that lower fertiliser loadings result in better financial outcomes, primarily due to the comparatively high cost of fertilizers compared to biomass. Figure 3.4 indicates that for a fertiliser loading < 20 %, the IRR becomes positive above a feeding rate of 13 855 kg day^{-1}. In contrast, the 50 % fertiliser loading exhibits a negative IRR for feed rates below 50 000 kg day^{-1}, rendering it economically unviable under the current parameters. To address uncertainties regarding the viability of loadings below and equal to 20 %, two payback period figures are presented in Figures 3.6 and 3.7. Figure 3.7 was introduced, with the y-axis limited to 20 years (the project's lifespan), to provide a clearer illustration of the feed rate's impact on the payback period, as Figure 3.6 alone does not clearly indicate when loadings below and equal to 20 % are economically feasible.

3.3.3 Enriched biochar yield optimisation

The data presented in Figure 3.3 – Figure 3.7 clearly indicate that an increase in feed rate leads to improved performance indicators. The enriched biochar yield was iterated between 10 % and 60 % with a constant feeding rate of 50 000 kg day^{-1}. This chosen biochar yield range reflects practical considerations. Numerous factors including heating rate, maximum temperature, pressure and holding time at maximum temperature [Basile et al., 2015, Titiladunayo et al., 2012, Wannapeera et al., 2011] impacts the final biochar yield.

Low temperature pyrolysis, torrefaction, occurs below 400 °C, with only primary decomposition taking place, forming mostly char (80 wt.% – 90 wt.% yield) [Shankar Tumuluru et al., 2011]. Wannapeera et al. [2011] found that temperatures as low as 275 °C resulted in cross-linking reactions to occur and as a result, structural changes. It is crucial to highlight that the model incorporates considerations for the combustion of synthesis gas and pyrolysis oil, or the potential sale of pyrolysis oil as wood vinegar and a phenolic fraction. Given the high biochar yields observed in Wannapeera et al. [2011], the volatile fraction is anticipated to be minimal. This poses a challenge in processing the pyrolysis oil and synthesis gas, highlighting the difficulties in handling these fractions due to the minimal amount of volatiles produced.

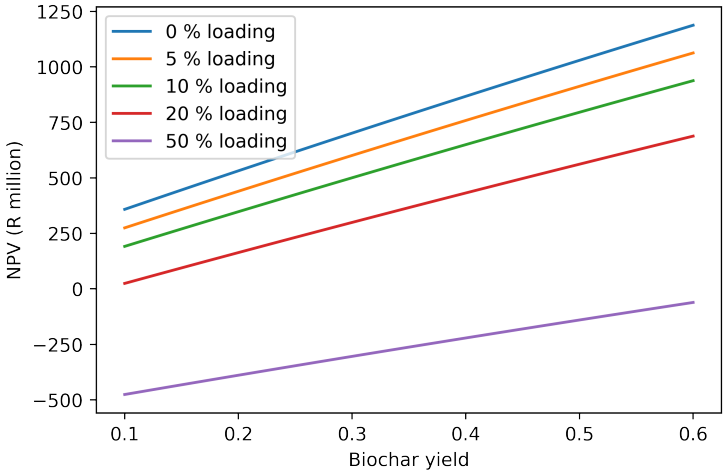

FIGURE 3.8: Net present value with a range of enriched biochar yields.

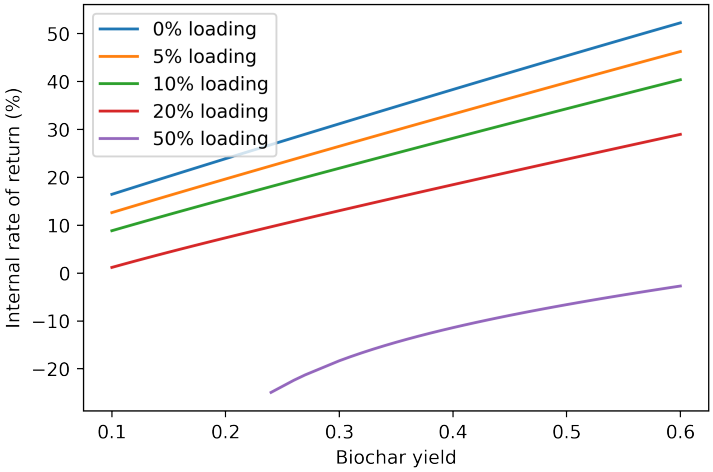

FIGURE 3.9: Internal rate of return with a range of enriched biochar yields.

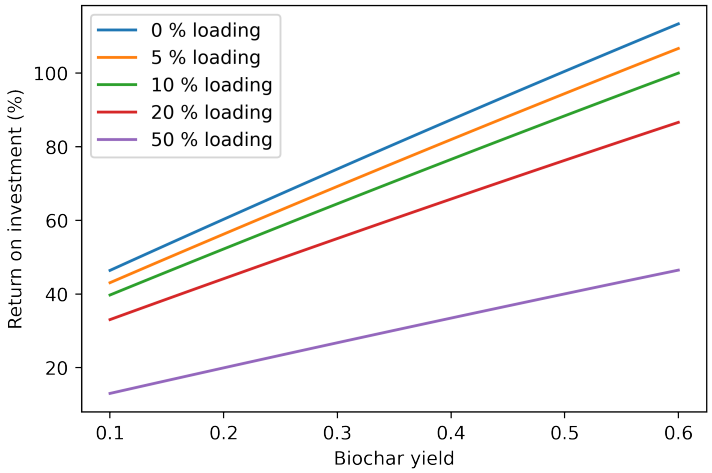

FIGURE 3.10: Return of investment with a range of enriched biochar yields.

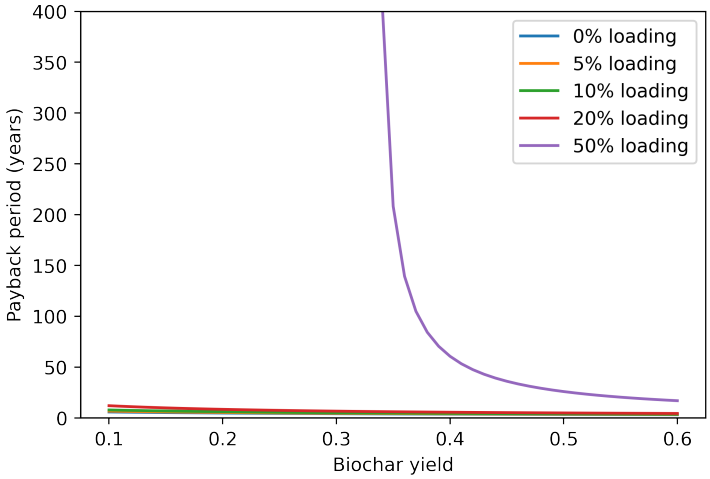

FIGURE 3.11: Payback period with a range of enriched biochar yields.

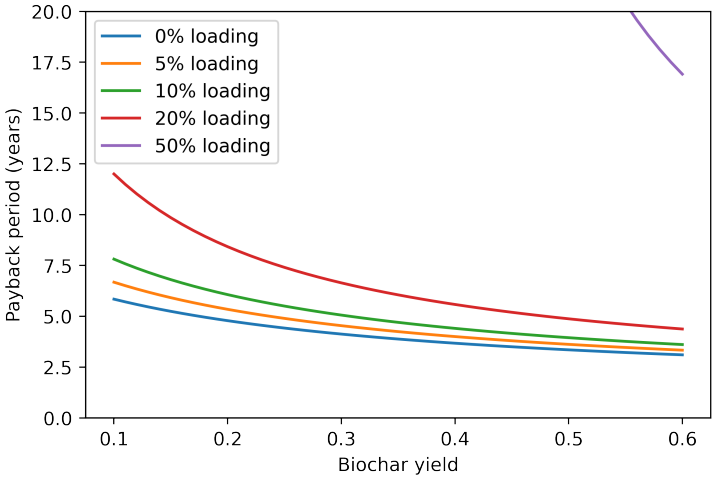

FIGURE 3.12: 20-year payback period with a range of enriched biochar yields.

As expected, an increase in biochar yield results to improved financial indicators. All the indicators have become much more viable with an increase in biochar yield. But, for the 50 % loading, a high enriched biochar yield still seems economically unfavourable, with a 60 % biochar yield resulting in an IRR of -1.8 %. Again, two payback period figures are depicted, as the 50 % loading reaches a maximum payback period of 400 years at just over 30 % enriched biochar yield. The remaining fertiliser loadings (0 %, 5 %, 10 % and 20 %) has a payback period of less 5 years.

Figure 2.3 indicates that a biochar yield of 60 % is achieved at a temperature of 313 °C, but the pyrolytic onset temperature was found to be 326 °C. Therefore, it is not recommended that neat biochar should be set to a yield of 60 %. As for fertiliser loadings greater and equal to 5 %, the pyrolytic onset temperature is 293 °C (Table 2.6) and 278 °C (Table 2.5) for K_3PO_4 and K_2CO_3, respectively.

3.3.4 Fertiliser ratio optimisation

The fertilising agents were introduced in a 1:1:1 ratio for all the previous iterations. It's important to highlight that despite each compound being added at approximately 33 %, the actual amounts of nitrogen, phosphorus, and potassium may not necessarily align with that ratio. Table 3.13 depicts the mass fraction of nitrogen, phosphorus and potassium that each fertilising agent contains as determined by Equation 2.1.

TABLE 3.13: NPK mass fractions of fertilising agents.

Compound	Nitrogen (N)	Phosphorus (P)	Potassium (K)
K_3PO_4	0.00	0.15	0.55
K_2CO_3	0.00	0.00	0.57
$Ca(NO_3)_2$	0.17	0.00	0.00

It should be noted from Table 3.13, that $Ca(NO_3)_2$ was used in this Chapter to represent nitrogen excluding the water of crystallisation (hydrate). Furthermore, it is clear from Table 3.13 that despite selecting K_3PO_4 as the representative compound for phosphorus, it contains three times more potassium than phosphorus Therefore, potassium will always be the main contributing agent to the mixture, as both K_3PO_4 and K_2CO_3 contains potassium. For example, if 33 % of each compound is added, it will result in an NPK ratio of 0.15:0.13:1 or 12 % N, 10 % P and 78 % K.

To find the operating range of the NPK ratio's, a ternary diagram was introduced. For each possible scenario, where a fertilising agents minimum introduced mass fraction is 0.1, a corresponding data point was calculated. It was found that the maximum mass fraction of phosphorus is 0.17 and in attempt to increase this number, K_2CO_3 was set to 0.05 and the other two fertilising agents were iterated in increments of 0.05. This resulted in maximum mass fraction of 0.2 for phosphorus. The ternary diagram is depicted in Figure 3.13.

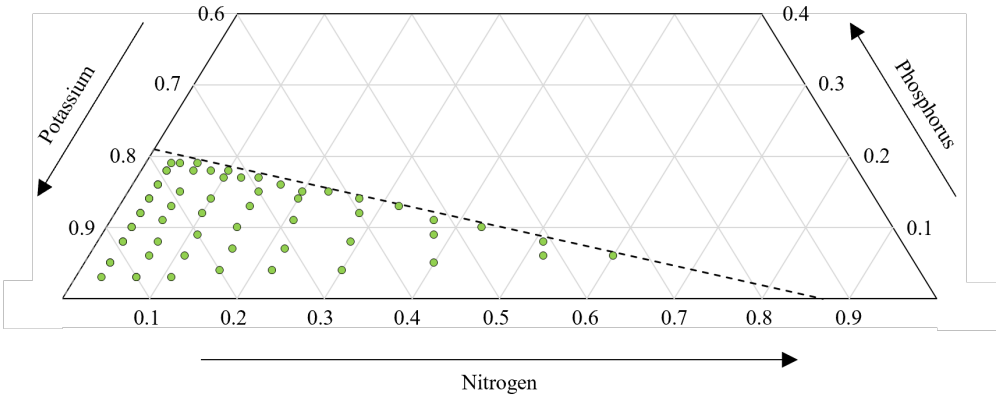

FIGURE 3.13: NPK ternary diagram.

Examining Table 3.2, it is evident that the prices of Urea and MOP, utilised as model compound prices for $Ca(NO_3)_2$ and K_2CO_3, fall within the same price range. On the other hand, DAP, the model compound for K_3PO_4 is approximately 2000 R ton^{-1} more expensive than Urea and MOP. Therefore, optimising the fertiliser ratio, to decrease the cost price, would not make a major difference as the maximum fraction possible of phosphorous is 0.2. For that reason, the fertiliser ratio was optimised for the most even distribution and not financially based. Feeding 45 % $Ca(NO_3)_2$, 50 % K_3PO_4 and 5 % results in a NPK ratio of 0.25:0.24:1 or 0.17 N, 0.16 P and 0.67 K.

3.3.5 Selling price optimisation and feasibility

The two main parameters that will be optimised during this section is the biochar selling price and the mark-up on the fertiliser. For all the previous iterations the average bulk and niche biochar price was set at R 20 per kg and R110 per kg, respectively, using a niche:bulk ratio of 10 %. This resulted in a biochar selling price of R29 per kilogram. A 75 % mark-up was set on the fertiliser costs, resulting in a fertiliser selling price of R26.43 per kg for the first iteration (Section 3.2). This then resulted in a enriched biochar selling price between R27.41 per kg (50 % loading) and R28.78 per kg (5 % loading). As the selling price of biochar was higher than the selling price of the fertiliser, an increase in fertiliser loading would result in lower profit and therefore the financial indicators were lower. Both Section 3.3.2 and Section 3.3.3 indicated financial viability for loadings $\leq$20 %. Therefore, the biochar selling price was iterated between R 0.01 per kg and R 25 per kg, using Scenario 2, in an attempt to compete as a industrially used fertiliser, depicted in Figures 3.14 – 3.18 The fertiliser mark-up was set to 0 %, to mitigate the impact of the profits made on the fertiliser.

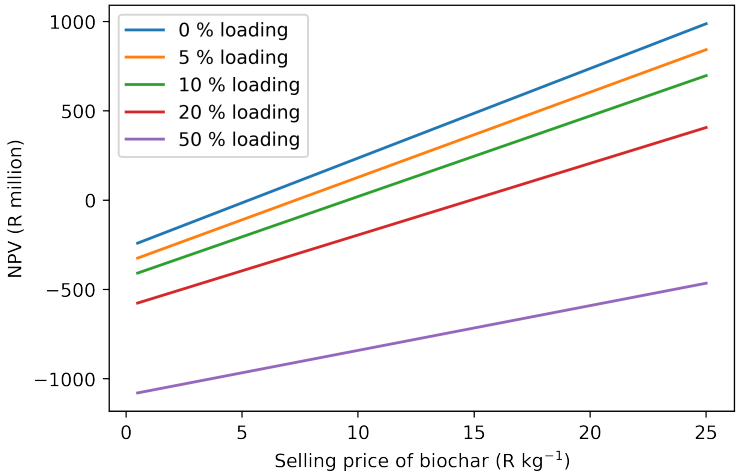

FIGURE 3.14: Net present value of a range of biochar selling prices.

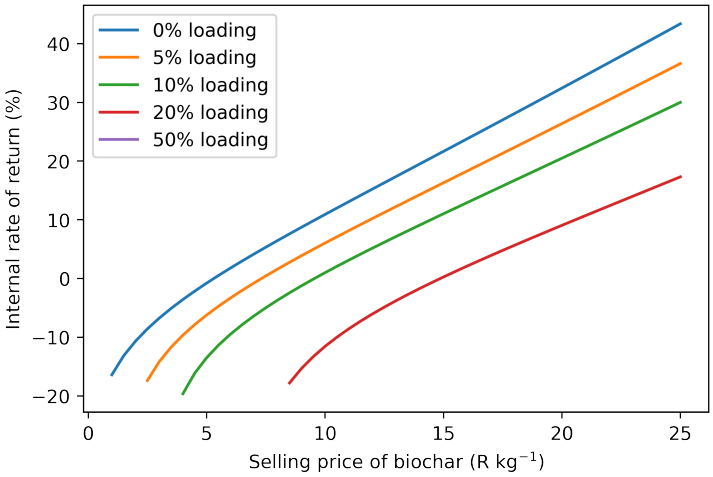

FIGURE 3.15: Internal rate of return of a range of biochar selling prices.

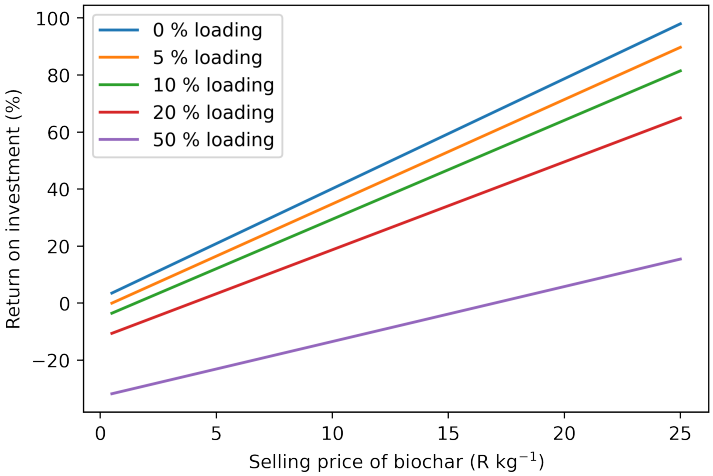

FIGURE 3.16: Return of investment of a range of biochar selling prices.

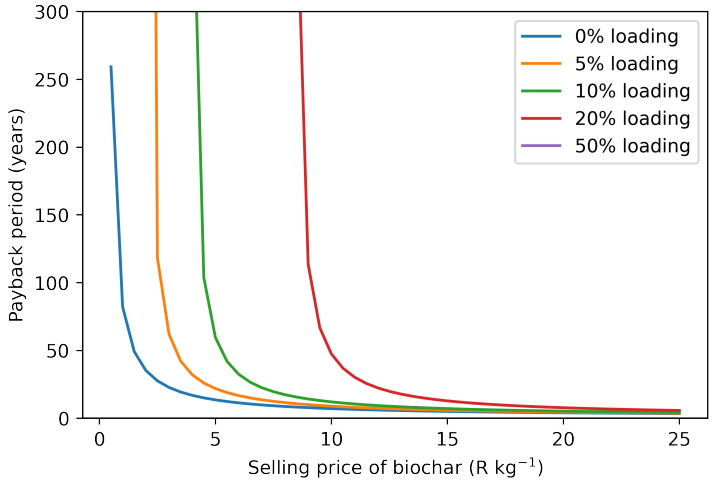

FIGURE 3.17: Payback period of a range of biochar selling prices.

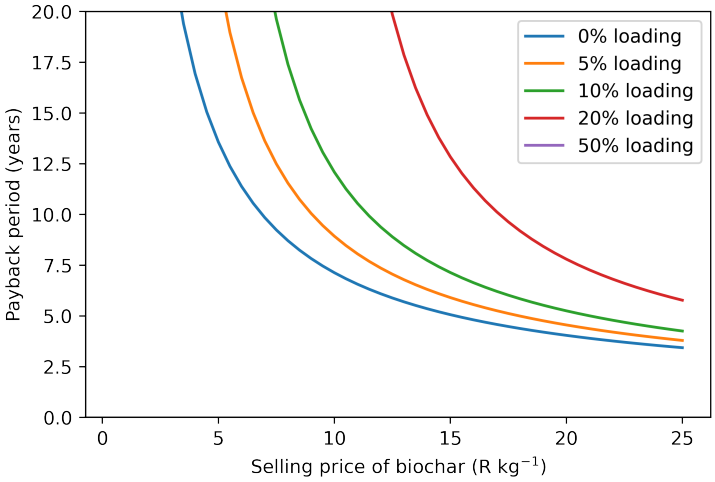

FIGURE 3.18: 20-year payback period of a range of biochar selling prices.

Figure 3.14 – Figure 3.18 depict the financial indicators as a function of the biochar selling price. As was previously observed, a 50 % loading is not viable at the current biochar selling price. Furthermore, Figure 3.18 was added for clarity of the PP over 20 years. It can be observed that none of the loadings results in a PP of less than 3.5 years.

The appraisal of a project proposal depend on a multitude of factors including the financial indicators, strategic positioning on the market and right to operate project. In this context, management invests in a project to align with granted permits, such as those pertaining to CO_2 emissions, ensuring compliance with established limits [Wagenmakers, 2020]. Industry specific financial indicators are difficult to set with each company having their own minimum levels for approval. Wagenmakers [2020] states that an IRR of between 14 % and 18 % is typical in the chemical industry with a PP of less than 3.5 years. Furthermore, Wagenmakers [2020] explains that exceptions do occur, such as high

risk projects, expansion projects, debottlenecking projects and right to operate projects. From the above information, an IRR of 14 % will be used as a benchmark for the selling price of the biochar. As the mark-up on the fertiliser will be added, the IRR will further increase. Table 3.14 illustrates the selling price of the biochar and financial indicators when the IRR is 14 %.

TABLE 3.14: Biochar selling price with IRR level at 14 %.

Loading (%)	Biochar selling price (R kg^{-1})	NPV (R mil)	ROI (%)	PP (Years)
0	11.42	306.8	45.6	6.4
5	13.88	312.7	49.0	6.4
10	16.57	316.7	52.2	6.4
20	22.96	324.8	58.7	6.4
50	57.64	353.1	78.4	6.4

Table 3.14 indicates that the biochar selling price should be set at R11.42 per kg, for the 0 % loading to have an IRR of 14 %. This is aligns with findings by other authors, who reported costs to be US$ 0.51 (R8.32) per kg [Keske et al., 2020] and US$ 0.58 (R9.62) per kg [Shackley et al., 2011], based on the average exchange rate of R16.47 to the US Dollar in 2022. Even though Section 3.3.1 indicates that neat biochar (0 % loading) will never be able to compete with coal, it was added for completeness. As for the 50 % loading, a biochar selling price of R57.64 per kg is required to attain an IRR of 14 %. The fertiliser mark-up was iterated and an enriched biochar (EB) price was calculated when the IRR reaches 16 %. An IRR of 16 % was chosen as it is the midpoint of the range Wagenmakers [2020] recommended. The results are depicted in Table 3.15.

TABLE 3.15: Enriched biochar selling price with IRR level at 16 %.

Loading (%)	Fertiliser mark-up (%)	EB selling price (R kg^{-1})	NPV (R mil)	ROI (%)	PP (Years)
5	115	14.87	359.2	52.6	6.0
10	59	17.36	364.4	55.9	6.0
20	30	22.26	373.2	62.4	6.0
50	13	36.68	405.7	82.4	6.0

It should be noted that there are different ways of reaching the enriched biochar selling price, as it consists of the biochar selling price as well as the fertiliser mark-up. For

instance, with a 50 % loading, a biochar selling price of R29.06 per kg and a fertiliser mark-up 190 %, also results in a enriched biochar selling price of R36.68 per kg and an IRR of 16 %.

Using the fertiliser costing in Table 3.2, urea [$CO(NH_2)_2$], DAP [$(NH_4)_2HPO_4$] and MOP (KCl) was converted to an equivalent N, P, K cost per kg (R kg^{-1}). FAO [2005] studied the required N, P_2O_5 and K_2O per hectare, required by crops. The data will be adapted (Table 3.16) to a N, P, K required per hectare (R ha^{-1}) in order to be compared to the enriched biochar. This will give a good indication of the extra cost involved for farmers by using the enriched biochar.

TABLE 3.16: Fertiliser application rates adapted from FAO [2005].

Crop	N (kg ha^{-1})	P (kg ha^{-1})	K (kg ha^{-1})
Maize	55	7	5
Wheat	30	9	3
Sunflower	15	5	2
Soybeans	7	5	7
Sugar cane	92	12	110
Lucerne	15	13	20
Other pastures	50	10	6
Tobacco	38	31	81
Cotton	36	5	2
Citrus	80	8	50
Subtropical fruits/nuts	180	12	199
Vines	50	8	20
Deciduous fruit	110	35	69
Vegetables	170	35	100
Potatoes	170	35	100

Table 3.16 includes field crops, industrial crops and horticulture crops. As highlighted in Section 3.3.4, it was determined that potassium had the highest mass fraction among the fertilising agents, with nitrogen ranking second and phosphorus having the lowest contribution to the ratio. Emphasis will be placed on sugar cane and subtropical fruits/nuts given their elevated potassium and nitrogen application rate.

TABLE 3.17: Current cost per hectare using neat fertiliser.

Crop	N (R ha^{-1})	P (R ha^{-1})	K (R ha^{-1})	Total Cost (R ha^{-1})
Sugarcane	128	20	326	474
Subtropical fruits/nuts	250	20	589	859

Table 3.17 indicates that it currently costs farmers R474 per hectare and R859 per hectare to fertilise sugarcane and subtropical fruits/nuts, respectively. It should be noted, that the percentage loading of the enriched biochar is based on the feed and not on the product. Equation 3.3 depicts the calculation of final enriched biochar fertiliser loading,

$$\eta_{\text{fertiliser fraction}} = \frac{\dot{m}_{\text{fertiliser}}}{\dot{m}_{\text{fertiliser}} + \dot{m}_{\text{neat biochar}}} \tag{3.3}$$

where $\eta_{\text{fertiliser fraction}}$ is the mass fraction of fertiliser in the enriched biochar, $\dot{m}_{\text{fertiliser}}$ and $\dot{m}_{\text{neat biochar}}$ is the mass flow of N, P, K fertiliser and neat biochar in kg day^{-1}, respectively. Finally, the mass fraction of fertiliser in the enriched biochar is multiplied by a hundred to get a fertiliser loading. The 5 %, 10 %, 20 % and 50 % feed loading results in an enriched biochar product loading of 5.3 %, 10.6 %, 21.1 % and 51.7 %. The cost per hectare using enriched biochar is illustrated in Table 3.18.

TABLE 3.18: Cost per hectare using enriched biochar.

Loading %	N (R ha^{-1})	P (R ha^{-1})	K (R ha^{-1})	Total Cost (R ha^{-1})
Sugarcane with enriched biochar				
5.3	18 517	2 435	39 326	60 278
10.6	10 809	1 421	22 956	35 186
21.1	6 963	915	14 787	22 665
51.7	4 682	616	9 945	15 243
Subtropical fruits/nuts with enriched biochar				
5.3	36 229	2 409	71 135	109 888
10.6	21 148	1 406	41 523	64 144
21.1	13 623	906	26 748	41 320
51.7	9 161	609	17 988	27 788

Table 3.18 depicts the cost per hectare using enriched biochar. From the data it can be inferred that using a higher loading results in a lower cost per hectare. This observation is due to high amount of enriched biochar required to produce 1 kg of fertiliser. Approximately 19 kg of enriched biochar contains 1 kg of fertiliser for a 5.3 % loading. Therefore, 19 times the amount of product has to be spread on a hectare of land when using enriched biochar compared to neat fertilisers. On the other hand, 1.93 kg of enriched biochar is required to produce 1 kg of fertiliser using a 51.7 % loading. Furthermore, Table 3.17 and Table 3.18 indicate that potassium contributes the highest cost of the fertilisers. This is intuitive, as potassium has the highest mass fraction of the fertilisers. MOP also contains the highest amount of fertilising agent (52.4 % K) compared to urea and DAP that contain 23.3 % N and 19.7 % P, respectively, which further increases the cost per kg of K.

Comparing the cost per hectare of Table 3.17 and Table 3.18, a major distinction can be observed. The cost of using enriched biochar is between 32 and 127 times the price of using neat fertiliser both for sugarcane and subtropical fruits/nuts. This is a significant increase in price which would not be sustainable for farmers.

The analysis results in a pressing question: does the benefits of using enriched biochar, such as improved soil health and fertility, outweigh the considerable rise in cost? In my perspective, the answer leans towards the negative. The major increase in expenses associated with enriched biochar, when compared to the more economical alternative of neat fertilisers, poses a significant financial burden for farmers. While the potential advantages of improved soil conditions are known, the daunting cost variation may render the use of enriched biochar economically impractical for many farmers.

3.4 Summary

A techno-economic feasibility analysis was conducted on fertilised biochar, using biomass loaded with K_2CO_3, K_3PO_4 and $Ca(NO_3)_2{\cdot}4H_2O$ as fertilising agents, to represent potassium (K), phosphorus (P) and nitrogen (N), respectively. As bulk prices were difficult to obtain for the fertilising agents, wholesale prices for urea, MOP and DAP were used. Four financial indicators were utilised to evaluate the economic viability of enriched biochar including net present value (NPV), internal rate of return (IRR), return on investment (ROI), and payback period (PP). To increase financial feasibility, offset routes for the byproducts (synthesis gas and pyrolysis oil) were investigated. Four scenarios were introduced, whereby the byproducts were sold, distilled or combusted to produce electricity. Process parameters such as daily tonnage, fertiliser loading, biochar

yield, fertiliser agents ratio and the final selling price were iterated to optimise the viability. An equipment bill, fixed capital investment, working capital, production costs and discounted cash flow was calculated for all iterations.

The analysis included a price comparison to coking coal, with neat biochar as a possible replacement. It was concluded that neat biochar has to be sold at $>$ R20 per kg to be economically viable. The average price (2022) for coking coal was R5.04 per kg. Substituting coking coal for neat biochar would result in a price increase of R14.96 per kg, almost four times the current cost of coking coal.

The feedrate, biochar yield, fertiliser ratio, and selling price were optimised to maximise financial performance. To ensure the project attracts interest from investors, the enriched biochar was set to a selling price whereby the IRR is 16 %. At the previously mentioned IRR level, fertiliser application rates were used as a baseline to compare the enriched biochar to commercial neat fertilisers. It was discovered that the use of enriched biochar is between 32 (51.7 % loading) and 127 (5.3 % loading) times the cost per hectare compared to that of neat fertiliser. The increase in price is attributed to the high amount of enriched biochar required per hectare to meet current fertilising practices. Enriched biochar with a 5.3 % loading requires spreading 19 times more product per hectare compared to neat fertilisers. Further research should be conducted on the diffusivity properties of biochar to determine its potential as a slow-release agent, potentially reducing the frequency of fertiliser application.

Chapter 4

Conclusions and recommendations

4.1 Conclusions

Even though the use of thermochemical processes dates to the time of the Neanderthals [Tiilikkala et al., 2010], there has been a resurgence in the use of pyrolysis. This renewed interest comes from the need to find alternative fuels to reduce the rate of depletion of fossil fuel reserves. Pyrolysis stands out as a promising process for addressing this challenge as it transforms biomass and waste materials into valuable energy resources.

The thermochemical treatment of woody biomass for the upgradation of biochar to a fertiliser led to this research. It was hypothesised that there exists a simplistic method of optimising biochar synthesis during pyrolysis to decrease the pyrolytic onset temperature of biomass. This optimisation strategy is anticipated to result in a decreased energy consumption during the process. Furthermore, the optimising had to provide a industrial benefit post-pyrolysis. Therefore, chemical compounds were identified that can act as a catalyst but also enrich the biochar with nutrients to be used as a fertiliser.

The biomass utilised during the analysis was *Eucalyptus grandis*, as it is an abundant hardwood in South Africa and is known for its rapid growth. In total, 79 potential catalytic fertilising agents were identified and through a rigorous selection process, three compounds were identified, each representing nitrogen, phosphorus and potassium, respectively. Thermogravimetric analysis (TGA) was employed to study the thermal decomposition of the biomass and assess the impact of the fertilising agents on the pyrolytic onset temperature of *E. grandis*.

Both potassium carbonate (K_2CO_3) and tripotassium phosphate (K_3PO_4) resulted in a significant suppression of the pyrolytic onset temperature of *Eucalyptus grandis* biomass, leading to major energy savings. The results are depicted in Table 4.1 and Table 4.2 for K_2CO_3 and K_3PO_4, respectively. On the other hand, calcium nitrate tetrahydrate ($Ca(NO_3)_2{\cdot}4H_2O$) did not have any considerable catalytic effect on the biomass. K_2CO_3 and K_3PO_4, due to their alkaline nature upon dissolution, increases the pH of the solution by releasing hydroxide ions (OH^{-1}), whereas $Ca(NO_3)_2{\cdot}4H_2O$ remains neutral. The alkalinity brought about by K_2CO_3 and K_3PO_4 therefore promotes the breakdown of saccharide molecules, possibly decreasing the pyrolytic onset temperature of *E. grandis*, unlike $Ca(NO_3)_2{\cdot}4H_2O$, which lacks a significant effect. The combination of alkaline substances with pyrolytic vapors may further influence the thermal decomposition of cellulose, suggesting numerous factors at play during biomass depolymerisation.

TABLE 4.1: Reducing pyrolytic onset temperature for energy savings *via* K_2CO_3 catalysis.

Fertiliser loading	$T_{pyrolytic\ onset}$ (°C)	$\Delta T_{suppression}$ (°C)	Energy saving (%)
Neat	326	0	0.0
1 wt.%	315	-11	1.5
2 wt.%	301	-25	3.6
5 wt.%	278	-48	7.7
10 wt.%	254	-71	11.2
20 wt.%	243	-83	13.6
50 wt.%	229	-97	18.7

TABLE 4.2: Reducing pyrolytic onset temperature for energy savings *via* K_2PO_4 catalysis.

Fertiliser loading	$T_{pyrolytic\ onset}$ (°C)	$\Delta T_{suppression}$ (°C)	Energy saving (%)
Neat	326	0	0.0
1 wt.%	324	-2	0.6
2 wt.%	315	-20	2.3
5 wt.%	293	-33	6.4
10 wt.%	277	-49	9.4
20 wt.%	271	-55	11.5
50 wt.%	251	-75	16.7

From Table 4.1 and Table 4.2, it is clear that the addition of fertilising agents, specifically K_2CO_3 and K_3PO_4, has a significant impact on reducing the pyrolytic onset temperature of *E. grandis*. The maximum observed temperature suppression was -97 °C and -75 °C for K_2CO_3 and K_3PO_4 respectively, highlighting the potential of these fertilising additives. This reduction in temperature results in major energy savings, amounting to 18.7 % and 16.7 % for K_2CO_3 and K_3PO_4, respectively.

The findings are not only significant in terms of the catalytic ignition temperature suppression and energy reductions, but also confirm the initial hypothesis with respect to the role of fertilising agents in pyrolysis. The ability of the fertilising agents to reduce the pyrolytic onset temperature presents opportunities to optimise biochar production at the synthesis stage. By adding equal amounts of K_2CO_3, K_3PO_4 and $Ca(NO_3)_2{\cdot}4H_2O$, it is possible to produce a NPK-fertilised biochar while simultaneously reducing the energy consumption of *E. grandis* pyrolysis.

Now that it has been established that the fertilising agents act as a catalyst, a financial viability, in the form of a techno-economical feasibility analysis, was conducted. Four financial indicators, including the net present value (NPV), internal rate of return (IRR), return on investment (ROI), and payback period (PP) were introduced to evaluate the economic feasibility of producing fertilised-catalysed biochar *via* pyrolysis. All of the above mentioned financial metrics were calculated and iterated, but special attention was given to the IRR and the PP. After parameters such as the feed rate, biochar yield and fertiliser ratios were optimised, the target IRR was set to 16 wt.% and payback period less than 10 years, as the lifespan of the plant was 20 years. This strategic decision ensured that the selling price of the enriched biochar remained appealing for farmers, while staying attractive for investors.

The cost of growing and cultivating Eucalyptus across five countries (Laos, Brazil, South Africa, Kenya and two in India) were examined using available literature. The aim was to determine what the cost difference would be between purchasing Eucalyptus on large scale and undertaking self cultivation. To ensure that the literature sources remained relevant and comparable, a country-specific inflation calculator was used to the year 2022. It was discovered that the average bulk purchasing cost of Eucalyptus is 961.28 R ton^{-1}, while self-cultivation would cost approximately 546.94 R ton^{-1}. Consequently, a value of 550 R ton^{-1} of Eucalyptus was used for the analysis.

Four scenarios were introduced in an effort to enhance the economic feasibility of the plant. As pyrolysis also produces pyrolysis oil and synthesis gas, offset streams were created for these products. These scenarios included selling electricity back to the grid by combustion of the synthesis gas, fractional condensation of the pyrolysis oil to recover a phenolic fraction and combustion of the pyrolysis oil for electricity, amongst others.

Scenario 2 (selling electricity to the grid through the combustion of the synthesis gas and the wood vinegar fraction, while extracting the phenolic fraction through distillation and selling it) was used as it was found to be the most economic scenario.

The first price comparison introduced was that of neat biochar and metallurgic (coking) coal. The financial indicators were calculated for a neat biochar price between 5 R kg^{-1} and 20 R kg^{-1} and compared to the average coking coal price of 2022 [Focus Economics, 2023]. An IRR of 3.4 %, ROI of 29.1 % and PP of 10.4 years was observed when the selling price of neat biochar was set to 20 R kg^{-1}. This is a 297 % price increase compared to that of coking coal (5.04 R kg^{-1}) with financial indicators that aren't that favourable. As previously mentioned in Chapter 3, this prompts a crucial question: is the price of coal currently undervalued? The issue at hand is factoring in the true cost of climate change and the toll coking coal has on the environment. While replacing and/or substituting coking coal to some degree with biochar may appear expensive and inflated, it may ultimately reduce other significant expenses associated with environmental damage.

As for the catalysed-fertilised biochar, a much more pessimistic outlook emerged. In order to be comparable to industrially-used fertilisers, a NPK fertiliser application rate was adapted from FAO [2005] for various crops. As Figure 3.13 indicated, the enriched biochar will contain a large fraction of potassium which is attributed to the presence of both K_2CO_3 and K_3PO_4. Therefore, crops that require a large fraction of potassium, such as sugar cane and subtropical fruits/nuts, were chosen to compare costs per hectare.

Figure 4.1 depicts the extra costs associated with using enriched biochar instead of neat fertiliser, that is currently used. The figure reveals a power relationship between fertiliser loading and cost, where b=-0.686 for both subtropical fruits/nuts and sugarcane, respectively. This was expected, as the variable b in a power equation influences the shape and behaviour of the graph.

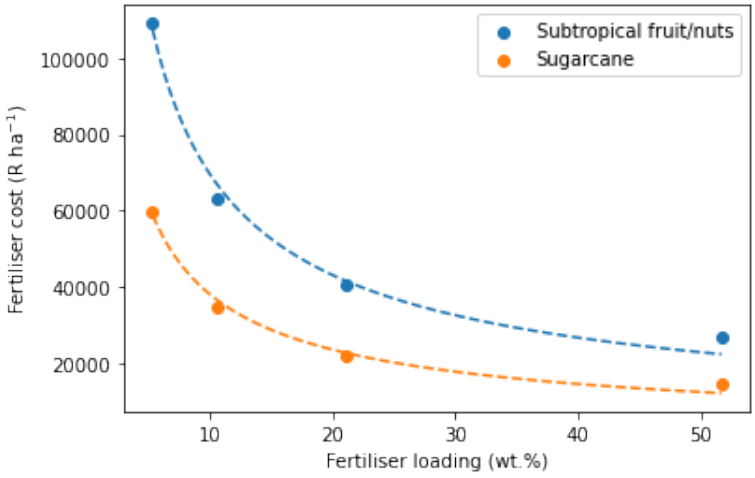

FIGURE 4.1: Additional cost per hectare using enriched biochar.

Figure 4.1 reiterates that replacing neat fertilisers with enriched biochar will result in significant financial stress, not only on farmers, but ultimately on us as consumers. As eluded to in Chapter 3, enriched biochar might be more beneficial to soil health and fertility, but at this stage remains economically unviable. This does not mean that it will forever remain that way. Take for instance the effect the Russia-Ukraine war has had on the price of crude oil. Even though bioplastics are currently much more expensive to produce than petroleum-based plastics, if the significant rise in crude oil continues, it might pave the way forward for the use and manufacture of bio-based plastics.

There exists a notable lack in literature and understanding to conduct a comprehensive and systematic techno-economical feasibility analysis on the sustainable application of biochar. This makes it difficult to create a baseline scenario for comparing different situations regarding the sustainability and profitability of enriched biochar. In conclusion, the feasibility analysis highlights the complex act of balancing economic viability with environmental sustainability. While more cost effective options such as coking coal and neat fertilisers (produced through the energy intensive Haber-Bosch process) may seem more attractive in the short term, the long-term effects on the environment should be considered.

4.2 Recommendations

This research has provided an introduction to the catalytic effect of fertilising agents on the pyrolytic onset temperature and ultimately, the energy consumption of *E. grandis* pyrolysis. Among the 79 prospective fertilising agents evaluated, three were selected for thermogravimetric analysis. However, this by no means indicates that there doesn't exist other fertilising agents that have a more profound effect on biomass pyrolysis, especially those containing nitrogen. That being said, clear suppression of pyrolytic onset temperature was observed for K_2CO_3 and K_3PO_4, but it is recommended that further research is conducted on the reaction kinetics of fertilised-catalysed *E. grandis*.

In the paper titled "Fertiliser-catalysed suppression of the pyrolytic temperature for synthesis of nutrient-enriched biochar", which was presented at the 14th International Conference on Applied Energy, reaction orders, activation energies, pre-exponential factors and mass fractions were estimated for cellulose, hemicellulose and lignin of *E. grandis*. It was realised that the deconvolution model of TG and dTG data can be a Master's research topic by itself, therefore falling outside of the research scope of this dissertation.

From the techno-economical feasibility analysis it was concluded that using fertilised biochar would result in a 32-fold price increase for farmers per hectare. But the longevity

and diffusivity of fertilised biochar is poorly understood. It is therefore recommended that more experimental work be conducted on the physical morphology (BET surface area, porosity, etc.) of fertilised-catalysed biochar to better understand the potential use as a slow-release agent, possibly leading to a reduction in the frequency of fertiliser application. Lastly, it is recommended that a life cycle analysis focusing on sustainability and environmental impact should be conducted.

References

Agrifarming. Eucalyptus cultivation project report, costs and profits, 2021. URL https://www.agrifarming.in/eucalyptus-cultivation-project-report-cost-and-profits.

MM Alam, M Maniruzzaman, and MM Morshed. Application and advances in microprocessing of natural fiber (jute)–based composites. 2014. URL https://www.sciencedirect.com/science/article/pii/B9780080965321007147.

Janine M Albaugh, Peter J Dye, John S King, et al. Eucalyptus and water use in south africa. *International Journal of Forestry Research*, 2013, 2013. URL https://www.hindawi.com/journals/ijfr/2013/852540/abs/.

Lyle Frederick Albright, Billy L Crynes, and William Harrison Corcoran. Pyrolysis, theory and industrial practice. 1983. URL https://www.osti.gov/biblio/5323862.

Farrukh Raza Amin, Yan Huang, Yanfeng He, Ruihong Zhang, Guangqing Liu, and Chang Chen. Biochar applications and modern techniques for characterization. *Clean Technologies and Environmental Policy*, 18(5):1457–1473, 2016. URL https://link.springer.com/article/10.1007/s10098-016-1218-8.

S Appleyard, O Schmoll, et al. Agriculture: potential hazards and information needs. *Protecting groundwater for health: managing the quality of drinking-water sources*, pages 243–273, 2006. URL https://www.cabidigitallibrary.org/doi/full/10.5555/20073117973.

John Baffes and Wee Chian Koh. Fertilizer prices expected to remain higher for longer, 2022. URL https://blogs.worldbank.org/opendata/fertilizer-prices-expected-remain-higher-longer.

Lucia Basile, Alessandro Tugnoli, and Valerio Cozzani. The role of pressure in the heat of pyrolysis of a lignocellulosic biomass. *Chemical Engineering Transactions*, 43:451–456, 2015. URL https://www.aidic.it/cet/15/43/076.pdf.

Nanthi Bolan, Son A Hoang, Jingzi Beiyuan, Souradeep Gupta, Deyi Hou, Ajay Karakoti, Stephen Joseph, Sungyup Jung, Ki-Hyun Kim, MB Kirkham, et al. Multifunctional applications of biochar beyond carbon storage. *International Materials Reviews*, pages 1–51, 2021. URL https://www.tandfonline.com/doi/abs/10.1080/09506608.2021.1922047.

Tristan R Brown, Mark M Wright, and Robert C Brown. Estimating profitability of two biochar production scenarios: slow pyrolysis vs fast pyrolysis. *Biofuels, Bioproducts and Biorefining*, 5(1):54–68, 2011. URL https://onlinelibrary.wiley.com/doi/abs/10.1002/bbb.254.

Benjamin Caballero, Luiz C Trugo, and Paul M Finglas. *Encyclopedia of food sciences and nutrition*. Academic, 2003. URL https://www.sciencedirect.com/science/article/pii/B012227055X005897.

Robert M Campbell, Nathaniel M Anderson, Daren E Daugaard, and Helen T Naughton. Financial viability of biofuel and biochar production from forest biomass in the face of market price volatility and uncertainty. *Applied energy*, 230:330–343, 2018. URL https://www.sciencedirect.com/science/article/abs/pii/S0306261918312558.

Marion Carrier, Anne Loppinet-Serani, Dominique Denux, Jean-Michel Lasnier, Frédérique Ham-Pichavant, François Cansell, and Cyril Aymonier. Thermogravimetric analysis as a new method to determine the lignocellulosic composition of biomass. *Biomass and Bioenergy*, 35(1):298–307, 2011. ISSN 0961-9534. doi: https://doi.org/10.1016/j.biombioe.2010.08.067. URL https://www.sciencedirect.com/science/article/pii/S0961953410003314.

José María Chaín, Esteban Tubert, Corina Graciano, Luis Nazareno Castagno, Marina Recchi, Fernando Luis Pieckenstain, María Julia Estrella, Gustavo Gudesblat, Gabriela Amodeo, and Irene Baroli. Growth promotion and protection from drought in eucalyptus grandis seedlings inoculated with beneficial bacteria embedded in a superabsorbent polymer. *Scientific Reports*, 10(1):1–17, 2020. URL https://www.nature.com/articles/s41598-020-75212-4.

Chemical Engineering. Chemical Engineering. 129(6), 2022. URL https://www.nxtbook.com/accessintelligence/ChemicalEngineering/chemical-engineering-june-intl-2022/index.php?startid=48.

Shuiliang Chen, Zheng Liu, Shaohua Jiang, and Haoqing Hou. Carbonization: A feasible route for reutilization of plastic wastes. *Science of the total environment*, 710: 136250, 2020. URL https://www.sciencedirect.com/science/article/abs/pii/S0048969719362461.

Lei Chu, Haifeng Liu, Zhenyu Zhang, Yue Zhan, Kang Wang, Deyu Yang, Ziqiang Liu, and Jialin Yu. Evaluation of wood vinegar as an herbicide for weed control. *Agronomy*, 12(12):3120, 2022. URL https://www.mdpi.com/2073-4395/12/12/3120.

Eric Craswell. Fertilizers and nitrate pollution of surface and ground water: an increasingly pervasive global problem. *SN Applied Sciences*, 3(4):518, 2021. URL https://link.springer.com/article/10.1007/s42452-021-04521-8.

Marc De Wit and André Faaij. European biomass resource potential and costs. *Biomass and bioenergy*, 34(2):188–202, 2010. URL https://www.sciencedirect.com/science/article/abs/pii/S0961953409001457.

Annabelle Déjardin, Françoise Laurans, Dominique Arnaud, Christian Breton, Gilles Pilate, and Jean-Charles Leplé. Wood formation in angiosperms. *Comptes rendus biologies*, 333(4):325–334, 2010. URL https://www.sciencedirect.com/science/article/pii/S1631069110000119.

Ayhan Demirbaş. Ethanol from cellulosic biomass resources. *International journal of green energy*, 1(1):79–87, 2004. URL https://www.cabdirect.org/cabdirect/abstract/20043164958.

Evelyn Desmidt, Karel Ghyselbrecht, Yang Zhang, Luc Pinoy, Bart Van der Bruggen, Willy Verstraete, Korneel Rabaey, and Boudewijn Meesschaert. Global phosphorus scarcity and full-scale p-recovery techniques: a review. *Critical Reviews in Environmental Science and Technology*, 45(4):336–384, 2015. URL https://lirias.kuleuven.be/retrieve/241561.

R Dewi, N Hastuti, and Y Nuraeni. Utilization of wood vinegar as plant based insecticide in mulberry (morus sp). In *IOP Conference Series: Materials Science and Engineering*, volume 935, page 012027. IOP Publishing, 2020. URL https://iopscience.iop.org/article/10.1088/1757-899X/935/1/012027/meta.

C Di Blasi, C Branca, and A Galgano. Biomass screening for the production of furfural via thermal decomposition. *Industrial & Engineering Chemistry Research*, 49(6):2658–2671, 2010. URL https://pubs.acs.org/doi/abs/10.1021/ie901731u.

Capucine Dupont, Rodica Chiriac, Guillaume Gauthier, and François Toche. Heat capacity measurements of various biomass types and pyrolysis residues. *Fuel*, 115: 644–651, 2014. URL https://www.sciencedirect.com/science/article/abs/pii/S0016236113006856.

Michael J Eden, Warwick Bray, Leonor Herrera, and Colin McEwan. Terra preta soils and their archaeological context in the caquetá basin of southeast colombia. *American Antiquity*, 49(1):125–140, 1984. URL https://www.jstor.org/stable/280517.

Saad A El-Sayed and Mohamed E Mostafa. Kinetic parameters determination of biomass pyrolysis fuels using tga and dta techniques. *Waste and Biomass Valorization*, 6:401–415, 2015. URL https://link.springer.com/article/10.1007/s12649-015-9354-7.

Saad A El-Sayed, Tarek M Khass, and Mohamed E Mostafa. Thermal degradation behaviour and chemical kinetic characteristics of biomass pyrolysis using tg/dtg/dta techniques. *Biomass Conversion and Biorefinery*, pages 1–25, 2023. URL https://link.springer.com/article/10.1007/s13399-023-03926-2.

AM Eremenko, IS Petrik, NP Smirnova, AV Rudenko, and YS Marikvas. Antibacterial and antimycotic activity of cotton fabrics, impregnated with silver and binary silver/copper nanoparticles. *Nanoscale research letters*, 11(1):1–9, 2016. URL https://link.springer.com/article/10.1186/s11671-016-1240-0.

Tamer YA Fahmy, Yehia Fahmy, Fardous Mobarak, Mohamed El-Sakhawy, and Ragab E Abou-Zeid. Biomass pyrolysis: past, present, and future. *Environment, Development and Sustainability*, 22(1):17–32, 2020. URL https://link.springer.com/article/10.1007/s10668-018-0200-5.

FAO. *Fertilizer use by crop in South Africa*. FOOD AND AGRICULTURE ORGANIZATION OF THE UNITED NATIONS, 2005. URL https://www.fao.org/3/y5998e/y5998e.pdf.

Focus Economics. Coking coal prices, 2023. URL https://www.focus-economics.com/commodities/energy/coking-coal/.

Shuo Fu, Haixiang Chen, Jiuling Yang, and Zhuo Yang. Kinetics of thermal pyrolysis of eucalyptus bark by using thermogravimetric-fourier transform infrared spectrometry technique. *Journal of Thermal Analysis and Calorimetry*, 139:3527–3535, 2020. URL https://link.springer.com/article/10.1007/s10973-019-08763-y.

JA Garcia-Nunez, MR Pelaez-Samaniego, ME Garcia-Perez, I Fonts, J Abrego, RJM Westerhof, and M Garcia-Perez. Historical developments of pyrolysis reactors: a review. *Energy & fuels*, 31(6):5751–5775, 2017. URL https://pubs.acs.org/doi/10.1021/acs.energyfuels.7b00641.

Don W Green and Robert H Perry. *Perry's chemical engineers' handbook*. McGraw-Hill Education, 2008.

Arthur Bachelor Lofté Grobler. *Scalable dual fluidised bed system for fast pyrolysis of woody biomass*. PhD thesis, University of Pretoria, 2015. URL https://repository.up.ac.za/handle/2263/43758.

Praveen Kumar Gupta, Shreeya Sai Raghunath, Deepali Venkatesh Prasanna, Priyadharsini Venkat, Vidhya Shree, Chandrananthi Chithananthan, Shreya Choudhary, Krithika Surender, and Keerthana Geetha. An update on overview of cellulose, its structure and applications. In Alejandro Rodríguez Pascual and María E. Eugenio Martín, editors, *Cellulose*, chapter 4. IntechOpen, Rijeka, 2019. doi: 10.5772/intechopen.84727. URL https://doi.org/10.5772/intechopen.84727.

Willis Gwenzi, Nhamo Chaukura, Chicgoua Noubactep, and Fungai ND Mukome. Biochar-based water treatment systems as a potential low-cost and sustainable technology for clean water provision. *Journal of environmental management*, 197:732–749, 2017. URL https://pubmed.ncbi.nlm.nih.gov/28454068/.

G Keith Harris and Maurice R Marshall. Ash analysis. *Food analysis*, pages 287–297, 2017. URL https://link.springer.com/chapter/10.1007/978-3-319-45776-5_16.

Krish Homagain, Chander Shahi, Nancy Luckai, and Mahadev Sharma. Life cycle cost and economic assessment of biochar-based bioenergy production and biochar land application in northwestern ontario, canada. *Forest ecosystems*, 3:1–10, 2016. URL https://link.springer.com/article/10.1186/s40663-016-0081-8.

Xun Hu and Mortaza Gholizadeh. Progress of the applications of bio-oil. *Renewable and Sustainable Energy Reviews*, 134:110124, 2020. URL https://www.sciencedirect.com/science/article/abs/pii/S1364032120304159.

Kefeng Huang, Xinyue Peng, Lingxun Kong, Wenzhao Wu, Yifu Chen, and Christos T. Maravelias. Greenhouse gas emission mitigation potential of chemicals produced from biomass. *ACS Sustainable Chemistry & Engineering*, 9(43):14480–14487, 2021. URL https://doi.org/10.1021/acssuschemeng.1c04836.

Stephen M Jasinski. Mineral commodity summaries 2020. *US Geological Survey*, page 200, 2022.

Tao Kan, Vladimir Strezov, and Tim J Evans. Lignocellulosic biomass pyrolysis: A review of product properties and effects of pyrolysis parameters. *Renewable and sustainable energy reviews*, 57:1126–1140, 2016. URL https://www.sciencedirect.com/science/article/abs/pii/S1364032115015683.

Adnan Asad Karim, Manish Kumar, Ekta Singh, Aman Kumar, Sunil Kumar, Arati Ray, and Nabin Kumar Dhal. Enrichment of primary macronutrients in biochar for sustainable agriculture: A review. *Critical Reviews in Environmental Science and Technology*, 52(9):1449–1490, 2022. URL https://www.tandfonline.com/doi/abs/10.1080/10643389.2020.1859271.

Menisha S Karunarathna and Rhett C Smith. Valorization of lignin as a sustainable component of structural materials and composites: Advances from 2011 to 2019. *Sustainability*, 12(2):734, 2020. URL https://www.mdpi.com/2071-1050/12/2/734.

Catherine Keske, Todd Godfrey, Dana LK Hoag, and Joinal Abedin. Economic feasibility of biochar and agriculture coproduction from canadian black spruce forest. *Food and energy security*, 9(1):e188, 2020. URL https://onlinelibrary.wiley.com/doi/full/10.1002/fes3.188.

Burak Koçak and İbrahim Ortaş. Short-term eucalyptus and phragmites biochar's efficiency in mineralization of soil carbon. *Journal of Soil Science and Plant Nutrition*, 21(4):3346–3353, 2021. URL https://link.springer.com/article/10.1007/s42729-021-00610-0.

IM Kolthoff. The lewis and the brönsted–lowry definitions of acids and bases. *The Journal of Physical Chemistry*, 48(1):51–57, 1944. URL https://pubs.acs.org/doi/pdf/10.1021/ed065p28.

MM Küçük and A Demirbaş. Biomass conversion processes. *Energy Conversion and Management*, 38(2):151–165, 1997. URL https://www.sciencedirect.com/science/article/abs/pii/0196890496000313.

David Langat, Joshua K Cheboiwo, and Mbae N Muchiri. Financial analysis of growing eucalyptus grandis for production of medium size power transmission poles and firewood in kenya. *African Journal of Agriculture and Utilisation of Natural Resources for Sustainable Development*, 1, 2015. URL https://www.academia.edu/download/57649650/Eucalyptus_paper__Pages_38-45_08-2-2015-4_21.pdf.

Richard L Lehman, Jefffery S Gentry, and Nick G Glumac. Thermal stability of potassium carbonate near its melting point. *Thermochimica Acta*, 316(1):1–9, 1998. URL https://www.sciencedirect.com/science/article/abs/pii/S0040603198002895.

Qingquan Liu, Le Luo, and Luqing Zheng. Lignins: biosynthesis and biological functions in plants. *International journal of molecular sciences*, 19(2):335, 2018. URL https://www.ncbi.nlm.nih.gov/pmc/articles/PMC5855557/.

JAR Lockhart and AJL Wiseman. *Lockhart & Wiseman's Crop Husbandry Including Grassland*. Elsevier, 2014. URL https://www.sciencedirect.com/book/9781782423713/lockhart-and-wisemans-crop-husbandry-including-grassland.

Gaojin Lyu, Shubin Wu, and Hongdan Zhang. Estimation and comparison of bio-oil components from different pyrolysis conditions. *Frontiers in Energy Research*, 3:28, 2015. URL https://www.frontiersin.org/articles/10.3389/fenrg.2015.00028/full.

Muhammad Aamer Maqsood, Imran Ashraf, Nasir Rasheed, et al. Sources of nitrogen for crop growth: Pakistan's case. In *Nitrogen assessment*, pages 13–28. Elsevier, 2022. URL https://www.sciencedirect.com/science/article/abs/pii/B9780128244173000058.

Peter McKendry. Energy production from biomass (part 1): overview of biomass. *Bioresource technology*, 83(1):37–46, 2002. URL https://www.sciencedirect.com/science/article/abs/pii/S0960852401001183.

D Meier and O Faix. State of the art of applied fast pyrolysis of lignocellulosic materials—a review. *Bioresource technology*, 68(1):71–77, 1999. URL https://www.sciencedirect.com/science/article/abs/pii/S0960852498000868.

Ryan David Merckel, Frederick Johannes Willem Jacobus Labuschagne, and MD Heydenrych. Oxygen consumption as the definitive factor in predicting heat of combustion. *Applied Energy*, 235:1041–1047, 2019. URL https://www.sciencedirect.com/science/article/abs/pii/S0306261918316829.

VR Mulkey, VN Owens, and DK Lee. Management of switchgrass-dominated conservation reserve program lands for biomass production in south dakota. *Crop science*, 46 (2):712–720, 2006. URL https://pubag.nal.usda.gov/catalog/1343308.

Alexander A Myburg, Dario Grattapaglia, Gerald A Tuskan, Uffe Hellsten, Richard D Hayes, Jane Grimwood, Jerry Jenkins, Erika Lindquist, Hope Tice, Diane Bauer, et al. The genome of eucalyptus grandis. *Nature*, 510(7505):356–362, 2014. URL https://www.nature.com/articles/nature13308.

Grace Nakabonge and Brian Matovu. Variation in susceptibility of eucalyptus grandis and selected hybrid clones to two termite species macrotermes bellicosus and m. subhyalinus in uganda. *All Life*, 14(1):120–126, 2021. URL https://doi.org/10.1080/26895293.2021.1883126.

Willem S Olivier and Graham D Rusk. Comparison of pine and eucalypt profitabilities and costs in south africa between 1991 and 1995. *Southern African Forestry Journal*, 179 (1):51–54, 1997. URL https://www.tandfonline.com/doi/abs/10.1080/10295925.1997.9631155.

Shusheng Pang. Advances in thermochemical conversion of woody biomass to energy, fuels and chemicals. *Biotechnology advances*, 37(4):589–597, 2019. URL https://www.sciencedirect.com/science/article/abs/pii/S0734975018301800.

Prakash Parthasarathy, Tareq Al-Ansari, Hamish R Mackey, and Gordon McKay. Effect of heating rate on the pyrolysis of camel manure. *Biomass Conversion and Biorefinery*, 13(7):6023–6035, 2023. URL https://link.springer.com/article/10.1007/s13399-021-01531-9.

Vamsee Pasangulapati, Karthikeyan D Ramachandriya, Ajay Kumar, Mark R Wilkins, Carol L Jones, and Raymond L Huhnke. Effects of cellulose, hemicellulose and lignin on thermochemical conversion characteristics of the selected biomass. *Bioresource technology*, 114:663–669, 2012. URL https://www.sciencedirect.com/science/article/abs/pii/S0960852412004798.

A Pattiya. Fast pyrolysis. In *Direct thermochemical liquefaction for energy applications*, pages 3–28. Elsevier, 2018. URL https://www.sciencedirect.com/science/article/pii/B9780081010297000011.

Bárbara Luísa Corradi Pereira, Angélica de Cássia Oliveira Carneiro, Ana Márcia Macedo Ladeira Carvalho, Jorge Luiz Colodette, Aylson Costa Oliveira, and Maurício Paulo Ferreira Fontes. Influence of chemical composition of eucalyptus wood on gravimetric yield and charcoal properties. *BioResources*, 8(3):4574–4592, 2013. URL https://www.researchgate.net/publication/269550337_Influence_of_Chemical_Composition_of_Eucalyptus_Wood_on_Gravimetric_Yield_and_Charcoal_Properties.

Somvang Phimmavong, Tek Narayan Maraseni, Rodney J Keenan, and Geoff Cockfield. Financial returns from collaborative investment models of eucalyptus agroforestry plantations in lao pdr. *Land Use Policy*, 87:104060, 2019. URL https://www.sciencedirect.com/science/article/pii/S0264837718319872.

Thomas Piketty. *Capital in the twenty-first century*. Harvard University Press, 2014.

Naveed Ahmed Qambrani, Md Mukhlesur Rahman, Seunggun Won, Soomin Shim, and Changsix Ra. Biochar properties and eco-friendly applications for climate change mitigation, waste management, and wastewater treatment: A review. *Renewable and Sustainable Energy Reviews*, 79:255–273, 2017. URL https://www.sciencedirect.com/science/article/abs/pii/S1364032117306937.

Cui Quan, Ningbo Gao, and Qingbin Song. Pyrolysis of biomass components in a tga and a fixed-bed reactor: Thermochemical behaviors, kinetics, and product characterization. *Journal of Analytical and Applied Pyrolysis*, 121:84–92, 2016. ISSN 0165-2370. doi: https://doi.org/10.1016/j.jaap.2016.07.005. URL https://www.sciencedirect.com/science/article/pii/S0165237016302054.

Harifara Rabemanolontsoa and Shiro Saka. Comparative study on chemical composition of various biomass species. *RSC advances*, 3(12):3946–3956, 2013. URL https://ui.adsabs.harvard.edu/abs/2013RSCAd...3.3946R/abstract.

Luis F Razon. Life cycle analysis of an alternative to the haber-bosch process: Non-renewable energy usage and global warming potential of liquid ammonia from cyanobacteria. *Environmental Progress & Sustainable Energy*, 33(2):618–624, 2014. URL https://aiche.onlinelibrary.wiley.com/doi/abs/10.1002/ep.11817.

Donald L. Rockwood, Martin F. Ellis, and Kyle W. Fabbro. Economic potential for carbon sequestration by short rotation eucalypts using biochar in florida, usa. *Trees, Forests and People*, 7:100187, 2022. ISSN 2666-7193. doi: https://doi.org/10.1016/j.tfp.2021.100187. URL https://www.sciencedirect.com/science/article/pii/S2666719321001266.

Emil Roduner. Understanding catalysis. *Chemical Society Reviews*, 43(24):8226–8239, 2014. URL https://pubs.rsc.org/de-ch/content/getauthorversionpdf/C4CS00210E.

Sahar Safarian. To what extent could biochar replace coal and coke in steel industries? *Fuel*, 339:127401, 2023. URL https://www.sciencedirect.com/science/article/pii/S0016236123000145.

Jitendra Kumar Saini, Reetu Saini, and Lakshmi Tewari. Lignocellulosic agriculture wastes as biomass feedstocks for second-generation bioethanol production: concepts and recent developments. *3 Biotech*, 5(4):337–353, 2015. URL https://link.springer.com/article/10.1007/s13205-014-0246-5.

Henrik Vibe Scheller and Peter Ulvskov. Hemicelluloses. *Annual review of plant biology*, 61:263–289, 2010. URL https://pubmed.ncbi.nlm.nih.gov/20192742/.

Simon Shackley, Jim Hammond, John Gaunt, and Rodrigo Ibarrola. The feasibility and costs of biochar deployment in the uk. *Carbon Management*, 2(3):335–356, 2011. URL ThefeasibilityandcostsofbiochardeploymentintheUK.

Jaya Shankar Tumuluru, Shahab Sokhansanj, J Richard Hess, Christopher T Wright, and Richard D Boardman. A review on biomass torrefaction process and product properties for energy applications. *Industrial Biotechnology*, 7(5):384–401, 2011. URL https://www.liebertpub.com/doi/abs/10.1089/ind.2011.7.384.

Janderson de Oliveira Silva, Fábio Gomes Monteiro, Leidy Alves dos Santos, Jonas Elias Castro da Rocha, and Gabriel Magalhães Miranda. Economic viability in eucalyptus spp. clonal plantation for production of pulp. *Floresta e Ambiente*, 27, 2020. URL https://www.scielo.br/j/floram/a/qGtdcCf3rrzJS66nQDw7hZN/?format=html&lang=en.

Aaron T. Simmons, Annette L. Cowie, and Cathy M. Waters. Pyrolysis of invasive woody vegetation for energy and biochar has climate change mitigation potential. *Science of The Total Environment*, 770:145278, 2021. ISSN 0048-9697. doi: https://doi.org/10.1016/j.scitotenv.2021.145278. URL https://www.sciencedirect.com/science/article/pii/S0048969721003442.

A. Skreiberg, Ø. Skreiberg, J. Sandquist, and L. Sørum. Tga and macro-tga characterisation of biomass fuels and fuel mixtures. *Fuel*, 90(6):2182–2197, 2011. ISSN 0016-2361. doi: https://doi.org/10.1016/j.fuel.2011.02.012. URL https://www.sciencedirect.com/science/article/pii/S0016236111000706.

P Sudha, V Ramprasad, M DV Nagendra, HD Kulkarni, and NH Ravindranath. Development of an agroforestry sequestration project in khammamdistrict of india. *Mitigation and Adaptation Strategies for GlobalChange*, 12(LBNL-61461), 2007. URL https://www.osti.gov/servlets/purl/926756.

Stephen David Swart. *Design, modelling and construction of a scalable dual fluidised bed reactor for the pyrolysis of biomass*. University of Pretoria (South Africa), 2012. URL https://repository.up.ac.za/bitstream/handle/2263/29849/dissertation.pdf?sequence=1.

Mohammad J Taherzadeh, Robert Eklund, Lena Gustafsson, Claes Niklasson, and Gunnar Lidén. Characterization and fermentation of dilute-acid hydrolyzates from wood. *Industrial & engineering chemistry research*, 36(11):4659–4665, 1997. URL https://pubs.acs.org/doi/10.1021/ie9700831.

Paul Tanger, John L Field, Courtney E Jahn, Morgan W DeFoort, and Jan E Leach. Biomass for thermochemical conversion: targets and challenges. *Frontiers in plant science*, 4:218, 2013. URL https://www.frontiersin.org/articles/10.3389/fpls.2013.00218/full.

Sonal K Thengane, Kevin Kung, Robert York, Shahabaddine Sokhansanj, C Jim Lim, and Daniel L Sanchez. Technoeconomic and emissions evaluation of mobile in-woods biochar production. *Energy Conversion and Management*, 223:113305, 2020. URL https://www.sciencedirect.com/science/article/pii/S0196890420308438.

Kari Tiilikkala, Leena Fagernäs, and Jasse Tiilikkala. History and use of wood pyrolysis liquids as biocide and plant protection product. 4:111–118, 2010. URL https://jukuri.luke.fi/bitstream/handle/10024/477784/Tiilikkala.pdf?sequence=1.

Isaac Femi Titiladunayo, Armando G McDonald, and Olorunnisola Peter Fapetu. Effect of temperature on biochar product yield from selected lignocellulosic biomass

in a pyrolysis process. *Waste and Biomass Valorization*, 3:311–318, 2012. URL https://link.springer.com/article/10.1007/s12649-012-9118-6.

Gavin Towler and Ray Sinnott. *Chemical engineering design: principles, practice and economics of plant and process design*. Butterworth-Heinemann, 2021. URL https://core.ac.uk/download/pdf/143491361.pdf.

US Energy Information Administration. Coal explained, 2022. URL https://www.eia.gov/energyexplained/coal/.

M Verma, Stéphane Godbout, Satinder Kaur Brar, Olga Solomatnikova, Stéphane P Lemay, and Jean-Pierre Larouche. Biofuels production from biomass by thermochemical conversion technologies. *International Journal of Chemical Engineering*, 2012, 2012. URL https://www.hindawi.com/journals/ijce/2012/542426/.

Paul Victor, SOOHYUN KIM, JIHO YOO, SIHYUN LEE, YOUNGJOON RHIM, JEONGHWAN LIM, SANGDO KIM, DONGHYUK CHUN, HOKYUNG CHOI, and YOUNGWOO RHEE. Deactivation behavior of k 2 co 3 catalyst in the steam gasification of kideco coal. *Transactions of the Korean hydrogen and new energy society*, 27(5):517–525, 2016. URL https://www.dbpia.co.kr/Journal/articleDetail?nodeId=NODE10599012.

Jan Wagenmakers. *Chapter 11: Economic Project Evaluation*. TU Delft OpenCourseWare, 2020. URL https://ocw.tudelft.nl/wp-content/uploads/Chapter_11.pdf.

Shurong Wang, Gongxin Dai, Haiping Yang, and Zhongyang Luo. Lignocellulosic biomass pyrolysis mechanism: a state-of-the-art review. *Progress in energy and combustion science*, 62:33–86, 2017. URL https://www.sciencedirect.com/science/article/abs/pii/S0360128517300266.

Janewit Wannapeera, Bundit Fungtammasan, and Nakorn Worasuwannarak. Effects of temperature and holding time during torrefaction on the pyrolysis behaviors of woody biomass. *Journal of analytical and applied pyrolysis*, 92(1):99–105, 2011. URL https://www.sciencedirect.com/science/article/abs/pii/S0165237011000805.

Gordon Harry Wood, Thomas M Kehn, M Devereux Carter, and William C Culbertson. *Coal resource classification system of the US Geological Survey*, volume 891. US Department of the Interior, Geological Survey, 1983. URL https://pubs.usgs.gov/circ/c891/crcs.htm.

Mark M Wright, Daren E Daugaard, Justinus A Satrio, and Robert C Brown. Techno-economic analysis of biomass fast pyrolysis to transportation fuels. *Fuel*, 89: S2–S10, 2010. URL https://www.sciencedirect.com/science/article/abs/pii/S0016236110003765.

Lei Ye, Zhiwei Peng, Liancheng Wang, Anton Anzulevich, Igor Bychkov, Dmitrii Kalganov, Huimin Tang, Mingjun Rao, Guanghui Li, and Tao Jiang. Use of biochar for sustainable ferrous metallurgy. *JOM*, 71(11):3931–3940, 2019. URL https://link.springer.com/article/10.1007/s11837-019-03766-4.

Michael Zeller, Krassimir Garbev, Luca Weigel, Tilman Saatzer, Daniela Merz, Salar Tavakkol, and Dieter Stapf. Thermogravimetric studies, kinetic modeling and product analysis of the pyrolysis of model polymers for technical polyurethane applications. *Journal of Analytical and Applied Pyrolysis*, 171:105976, 2023. ISSN 0165-2370. doi: https://doi.org/10.1016/j.jaap.2023.105976. URL https://www.sciencedirect.com/science/article/pii/S0165237023001201.

J Zhang and JM He. Soil acidification and nutrient depletion from long-term use of nitrogen fertilizers on winter wheat. *Journal of Environmental Quality*, 38(4):1521–1529, 2009. URL https://acsess.onlinelibrary.wiley.com/journal/15372537.

Junhua Zhang, Matti Siika-Aho, Maija Tenkanen, and Liisa Viikari. The role of acetyl xylan esterase in the solubilization of xylan and enzymatic hydrolysis of wheat straw and giant reed. *Biotechnology for Biofuels*, 4:1–10, 2011. URL https://link.springer.com/article/10.1186/1754-6834-4-60.

Angran Zhao, Bowen Xiong, Yongqiang Han, and Huiling Tong. Thermal decomposition paths of calcium nitrate tetrahydrate and calcium nitrite. *Thermochimica Acta*, 714: 179264, 2022. URL https://www.sciencedirect.com/science/article/abs/pii/S0040603122001204.

Yingdong Zhou and Changwei Hu. Catalytic thermochemical conversion of algae and upgrading of algal oil for the production of high-grade liquid fuel: A review. *Catalysts*, 10(2):145, 2020. URL https://www.mdpi.com/2073-4344/10/2/145.

Appendix A

Chapter 2.1.2.5: Chemical Selection

Compound	Molecular weight	n_N	n_P	n_K	ω_N	ω_P	ω_K	f_1	Soluibility (kg/kg H2O) at 20 C	Cost (R/kg)	f_2	Warning	Decomposition temperature	Decomposition rating	Thermal stability	Thermal stability rating	f3	Non human toxicity (mg/kg bw)	f_4	F	
KNO_3	101.10	1.00	0.00	1.00	0.14	0.00	0.39	0.53	0.32	1916.00	0.97	O, explosive	550	0.33	1.00	0.33	0.66	3015.00	0.18	2.33	
$NaNO_3$	84.99	1.00	0.00	0.00	0.16	0.00	0.00	0.16	0.91	1806.00	0.97	O, explosive	380	0.23	1.00	0.33	0.56	1267.00	0.07	1.77	
$Ca(NO_3)_2$	**164.09**	**2.00**	**0.00**	**0.00**	**0.17**	**0.00**	**0.00**	**0.17**	**1.21**	**1826.00**	**0.97**	**O**	**550**	**0.33**	**1.75**	**0.58**	**0.91**	**4900.00**	**0.29**	**2.34**	*
$Mg(NO_3)_2$	148.31	2.00	0.00	0.00	0.19	0.00	0.00	0.19	0.71	1582.00	0.97	O	330	0.20	1.75	0.58	0.78	500.00	0.03	1.97	
$Zn(NO_3)_2$	189.39	2.00	0.00	0.00	0.15	0.00	0.00	0.15	1.84	1780.00	0.97	O	125	0.07	1.75	0.58	0.66	1400.00	0.08	1.86	
$Cu(NO_3)_2$	187.56	2.00	0.00	0.00	0.15	0.00	0.00	0.15	0.38	58200.00	0.00	O,C	180	0.11	1.50	0.50	0.61	940.00	0.06	0.81	
$Fe(NO_3)_3$	241.86	3.00	0.00	0.00	0.17	0.00	0.00	0.17	0.15	2648.00	0.95	O	345	0.21	1.75	0.58	0.79	3250.00	0.19	2.11	
$Ni(NO_3)_2$	244.71	3.00	0.00	0.00	0.17	0.00	0.00	0.17	2.43	31860.00	0.45	O,C	225	0.13	1.50	0.50	0.63	1.62	0.00	1.26	
$NaNO_2$	69.00	1.00	0.00	0.00	0.20	0.00	0.00	0.20	0.85	1547.00	0.97	O	320	0.19	1.75	0.58	0.77	186.00	0.01	1.96	
KNO_2	85.10	1.00	0.00	1.00	0.16	0.00	0.46	0.62	3.12	18600.00	0.68	O	400	0.24	1.75	0.58	0.82	200.00	0.01	2.14	
NH_4NO_2	64.04	2.00	0.00	0.00	0.44	0.00	0.00	0.44	1.18	2110.00	0.96	O, explosive	85	0.05	1.00	0.33	0.38	2217.00	0.13	1.92	
$(NH_4)_3PO_4$	149.09	3.00	1.00	0.00	0.28	0.21	0.00	0.49	0.58	1946.00	0.97	none	210	0.13	1.00	0.33	0.46	5750.00	0.34	2.25	
$(NH_4)_2SO_4$	132.14	2.00	0.00	0.00	0.21	0.00	0.00	0.21	0.74	1665.00	0.97	none	250	0.15	0.50	0.17	0.32	3000.00	0.18	1.68	
$(NH_4)_2HPO_4$	132.06	2.00	1.00	0.00	0.21	0.23	0.00	0.45	0.66	1724.80	0.97	none	70	0.04	3.00	1.00	1.04	6500.00	0.38	2.84	
$(NH_4)_2CO_3$	96.09	2.00	0.00	0.00	0.29	0.00	0.00	0.29	0.25	2227.00	0.96	O,C	58	0.03	2.00	0.67	0.70	2.00	0.00	1.95	
NH_4Cl	53.49	1.00	0.00	0.00	0.26	0.00	0.00	0.26	0.38	926.00	0.98	none	337	0.20	3.00	1.00	1.20	1650.00	0.10	2.54	
$(NH_4)_2SO_3$	116.14	2.00	0.00	0.00	0.24	0.00	0.00	0.24	0.35	1562.00	0.97	C	65	0.04	2.00	0.67	0.71	0.00	0.00	1.92	
NaH_2PO_4	119.98	0.00	1.00	0.00	0.00	0.26	0.00	0.26	0.60	5633.00	0.90	none	169	0.10	3.00	1.00	1.10	8290.00	0.49	2.75	
$Ca(H_2PO_4)_2$	234.05	0.00	2.00	0.00	0.00	0.26	0.00	0.26	0.02	9022.00	0.84	C	225	0.13	2.00	0.67	0.80	3986.00	0.23	2.15	
KH_2PO_4	136.09	0.00	1.00	1.00	0.00	0.23	0.29	0.51	0.23	1348.00	0.98	none	400	0.24	3.00	1.00	1.24	4640.00	0.27	3.00	
NaH_2PO_3	103.98	0.00	1.00	0.00	0.00	0.30	0.00	0.30	0.83	1131.00	0.98	none	175	0.10	1.00	0.00	0.10	7640.00	0.45	1.83	
KH_2PO_3	120.09	0.00	1.00	1.00	0.00	0.26	0.33	0.58	0.22	-	0.00	none	180	0.11	3.00	1.00	1.11	2000.00	0.12	1.81	
K_2HPO_4	174.18	0.00	1.00	2.00	0.00	0.18	0.45	0.63	1.49	1420.00	0.98	none	465	0.28	3.00	1.00	1.28	6000.00	0.35	3.23	
Na_2HPO_4	141.96	0.00	1.00	0.00	0.00	0.22	0.00	0.22	0.08	1026.00	0.98	none	250	0.15	3.00	1.00	1.15	17000.00	1.00	3.35	
$MgHPO_4$	120.28	0.00	1.00	0.00	0.00	0.26	0.00	0.26	0.00	2272.00	0.96	C	400	0.24	1.00	0.33	0.57	0.00	0.00	1.79	
$CaHPO_4$	136.06	0.00	1.00	0.00	0.00	0.23	0.00	0.23	0.00	1029.00	0.98	none	450	0.27	3.00	1.00	1.27	2000.00	0.12	2.60	
$MnHPO_4$	150.92	0.00	1.00	0.00	0.00	0.21	0.00	0.21	0.00	-	0.00	none	500	0.30	3.00	1.00	1.30	0.00	0.00	1.50	
$NiHPO_4$	154.67	0.00	1.00	0.00	0.00	0.20	0.00	0.20	0.00	-	0.00	O	500	0.30	3.00	1.00	1.30	0.00	0.00	1.50	
$Ca_3(PO_4)_2$	310.18	0.00	2.00	0.00	0.00	0.20	0.00	0.20	0.00	1394.00	0.98	none	1670	1.00	3.00	1.00	2.00	500.00	0.03	3.21	
K_3PO_4	**212.27**	**0.00**	**1.00**	**3.00**	**0.00**	**0.15**	**0.55**	**0.70**	**0.10**	**1473.00**	**0.97**	**none**	**1380**	**0.83**	**3.00**	**1.00**	**1.83**	**2000.00**	**0.12**	**3.62**	*
$FePO_4$	150.82	0.00	1.00	0.00	0.00	0.21	0.00	0.21	0.00	3731.00	0.94	none	600	0.36	2.00	0.67	1.03	2000.00	0.12	2.28	
Na_3PO_4	163.94	0.00	1.00	0.00	0.00	0.19	0.00	0.19	0.12	977.60	0.98	C	600	0.36	3.00	1.00	1.36	5950.00	0.35	2.88	
K_2CO_3	**138.21**	**0.00**	**0.00**	**2.00**	**0.00**	**0.00**	**0.57**	**0.57**	**1.10**	**1167.00**	**0.98**	**none**	**891**	**0.53**	**3.00**	**1.00**	**1.53**	**1870.00**	**0.11**	**3.19**	*
KCl	74.55	0.00	0.00	1.00	0.00	0.00	0.52	0.52	0.34	2274.00	0.96	none	600	0.36	3.00	1.00	1.36	2600.00	0.15	3.00	
K_2SO_4	174.26	0.00	0.00	2.00	0.00	0.00	0.45	0.45	0.11	1538.00	0.97	C	1069	0.64	2.00	0.67	1.31	6600.00	0.39	3.12	
$KHCO_3$	100.12	0.00	0.00	2.00	0.00	0.00	0.78	0.78	0.22	1603.20	0.97	C	100	0.06	3.00	1.00	1.06	2000.00	0.12	2.93	
$KHSO_4$	136.17	0.00	0.00	2.00	0.00	0.00	0.57	0.57	0.49	1888.00	0.97	C	300	0.18	2.00	0.67	0.85	2340.00	0.14	2.53	
K_2SO_3	158.26	0.00	0.00	2.00	0.00	0.00	0.49	0.49	1.00	1642.00	0.97	none	400	0.24	3.00	1.00	1.24	0.00	0.00	2.71	

FIGURE A.1: Full list of prospective chemical compounds analysed

Appendix B

Chapter 3.2.4: Discounted Cash Flow and Financial Indicators

DISCOUNTED CASHFLOW TABLE: MODERATE (CONSERVATIVE) CASE								
YEAR:		**1**	**2**	**3**	**17**	**18**	**19**	**20**
Fixed Capital Investment	1	-R 52 702 578	R -	R -	R -	R -	R -	R -
Working Capital	1	R -	-R 1 965 035	-R 5 895 106	R -	R -	R -	R 7 860 142
Total Capital Investment		-R 52 702 578	-R 1 965 035	-R 5 895 106	R -	R -	R -	R 7 860 142
ANNUAL SALES								
Plant performance %		0	75	100	100	100	100	100
Biochar mass production (tpa)		0	619	825	224	224	224	224
Wood vinegar sales (tpa)		0	104	139	206	206	206	206
Phenolic-type compounds sales (tpa)		0	296	394	241	241	241	241
Liquid to electricity production		0	592	789	470	470	470	470
Biochar sales	1	R -	R 17 938 530	R 23 918 040	R 23 918 040	R 23 918 040	R 23 918 040	R 23 918 040
Fertiliser sales	1	R -	R 2 912 606	R 3 883 474	R 3 883 474	R 3 883 474	R 3 883 474	R 3 883 474
Electricity sales: syngas	1	R -	R 5 694 090	R 7 592 120	R 7 592 120	R 7 592 120	R 7 592 120	R 7 592 120
Wood vinegar sales	1	R -	R -	R -	R -	R -	R -	R -
Phenolics sales	1	R -	R -	R -	R -	R -	R -	R -
TOTAL ANNUAL INCOME	**1**	**R -**	**R 26 545 226**	**R 35 393 634**	**R 35 393 634**	**R 35 393 634**	**R 35 393 634**	**R 35 393 634**
CO2 Emissions rebate (@R120/eq.ton_CO_2)	*1*	R -	R 245 203	R 326 938	R 326 938	R 326 938	R 326 938	R 326 938
ANNUAL MANUFACTURING COST								
Fixed cost	**1**	R -	R 14 102 015	R 18 802 686	R 18 802 686	R 18 802 686	R 18 802 686	R 18 802 686
Variable cost	**1**	R -	R 6 842 065	R 9 122 754	R 9 122 754	R 9 122 754	R 9 122 754	R 9 122 754
TOTAL COST OF SALES	**1**	**0**	**R 20 944 080**	**R 27 925 440**	**R 27 925 440**	**R 27 925 440**	**R 27 925 440**	**R 27 925 440**
Less book depreciation	**1**	R -	R 10 540 516	R 8 432 412	R 370 861	R 296 689	R 237 351	R 189 881
Gross profit		R -	R 3 881 313	R 1 900 026	R 7 795 132	R 7 795 132	R 7 795 132	R 15 655 274
OPERATING PROFIT (PBIT)		R -	-R 6 659 202	-R 6 532 387	R 7 424 270	R 7 498 443	R 7 557 781	R 15 465 392
Add book depreciation		R -	R 10 540 516	R 8 432 412	R 370 861	R 296 689	R 237 351	R 189 881
Less tax depreciation (@ 50 %, 30 %, 20 %)		R -	R 26 351 289	R 20 664 288	R -	R -	R -	R -
Taxable Income		R -	-R 22 469 975	-R 18 764 262	R 7 795 132	R 7 795 132	R 7 795 132	R 15 655 274
Less income tax @ 28 %		R -	-R 6 291 593	-R 5 253 993	R 2 182 637	R 2 182 637	R 2 182 637	R 4 383 477
PROFIT AFTER TAX		**R -**	**-R 367 609**	**-R 1 278 393**	**R 5 241 634**	**R 5 315 806**	**R 5 375 144**	**R 11 081 916**
Net cash flow (R_c)		-R 52 702 578	-R 16 178 382	-R 13 510 269	R 5 612 495	R 5 612 495	R 5 612 495	R 11 271 797
CUMULATIVE NET CASH FLOW		**-R 52 702 578**	**-R 68 880 960**	**-R 82 391 229**	**-R 15 680 637**	**-R 10 068 142**	**-R 4 455 647**	**R 6 816 150**
Discounted cash flow		-R 52 702 578	-R 15 262 625	-R 12 024 091	R 2 209 338	R 2 084 281	R 1 966 303	R 3 725 476
Cumulative discounted cash flow		-R 52 702 578	-R 67 965 203	-R 79 989 294	-R 43 521 441	-R 41 437 160	-R 39 470 857	-R 35 745 382
Discounted cash flow @ IRR		-R 52 702 578	-R 69 738 325	-R 84 718 476	R 32 558 644	R 46 060 690	R 60 278 271	R 90 345 194

FINANCIAL INDICATORS		
Inflation rate		**6.0%**
Net present value (NPR)	**-R**	**35 745 382**
Internal rate of return (IRR)		**-5.0%**
Return on investment (ROI)		**21.4%**
Packback period		**19.8**

Figure B.1: Discounted cash flow and financial indicators of Scenario 1

DISCOUNTED CASHFLOW TABLE: MODERATE (CONSERVATIVE) CASE																					
YEAR:			**1**		**2**		**3**		**17**		**18**		**19**		**20**						
Fixed Capital Investment	1	-R	52 702 578	R	-	R	-	R	-	R	-	R	-	R	-						
Working Capital	1	R	-	-R	1 816 229	-R	5 448 687	R	-	R	-	R	-	R	7 264 916						
Total Capital Investment		-R	52 702 578	-R	1 816 229	-R	5 448 687	R	-	R	-	R	-	R	7 264 916						
ANNUAL SALES																					
Plant performance %			0		75		100		100		100		100		100						
Biochar mass production (tpa)			0		619		825		224		224		224		224						
Wood vinegar sales (tpa)			0		104		139		206		206		206		206						
Phenolic-type compounds sales (tpa)			0		296		394		241		241		241		241						
Liquid to electricity production			0		592		789		470		470		470		470						
Biochar sales	1	R	-	R	17 938 530	R	23 918 040	R	23 918 040	R	23 918 040	R	23 918 040	R	23 918 040						
Fertiliser sales	1	R	-	R	2 912 606	R	3 883 474	R	3 883 474	R	3 883 474	R	3 883 474	R	3 883 474						
Electricity sales: syngas	1	R	-	R	3 075 955	R	4 101 273	R	4 101 273	R	4 101 273	R	4 101 273	R	4 101 273						
Wood vinegar sales	1	R	-	R	-	R	-	R	-	R	-	R	-	R	-						
Phenolics sales	1	R	-	R	6 447 887	R	8 597 183	R	8 597 183	R	8 597 183	R	8 597 183	R	8 597 183						
TOTAL ANNUAL INCOME	**1**	**R**	**-**	**R**	**30 374 977**	**R**	**40 499 970**	**R**	**40 499 970**	**R**	**40 499 970**	**R**	**40 499 970**	**R**	**40 499 970**						
CO2 Emissions rebate (@R120/eq.ton_CO_2)	*1*	R	-	R	245 203	R	326 938	R	326 938	R	326 938	R	326 938	R	326 938						
ANNUAL MANUFACTURING COST																					
Fixed cost	**1**	R	-	R	14 043 761	R	18 725 015	R	18 725 015	R	18 725 015	R	18 725 015	R	18 725 015						
Variable cost	**1**	R	-	R	6 658 796	R	8 878 395	R	8 878 395	R	8 878 395	R	8 878 395	R	8 878 395						
TOTAL COST OF SALES	**1**		**0**	**R**	**20 702 557**	**R**	**27 603 409**	**R**	**27 603 409**	**R**	**27 603 409**	**R**	**27 603 409**	**R**	**27 603 409**						
Less book depreciation	**1**	R	-	R	10 540 516	R	8 432 412	R	370 861	R	296 689	R	237 351	R	189 881						
Gross profit		R	-	R	8 101 395	R	7 774 811	R	13 223 498	R	13 223 498	R	13 223 498	R	20 488 414						
OPERATING PROFIT (PBIT)		R	-	-R	2 439 121	-R	657 601	R	12 852 637	R	12 926 809	R	12 986 147	R	20 298 533						
Add book depreciation		R	-	R	10 540 516	R	8 432 412	R	370 861	R	296 689	R	237 351	R	189 881						
Less tax depreciation (@ 50 %, 30 %, 20 %)		R	-	R	26 351 289	R	19 752 750	R	-	R	-	R	-	R	-						
Taxable Income		R	-	-R	18 249 894	-R	11 977 939	R	13 223 498	R	13 223 498	R	13 223 498	R	20 488 414						
Less income tax @ 28 %		R	-	-R	5 109 970	-R	3 353 823	R	3 702 579	R	3 702 579	R	3 702 579	R	5 736 756						
PROFIT AFTER TAX		**R**	**-**	**R**	**2 670 850**	**R**	**2 696 222**	**R**	**9 150 057**	**R**	**9 224 230**	**R**	**9 283 567**	**R**	**14 561 777**						
Net cash flow (R_t)		-R	52 702 578	-R	13 139 924	-R	8 624 116	R	9 520 919	R	9 520 919	R	9 520 919	R	14 751 658						
CUMULATIVE NET CASH FLOW		**-R**	**52 702 578**	**-R**	**65 842 502**	**-R**	**74 466 618**	**R**	**48 103 051**	**R**	**57 623 970**	**R**	**67 144 889**	**R**	**81 896 547**						
Discounted cash flow		-R	52 702 578	-R	12 396 155	-R	7 675 433	R	3 747 874	R	3 535 730	R	3 335 595	R	4 875 615						
Cumulative discounted cash flow		-R	52 702 578	-R	65 098 732	-R	72 774 165	-R	3 015 740	R	519 991	R	3 855 586	R	8 731 200						
Discounted cash flow @ IRR		-R	52 702 578	-R	65 695 303	-R	74 127 281	R	35 393 710	R	43 255 202	R	51 028 626	R	62 937 804						

FINANCIAL INDICATORS		
Inflation rate		**6.0%**
Net present value (NPR)	**R**	**8 731 200**
Internal rate of return (IRR)		**1.1%**
Return on investment (ROI)		**28.0%**
Packback period		**11.9**

FIGURE B.2: Discounted cash flow and financial indicators of Scenario 2

DISCOUNTED CASHFLOW TABLE: MODERATE (CONSERVATIVE) CASE									
YEAR:		**1**	**2**	**3**	**17**	**18**	**19**	**20**
Fixed Capital Investment	1	-R 52 702 578	R -	R -	R -	R -	R -	R -
Working Capital	1	R -	-R 1 814 217	-R 5 442 652	R -	R -	R -	R 7 256 870
Total Capital Investment		-R 52 702 578	-R 1 814 217	-R 5 442 652	R -	R -	R -	R 7 256 870
ANNUAL SALES								
Plant performance %		0	75	100	100	100	100	100
Biochar mass production (tpa)		0	619	825	224	224	224	224
Wood vinegar sales (tpa)		0	104	139	206	206	206	206
Phenolic-type compounds sales (tpa)		0	296	394	241	241	241	241
Liquid to electricity production		0	592	789	470	470	470	470
Biochar sales	1	R -	R 17 938 530	R 23 918 040	R 23 918 040	R 23 918 040	R 23 918 040	R 23 918 040
Fertiliser sales	1	R -	R 2 912 606	R 3 883 474	R 3 883 474	R 3 883 474	R 3 883 474	R 3 883 474
Electricity sales: syngas	1	R -	R -	R -	R -	R -	R -	R -
Wood vinegar sales	1	R -	R 3 040 564	R 4 054 085	R 4 054 085	R 4 054 085	R 4 054 085	R 4 054 085
Phenolics sales	1	R -	R -	R -	R -	R -	R -	R -
TOTAL ANNUAL INCOME	**1**	**R -**	**R 23 891 700**	**R 31 855 599**	**R 31 855 599**	**R 31 855 599**	**R 31 855 599**	**R 31 855 599**
CO2 Emissions rebate (@R120/eq.ton_CO_2)	*1*	R -	R 245 203	R 326 938	R 326 938	R 326 938	R 326 938	R 326 938
ANNUAL MANUFACTURING COST								
Fixed cost	**1**	R -	R 14 042 974	R 18 723 965	R 18 723 965	R 18 723 965	R 18 723 965	R 18 723 965
Variable cost	**1**	R -	R 6 656 319	R 8 875 091	R 8 875 091	R 8 875 091	R 8 875 091	R 8 875 091
TOTAL COST OF SALES	**1**	**0**	**R 20 699 292**	**R 27 599 056**	**R 27 599 056**	**R 27 599 056**	**R 27 599 056**	**R 27 599 056**
Less book depreciation	1	R -	R 10 540 516	R 8 432 412	R 370 861	R 296 689	R 237 351	R 189 881
Gross profit		R -	R 1 623 393	-R 859 172	R 4 583 481	R 4 583 481	R 4 583 481	R 11 840 351
OPERATING PROFIT (PBIT)		R -	-R 8 917 122	-R 9 291 584	R 4 212 619	R 4 286 792	R 4 346 129	R 11 650 470
Add book depreciation		R -	R 10 540 516	R 8 432 412	R 370 861	R 296 689	R 237 351	R 189 881
Less tax depreciation (@ 50 %, 30 %, 20 %)		R -	R 26 351 289	R 21 151 999	R -	R -	R -	R -
Taxable Income		R -	-R 24 727 896	-R 22 011 170	R 4 583 481	R 4 583 481	R 4 583 481	R 11 840 351
Less income tax @ 28 %		R -	-R 6 923 811	-R 6 163 128	R 1 283 375	R 1 283 375	R 1 283 375	R 3 315 298
PROFIT AFTER TAX		**R -**	**-R 1 993 312**	**-R 3 128 456**	**R 2 929 245**	**R 3 003 417**	**R 3 062 755**	**R 8 335 171**
Net cash flow (R_t)		-R 52 702 578	-R 17 804 085	-R 15 848 043	R 3 300 106	R 3 300 106	R 3 300 106	R 8 525 052
CUMULATIVE NET CASH FLOW		**-R 52 702 578**	**-R 70 506 663**	**-R 86 354 705**	**-R 52 588 297**	**-R 49 288 191**	**-R 45 988 085**	**-R 37 463 032**
Discounted cash flow		-R 52 702 578	-R 16 796 307	-R 14 104 702	R 1 299 075	R 1 225 542	R 1 156 172	R 2 817 641
Cumulative discounted cash flow		-R 52 702 578	-R 69 498 884	-R 83 603 586	-R 66 744 180	-R 65 518 638	-R 64 362 467	-R 61 544 826
Discounted cash flow @ IRR		-R 52 702 578	-R 72 385 441	-R 91 754 693	R 21 311 418	R 39 474 700	R 59 554 664	R 116 900 343

FINANCIAL INDICATORS		
Inflation rate		**6.0%**
Net present value (NPR)	**-R**	**61 544 826**
Internal rate of return (IRR)		**-9.5%**
Return on investment (ROI)		**16.2%**
Packback period		**32.9**

FIGURE B.3: Discounted cash flow and financial indicators of Scenario 3

DISCOUNTED CASHFLOW TABLE: MODERATE (CONSERVATIVE) CASE																					
YEAR:			**1**		**2**		**3**		**17**		**18**		**19**		**20**						
Fixed Capital Investment	1	-R	52 702 578	R	-	R	-	R	-	R	-	R	-	R	-						
Working Capital	1	R	-	-R	1 814 217	-R	5 442 652	R	-	R	-	R	-	R	7 256 870						
Total Capital Investment		-R	52 702 578	-R	1 814 217	-R	5 442 652	R	-	R	-	R	-	R	7 256 870						
ANNUAL SALES																					
Plant performance %			0		75		100		100		100		100		100						
Biochar mass production (tpa)			0		619		825		224		224		224		224						
Wood vinegar sales (tpa)			0		104		139		206		206		206		206						
Phenolic-type compounds sales (tpa)			0		296		394		241		241		241		241						
Liquid to electricity production			0		592		789		470		470		470		470						
Biochar sales	1	R	-	R	17 938 530	R	23 918 040	R	23 918 040	R	23 918 040	R	23 918 040	R	23 918 040						
Fertiliser sales	1	R	-	R	2 912 606	R	3 883 474	R	3 883 474	R	3 883 474	R	3 883 474	R	3 883 474						
Electricity sales: syngas	1	R	-	R	-	R	-	R	-	R	-	R	-	R	-						
Wood vinegar sales	1	R	-	R	3 040 564	R	4 054 085	R	4 054 085	R	4 054 085	R	4 054 085	R	4 054 085						
Phenolics sales	1	R	-	R	6 447 887	R	8 597 183	R	8 597 183	R	8 597 183	R	8 597 183	R	8 597 183						
TOTAL ANNUAL INCOME	**1**	**R**	-	**R**	**30 339 587**	**R**	**40 452 782**	**R**	**40 452 782**	**R**	**40 452 782**	**R**	**40 452 782**	**R**	**40 452 782**						
CO2 Emissions rebate (@R120/eq.ton_CO_2)	*1*	R	-	R	245 203	R	326 938	R	326 938	R	326 938	R	326 938	R	326 938						
ANNUAL MANUFACTURING COST																					
Fixed cost	**1**	R	-	R	14 042 974	R	18 723 965	R	18 723 965	R	18 723 965	R	18 723 965	R	18 723 965						
Variable cost	**1**	R	-	R	6 656 319	R	8 875 091	R	8 875 091	R	8 875 091	R	8 875 091	R	8 875 091						
TOTAL COST OF SALES	**1**		**0**	**R**	**20 699 292**	**R**	**27 599 056**	**R**	**27 599 056**	**R**	**27 599 056**	**R**	**27 599 056**	**R**	**27 599 056**						
Less book depreciation	**1**	R	-	R	10 540 516	R	8 432 412	R	370 861	R	296 689	R	237 351	R	189 881						
Gross profit		R	-	R	8 071 280	R	7 738 011	R	13 180 664	R	13 180 664	R	13 180 664	R	20 437 534						
OPERATING PROFIT (PBIT)		R	-	-R	2 469 235	-R	694 401	R	12 809 802	R	12 883 975	R	12 943 313	R	20 247 653						
Add book depreciation		R	-	R	10 540 516	R	8 432 412	R	370 861	R	296 689	R	237 351	R	189 881						
Less tax depreciation (@ 50 %, 30 %, 20 %)		R	-	R	26 351 289	R	19 759 255	R	-	R	-	R	-	R	-						
Taxable Income		R	-	-R	18 280 008	-R	12 021 244	R	13 180 664	R	13 180 664	R	13 180 664	R	20 437 534						
Less income tax @ 28 %		R	-	-R	5 118 402	-R	3 365 948	R	3 690 586	R	3 690 586	R	3 690 586	R	5 722 509						
PROFIT AFTER TAX		**R**	-	**R**	**2 649 167**	**R**	**2 671 547**	**R**	**9 119 217**	**R**	**9 193 389**	**R**	**9 252 727**	**R**	**14 525 143**						
Net cash flow (R_t)		-R	52 702 578	-R	13 161 606	-R	8 655 295	R	9 490 078	R	9 490 078	R	9 490 078	R	14 715 024						
CUMULATIVE NET CASH FLOW		**-R**	**52 702 578**	**-R**	**65 864 184**	**-R**	**74 519 479**	**R**	**47 610 807**	**R**	**57 100 885**	**R**	**66 590 963**	**R**	**81 305 988**						
Discounted cash flow		-R	52 702 578	-R	12 416 610	-R	7 703 182	R	3 735 734	R	3 524 277	R	3 324 790	R	4 863 507						
Cumulative discounted cash flow		-R	52 702 578	-R	65 119 187	-R	72 822 369	-R	3 325 465	R	198 812	R	3 523 602	R	8 387 109						
Discounted cash flow @ IRR		-R	52 702 578	-R	65 722 410	-R	74 192 245	R	35 405 427	R	43 299 671	R	51 108 880	R	63 087 169						

FINANCIAL INDICATORS		
Inflation rate		**6.0%**
Net present value (NPR)	**R**	**8 387 109**
Internal rate of return (IRR)		**1.1%**
Return on investment (ROI)		**27.9%**
Packback period		**12.0**

FIGURE B.4: Discounted cash flow and financial indicators of Scenario 4